INFORMATION TO USERS

This manuscript has been reproduced from the microfilm master. UMI films the text directly from the original or copy submitted. Thus, some thesis and dissertation copies are in typewriter face, while others may be from any type of computer printer.

The quality of this reproduction is dependent upon the quality of the copy submitted. Broken or indistinct print, colored or poor quality illustrations and photographs, print bleedthrough, substandard margins, and improper alignment can adversely affect reproduction.

In the unlikely event that the author did not send UMI a complete manuscript and there are missing pages, these will be noted. Also, if unauthorized copyright material had to be removed, a note will indicate the deletion.

Oversize materials (e.g., maps, drawings, charts) are reproduced by sectioning the original, beginning at the upper left-hand corner and continuing from left to right in equal sections with small overlaps.

Photographs included in the original manuscript have been reproduced xerographically in this copy. Higher quality 6" x 9" black and white photographic prints are available for any photographs or illustrations appearing in this copy for an additional charge. Contact UMI directly to order.

Bell & Howell Information and Learning
300 North Zeeb Road, Ann Arbor, MI 48106-1346 USA

UMI®
800-521-0600

Université d'Ottawa • University of Ottawa

THE MECHANISM OF FOULING AND SYNTHETIC MEMBRANE DEVELOPMENT FOR TREATING COATING PLANT EFFLUENT FROM A PULP AND PAPER MILL

Surendra Singh

A thesis submitted to the School of Graduate Studies and Research
in partial fulfillment of the requirements for the
degree of
DOCTOR OF PHILOSOPHY
in the Department of Chemical Engineering
University of Ottawa

June 1999

To my lovely kids, Rahul and Neha,

who persistently encourage me to work hard.

Abstract

The use of the membrane is ever increasing with the development of membranes which can tolerate higher temperatures and a wider range of pH. In the pulp and paper industry, to comply with the strict effluent regulations and to reduce the water consumption, more and more water has to be recycled within the process after some internal treatments. Paper coating plant effluent and paper machine white-water are the streams that would allow for the application of membranes in pulp and paper. Therefore, in this research an attempt was made to develop synthetic membranes and also to study the mechanism of fouling for treating these streams.

Asymmetric membranes having different pore sizes were prepared from polyethersulfone by the phase inversion technique using casting solutions of different polymer concentrations. These membranes were further modified by coating a thin layer of SPPO (sulfonated polyphenylene oxide) material. Each type of membrane used in this study was characterized in terms of mean pore size, pore size distribution, pore density, surface porosity and surface roughness by solute transport and also by atomic force microscope (AFM). Fouled membranes after ultrafiltration experiments were also characterized. Membranes were tested for laboratory made feed solutions which included clay and/or styrene butadiene rubber (SBR) as solutes to simulate coating plant effluent and white-water from a pulp and paper mill.

The mean pore size of the membrane was substantially reduced on coating of a SPPO layer on the membrane surface. The mean pore sizes measured by AFM were about 3.5 times larger than those calculated from solute transport data. Pore sizes, obtained from both AFM and solute transport studies fitted remarkably well to the log-normal distribution curve. A very sharp flux decline was observed immediately after the start of the experiment when membranes were tested for a feed solution containing clay and/or SBR. Flux reduction was attributed mainly to pore plugging and cake layer formation on the membrane surface.

A procedure was developed to determine the resistances of cake layer and membrane to the permeate flow. Cake layer resistance to the permeate flow was substantially higher than the resistance of the membrane and hence was the controlling factor. The resistance of the cake layer was, however, lower for the SPPO coated membranes compared to unmodified membranes. Both mass and thickness of cake layer attained their maximum in the first hour of operation and remained unchanged thereafter. Clay particles in the cake layer were substantially smaller in size compared to those in the feed solution. Specific resistance of the cake layer increased while its void space decreased with the operating time. More pore plugging was observed with the membranes having bigger pores. Reduction in the pore densities of the membranes after treating clay/SBR solution indicated that some of the pores were blocked either completely or partially.

Characterization of the changes in the membrane morphology after coating a thin layer of SPPO will help in selecting design parameters for the development of a new thin film composite membrane. The usefulness of AFM was demonstrated in studying fouling and also in characterizing the membrane morphology. A detailed study of fouling was also conducted.

Acknowledgements

I would like to thank Prof. T. Matsuura for his supervision and the guidance throughout this research work. Thanks are also due to Dr. P. Ramamurthy of the Pulp and Paper Research Institute of Canada, Montreal for his help and invaluable advice from time to time. I am also very thankful to Dr. S. Sourirajan for his comments and suggestions for this research work.

Financial support from the Government of Canada in the form of a Canadian Commonwealth Fellowship is greatly appreciated. Technical support provided by the machine shop in the Department of Chemical Engineering is also appreciated.

I would also like to take this opportunity to thank all my fellow students and researchers at the Industrial Membrane Research Institute with whom I truly enjoyed working. Support from my family is greatly acknowledged.

List of Publications and Presentations

The following are the publications/presentations based on this research work.

Publications

- "Membrane Characterization by Solute Transport and Atomic Force Microscopy", S. Singh, K. C. Khulbe, T. Matsuura and P. Ramamurthy, *J. Membrane Science*, 142(1) : 111-127(1998)

- "Coating Plant Effluent Treatment by Ultrafiltration Membrane", S. Singh, T. Matsuura and P. Ramamurthy, *TAPPI JOURNAL* ,82(4) : 146-157(1999).

- "Study of Thin Film Composite Membrane Prepared from Sulfonated Polyphenylene Oxide: Preparation, Characterization, Performance and Transport", G. Chowdhary, S. Singh, C. Tsang and T. Matsuura, Accepted for publication in *ACS Symp. Series*.

- "Coating Plant Effluent Treatment by Modified Polyethersulfone Membrane" S. Singh, T. Matsuura and P. Ramamurthy, Submitted to *TAPPI JOURNAL*, under review.

Three more papers based on the results data presented in Chapter 8, 9 and 10, respectively, are under preparation for publications.

Presentations

- "Performance of Charged Polyethersulfone Membrane for Treating Coating Plant Effluent", S. Singh, T. Matsuura and P. Ramamurthy, *1st France-Canada Nanofiltration and Application Workshop*, Trois-Rivières, Canada, June 2-4, 1997.

- "Treatment of Excess White Water and Coating Plant Effluent by Modified Polyethersulfone Ultrafiltration Membrane", S. Singh, T. Matsuura and P. Ramamurthy, *TAPPI International Environmental Conference*, Minneapolis, USA, May 5-7, 1997, 881-898.

- "White Water System Closure by Ultrafiltration Membrane", S. Singh, T. Matsuura and P. Ramamurthy, *IPPTA Conference*, New Delhi, India, December 14 & 15, 1996, 15-23.

- "Ultrafiltration Membrane Application for Treating Coating Plant Effluent from a Pulp and Paper Mill", S. Singh, T. Matsuura and P. Ramamurthy, *8th Annual Meeting of North American Membrane Society*, Ottawa, Canada May 20-23, 1996, 52.

Table of Contents

List of Tables

List of Figures

Nomenclature

List of symbols

A	membrane surface area, [m^2]
a	Stokes radius, [cm]
A_0	intercept of linear regression on log-normal probability paper, [-]
A_1	slope of linear regression on log-normal probability paper, [-]
A_r	aspect ratio of clay particle, [-]
a_v	specific surface area of clay particle, [m^{-1}]
c_f	solute concentration in the feed solution, [ppm, %]
c_g	gel concentration, [%]
c_m	solute concentration on membrane surface, [ppm, %]
c_p	solute concentration in the permeate, [ppm, %]
D	diffusivity of solute in Eq. (3.10), [cm^2/s]
D	equivalent spherical diameter of clay particle in Eq. (9.8), [μm, m]
D_p	effective particle diameter (of clay particle), [μm, m]
d_{max}	maximum pore size, [nm]
d_{min}	minimum pore size, [nm]
d_p	pore size, [nm]
d_s	solute size, [nm]
f	solute separation, [%]
$f(x, y)$	surface relative to the center line, [-]
f_i	fraction of pores of diameter d_i, [-]
Fr_t	flux reduction at operating time t, [%]
f_s	steady state sodium chloride separation in Eq. (8.1), [%]
f_t	sodium chloride separation at operating time t in Eq (8.1), [%]
g	acceleration due to gravity, [m/s^2]
h	distance fallen by clay particle in time t, [m]
I	target value of IEC, [meq/g of polymer]
j	order number of pore when arranged in ascending order, [-]
J	total solvent flux through all the pores, [m^3/m^2s]
J_{lim}	limiting flux, [L/m^2h, m^3/m^2s]
J_i	solvent flux through the pores of diameter d_i, [m^3/m^2s]
$J_{p(25)}$	permeate flux value converted at 25°C, [L/m^2h, m^3/m^2s]
$J_{p(T)}$	permeate flux at operating temperature of T°C, [L/m^2h, m^3/m^2s]
J_s	solvent (water) permeation flux, [m^3/m^2s]
J_{wf}	pure water permeation flux of fouled membrane, [L/m^2h, m^3/m^2s]
$J_{p_{24}}$	final permeate flux, [L/m^2h, m^3/m^2s]

J_{p_t}	permeate flux at time t, [L/m^{2}h, m^3/m^{2}s]
J_w	pure water permeation flux, [L/m^{2}h, m^3/m^{2}s]
k	Boltzmann's constant in Eq (3.10), [-]
k	mass transfer coefficient in Eq. (3.43), [m/s]
L	length/width of clay particle, [μm, m]
L_x, L_y	dimensions of the surface f(x, y), [nm]
m	mass of cake layer in Eq. (9.1), [mg, kg]
m_c	molecular weight of chlorosulfonic acid, [g/mol]
M	molecular weight of PEG/PEO, [g/mol]
n	total number of pores measured from AFM images, [-]
N	total number of pores per unit area, [-]
N_i	number of pores of diameter d_i per unit area, [-]
N_p	number of points within a given area, [-]
r	coefficient of correlation, [-]
R_1	total resistance of a virgin membrane, [m^{-1}]
R_2	total resistance of a fouled membrane, [m^{-1}]
R_3	total resistance of fouled membrane with cake layer, [m^{-1}]
R_a	mean roughness, [nm]
R_c	resistance contributed by the cake layer, [m^{-1}]
R_f	combined fouling resistance, [m^{-1}]
R_m	resistance contributed by membrane in Eqs. (7.1 – 7.3), [m^{-1}]
R_m	resistance due to membrane matrix in Eqs. (3.20-3.22, 3.28, 3.29, 3.35, 3.37, 3.38) [m^{-1}]
R_p	resistance due to pores in virgin membrane, [m^{-1}]
R_p^1	resistance due to pores in fouled membrane, [m^{-1}]
R_q	root mean square of Z data, [nm]
R_z	mean difference between five highest peaks and five lowest valleys, [nm]
S	surface area of clay particle, [m^2]
S_p	surface porosity of membrane, [%]
T	absolute temperature, [K]
t	operating time, [h, s]
t	thickness of clay particle in Eq.(9.6), [μm, m]
v	terminal falling velocity of clay particle, [m/s]
V	volume of clay particle, [m^3]
v_1	volume of 0.1N NaOH used for soaking SPPOH, [mL]
v_2	volume of 0.1N HCl consumed in titration, [mL]
v_c	volume of chlorosulfonic acid, [mL]
w_p	weight of PPO used for sulfonation, [g]

w_s	weight of SPPOH polymer soaked in 0.1N NaOH, [g]
Z_{avg}	average of the Z values, [nm]
Z_i	current Z value, [nm]

Greek letters

α	specific resistance of the cake, [m/kg]
α	permeate flux conversion factor for temperature in Eq. (C.1), [-]
β_0 β_1	constant, [-]
σ_g	geometric standard deviation of solute size, [-]
σ_p	geometric standard deviation of pore size, [-]
μ_p	geometric mean pore size of the membrane, [nm]
μ_s	geometric mean solute size, [nm]
δ_{bl}	boundary layer thickness, [μm, m]
δ	thickness of cake layer in Eq. (9.5), [μm, m]
δ	skin layer thickness in Eq. (3.6), [μm, m]
ε	void space of the cake layer, [-]
ρ	feed (water) density, [g/cm^3 kg/m^3]
ρ	clay particle density in Eq. (9.2), [kg/m^3]
ρ_c	density of chlorosulfonic acid, [g/cm^3]
η	solvent (water) viscosity, [N s/m^2]
$[\eta]$	intrinsic viscosity of PEG/PEO, [dL/g]
Δp	pressure difference across the pores/membrane, [kPa, Pa]

Abbreviations

AFM	atomic force microscope
AOX	absorbable organic halogen
BOD.	biochemical oxygen demand
COD	chemical oxygen demand
CR	cross-rotational
EPD	effective particle diameter
ESD	equivalent spherical diameter
FESEM	field emission scanning electron microscope
IEC	ion exchange capacity
MWCO	molecular weight cut-off
NMP	N-methylpyrrolidone
PEG	polyethylene glycol
PEO	polyethylene oxide
PES	polyethersulfone
PF	product flux

PPO	polyphenylene oxide
PSA	particle size analysis
PVP	polyvinylpyrrolidone
PWP	pure water permeation
RO	reverse osmosis
S	nomenclature to represent modified SPPO coated membrane
SBR	styrene butadiene rubber
SEM	scanning electron microscope
SPPO	sulfonated polyphenylene oxide
TEM	transmission electron microscope
TFC	thin film composite
TM	tapping mode
TOC	total organic carbon
TOCl	total organic chloride
U	nomenclature to represent unmodified never dried membrane
UD	nomenclature to represent glycerol treated dried membrane
UF	ultrafiltration

PART I

Introduction

Literature Review

Theoretical

Methodology and Experimental

CHAPTER 1

Introduction

1.1. Motivation

The pulp and paper industry is currently faced with the challenge of substantially reducing the discharge of contaminants to the receiving environment. Water is of primary importance in the paper making process. The pulp and paper industry has been a very large user of fresh water in comparison to several other manufacturing industries. Continuous progress has been made by the pulp and paper industry in reducing the fresh water use because of growing environmental concerns and stricter government regulations,. In a survey, it was found that in 1988, compared to 1959, 70% less water was required to produce one ton of paper (Miner and Unwin, 1991). Water use reduction in paper machine has been accomplished primarily by closing up the water system. Water closure, however, results in an increased concentration of suspended, dissolved and colloidal materials in the white water system of the paper machine which in turn could result in a poor quality of paper and operational problems. A reduction in fresh water intake from 30 m^3/ton to 10 m^3/ton of paper will result in an increase of 40% in the concentration of dissolved solids in the white water system (Lindstrom et al., 1977). Paper mills are looking for alternative processes for internal treatment of water because of these solids buildup problems,. Among the alternative processes, membrane separation process is getting an ever-increasing acceptance.

The membranes which were used in the early days of membrane filtration were made of cellulose acetate, and the application of these membranes was limited, especially with respect to pH and temperature. These drawbacks resulted in serious limitations in the use of membrane filtration in the pulp and paper industry. However, today, with the development of more pH and temperature resistant membranes, membrane filtration is now a well-established separation process in the pulp and paper industry. One of the major problems of membrane application to pulp and paper stream treatment is the flux decline due to fouling.

1.2. Objectives of the research

Objectives of the research were formulated after critically reviewing the available literature (Chapter 2) and identifying the potential of membrane applications to treat coating plant effluent and paper machine white water in a paper mill.

Although there are a few commercial scale ultrafiltration plants to treat bleach plant effluent from a Kraft mill, not much work has been reported on the recycling of waste water and process chemicals from other sections of the paper mill. In most of the studies, commercially available membranes have been tested to find out if they suit a specific application in the pulp and paper industry. Hardly any attempt has been made to develop a membrane for waste water treatment from a pulp and paper mill. Almost all the researchers have reported a flux decline due to fouling, however, no systematic study has been carried out to understand the mechanisms of fouling while treating white water and coating plant effluent. The basic objectives of this research are:

1. to develop synthetic polymeric ultrafiltration membranes to treat excess white water and coating plant effluent from a pulp and paper mill.
2. to study the mechanisms of fouling, which is one of the main constraints for these applications.

3. to study the membrane morphology by microscopic tools and by solute transport and to correlate the performance and fouling behavior of a membrane to its morphology.
4. to modify the membrane surface in order to reduce the fouling.
5. to study the morphology of the foulants layer on the membrane surface.

1.3. Originality of the research and milestones achieved

- The approach adopted in this research was entirely different from the so-called "traditional approach" of finding the best membrane (for a particular application) among the available ones. Knowing the application, an attempt was made to develop a membrane unique to the particular application. Therefore, this research was very focussed.
- Membranes were made in the laboratory to control their structures. The morphology of membranes prepared under various conditions was characterized in terms of various parameters such as mean pore size and pore size distribution, pore density, surface porosity and surface roughness. These parameters were determined from solute transport data and by atomic force microscopy. Results obtained from these two techniques were compared. No such detailed study is found in the literature. Characterization of the fouled membranes was also performed in order to identify any changes in the morphology of the membranes.
- Characterization of the membrane morphology after coating of a thin layer of sulfonated polyphenylene oxide (SPPO) polymer on the ultrafiltration membrane was done. This will help in selecting design parameters for a new thin film composite (TFC) membrane.
- Atomic force microscope (AFM) and scanning electron microscope (SEM) were used for not only to characterize virgin membranes but also to characterize the fouled membranes. AFM has not been applied so extensively by any researcher to study fouling.

- The effect of membrane modification (SPPO coating) on the membrane performance was clearly demonstrated by comparing the performance with unmodified membrane.
- The range of the size of particles that is responsible for the cake layer formation was identified by comparing the clay particle size distribution in the cake layer and in the feed solution. Particle size analysis (PSA) was performed by a Sedigraph 5100. The PSA of the cake layer was also performed by image analysis software built into the AFM.
- A procedure was developed to calculate the individual resistances, such as the resistance due to the membrane, due to the pores, due to partially plugged pores in fouled membranes and due to the cake layer.
- A detailed study on the cake layer formation during ultrafiltration experiments was conducted. The mass of the cake layer and its thickness were measured and its specific resistance and void space were determined for different operating periods. No such detailed study on the formation of the cake layer is available in the literature.
- The formation of the cake layer was monitored in an innovative way by monitoring the change in the sodium chloride separation with time.
- This research is very relevant and has a potential for application, as any reduction in the fouling (by better understanding of its mechanism) will lead to a higher permeate flux and improved economic feasibility of the process.

1.4. Contributions to science and technology

The following are the expected contributions from this research work to the fields of chemical engineering and membrane science and technology.

- Development of polymeric ultrafiltration membranes for treating white water and coating plant effluent from a pulp and paper mill
- Thorough characterization of both virgin and fouled membranes by solute transport measurement and by microscopic techniques

- Introduction of AFM for characterizing the fouling on the membrane
- Understanding the fouling mechanism by study of the cake layer formation process
- A procedure development to calculate the individual resistances

1.5. Pulp and paper making process

A generalized flow diagram of a bleached Kraft pulp and paper making process is given in Figure 1.1. Wood is the chief fibrous raw material used for pulp and paper industry. Wood is cut into small chips which undergo chemical and/or mechanical treatment. Various pulping processes exist depending on chemical, pressure, temperature treatment or a combination thereof to remove the lignin and other non-cellulosic components of wood. In the mechanical pulping process, lignin is not necessarily removed from the pulp. The product of the chemical pulping process is divided into two components in a brown stock washer. Liquor obtained from the washer is called black liquor, which consists of spent cooking chemicals, lignin and other compounds extracted from the wood. The cellulosic fibers obtained are called pulp, which goes for bleaching to improve its whiteness and brightness by removing residual lignin. Bleaching is carried out in different stages at which different chemicals are used, often with a washing stage in between. Chlorination (C-stage), used for degradation of lignin, is followed by alkali extraction (E-stage). After extraction a mild bleaching is carried out to further improve the brightness. Bleaching sequences vary from mill to mill but usually have chlorination (with or without chlorine dioxide) and extraction stages. It is the wash water from C-stage and E-stage which constitute major sources of pollution from the paper industry.

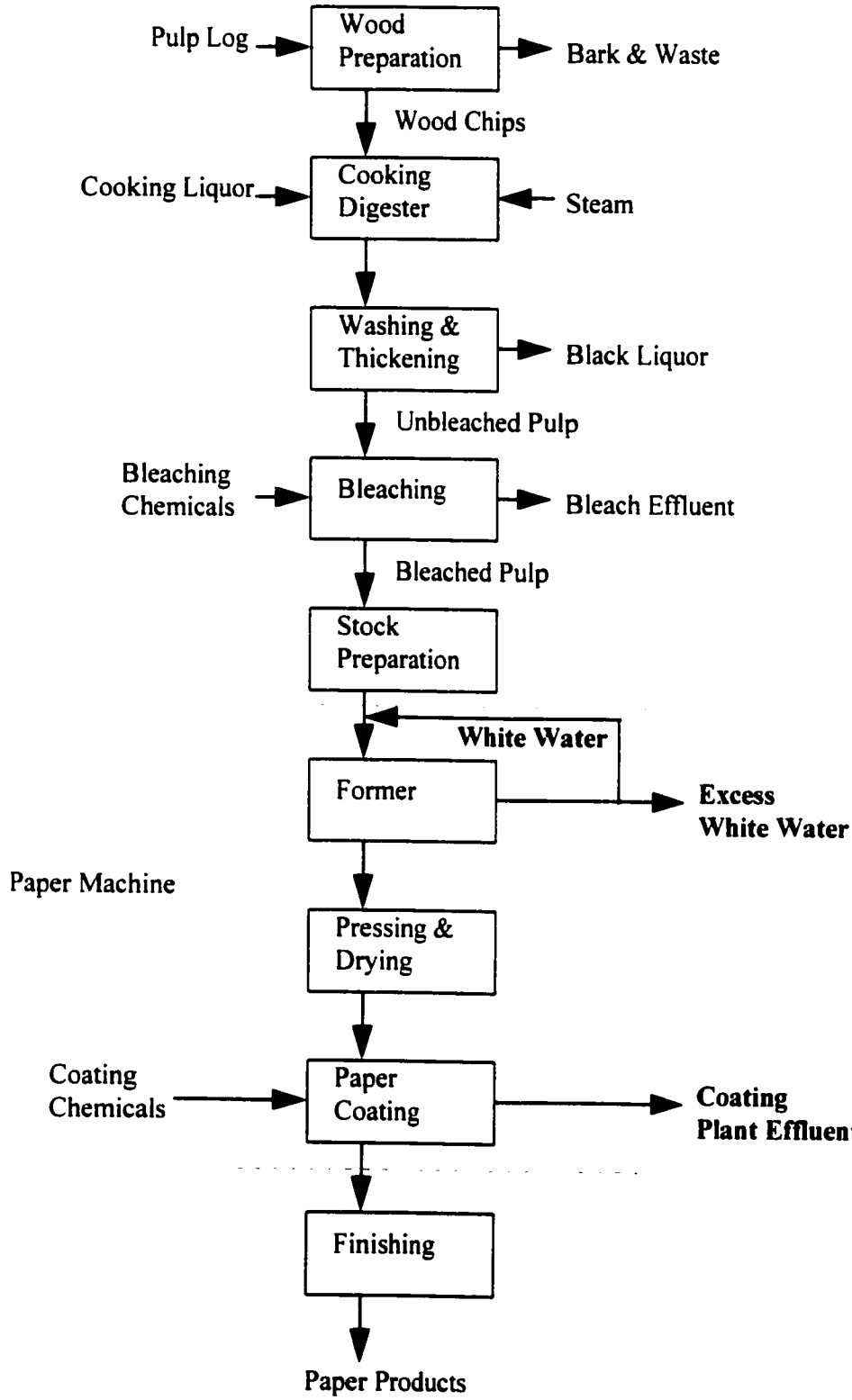

Figure 1.1. Generalized flow diagram of a bleached Kraft pulp and paper making process

In the stock preparation, pulp undergoes various treatments such as refining, blending, cleaning and chemicals addition to impart desired properties to the pulp in order to make the required quality of paper. A very dilute pulp suspension (< 0.5 wt.%) is supplied to the paper machine fabric former. Dewatering takes place through the fabric, resulting in a paper web formation over the fabric. Water coming out from the pulp through the fabric is called white water. Most of the white water is reused for the pulp dilution before pulp is supplied to the paper machine. Further dewatering from the paper web is achieved by mechanical pressing and thermal drying. Paper is often coated with pigments and binders to enhance the paper quality (gloss, smoothness, printing quality etc.).

1.6. Chemical composition of white water and coating emulsion

Paper machine white water contains various proportions of fines (smaller cellulosic fibers), fillers, wet strength resins, biocides, dyes, starch, alum, rosin and other wet-end additives. The total amount of solids in white water depends on the quality of paper produced, types of equipment used and their performance efficiencies (Panchapakesan, 1991).

A paper coating emulsion is a complex mixture of different chemical components. Coating emulsions consist of three main groups of components: pigments, binders and additives. The pigments make up the largest part of the total solids of the emulsion, 80-95%. Common pigment components are different types of clay (kaolin, calcium carbonate), titanium dioxide and plastic pigments. The binders constitute 5-20% of the solid content. Latex, starch and soy protein are commonly used binders. The additives make up only 1-2% of the color. The additives are a complex mixture of the compounds such as dispersants, viscosity modifiers, lubricants, crosslinkers or insolubilizers, biocides and dyes (Jonsson et al. 1996a).

1.7. Organization of the thesis

The contents of this thesis are divided into four parts. Part I contains four chapters; i.e. 'Introduction', 'Literature Review', 'Theoretical' and 'Methodology and Experimental'. Part II deals with results and discussion and has seven chapters from Chapter 5 to Chapter 11. Chapters 5, 6 and 7 have been reproduced with little or no change from the papers published/submitted in journals. Conclusions pertinent to the individual chapters in part II are provided at the end of the each chapter. Part III has only one chapter (#12) where all the conclusions are summarized along with the recommendations. All the appendices are compiled in Part IV.

CHAPTER 2

Literature Review

2.1. Membrane applications in the pulp and paper industry

Paleologou et al. (1994) discussed membrane applications in the pulp and paper industry with respect to technical feasibility, process integration and the economics of the mill system. Since MacLeod (1974) and Bansal (1977) presented ultrafiltration and reverse osmosis as efficient methods of treating process water from the pulp and paper industry, technology of the field has steadily progressed. The following are some applications of membrane separation processes in the pulp and paper industry.

2.1.1. Bleach plant effluent

The two most contaminated bleach plant effluents are the acidic filtrate from the chlorination stage (C-stage) or from the chlorine dioxide stage (D-stage) washer and the first alkaline extraction filtrate from the extraction stage (E-stage) washer, as most of the chlorinated substances and colored materials originate from these two stages.

Most of the published works on membrane applications in the pulp and paper industry have focused on E-stage effluent treatment. E-stage effluent is very well suited for treatment by the ultrafiltration process because it has a comparatively small volume and contains relatively high-molecular-weight-substances. There are several ultrafiltration plants of commercial

scale, for example, the Sanyo Kokusaku Pulp Mill and Taio Paper Co., Japan (Jonsson, 1987). In a typical plant, E-stage effluent contributes 140-150 kg of color and 5-6 kg of BOD_7 (Biochemical Oxygen Demand) per ton of pulp. Ultrafiltration of this effluent can reduce TOCl (Total Organic Chloride) by 60-70% (Jonsson, 1987), COD (Chemical Oxygen Demand) by 50-80%, AOX (Absorbable Organic Halogen) by 90% (Jonsson, 1989), color by 90% and BOD_7 by 25-50% (Lundahl and Mansson, 1980). The overall effect of the ultrafiltration of E-stage effluent on the total mill effluent is 65-70% reduction in color, 40% reduction in COD and 10% reduction in BOD_7. Pinho et al. (1996) and Geraldes and Pinho (1996) reported that if nanofiltration and electrodialysis were used in combination to treat E-stage effluent, the final resulting permeate would be good enough to be reused in the bleaching plant.

C-stage effluent contains mostly low-molecular-weight-substances. Most of the substances in the C-stage effluent are too small to be retained, even by a very dense ultrafiltration membrane. The low-molecular weight organics make it difficult to treat C-stage effluent by ultrafiltration. The large amount of effluent is a factor that makes the membrane treatment of C-stage even more difficult (Jonsson and Petersson, 1989). Considering the results of both laboratory and pilot plant scale experimentation, at present it seems impractical to apply ultrafiltration to treat chlorination stage effluent on a commercial scale. Jonsson and Petersson (1988) conducted experiments by mixing C-stage and E-stage effluents in their actual proportions; however, the results were not very encouraging. Yao et al. (1994) tested a series of laboratory made and also commercial membranes for the treatment of E-stage effluent mixed with a small amount (4%) of C-stage effluent. Using three membranes (molecular weight cut-off (MWCO) of 130,000, 15,000 and 5,000 Daltons, MWCO is defined as a molecular weight of a solute at which 90% separation can be achieved) in series they achieved high reduction in TOC (78%), COD (80%), and AOX (88%).

2.1.2. Paper machine white-water

Among the new and promising applications of membranes are treatments of paper machine white water, coating plant effluent and spent liquor from chemi-mechanical pulping (Jonsson and Wimmerstedt, 1985). A closed white water system would not only reduce the consumption of chemicals, but also lower the amount of water discharged, and hence lower the effluent treatment costs.

Ultrafiltration is an effective method of white water treatment as it is capable of removing colloidal and dissolved matter present in white water while allowing salts to pass through. Membrane performance depends on the composition of the feed water components and can vary from mill to mill as white water differs in its constituents because of the different raw materials and the types of processes used (Sierka et al., 1994). The suspended solids in white water are primarily made up of fibers, clays, fillers, sizing agents and dyes. For white water treatment, the first full scale membrane based plant was put into operation in 1972 at Green Bay Packaging Inc., Wis., USA (Nelson et al., 1973; McLeod, 1974). This installation formed an integrated part of the closed white water system of the mill for a couple of years before it was discontinued due to mill expansion and consequent changes in the white water requirements.

The permeate fluxes obtained by Nuortila-Jokinen et al. (1995a) in a laboratory scale white water treatment by a CR (Cross-Rotational) Ultrafilter were adequate (over 200 L/m^2h) for industrial application. In a pilot plant trial with 3 ultra-fine inorganic membranes, the solid rejection achieved was over 99% with a permeate flux of 90 L/m^2h (Bansal, 1977). With ultrafiltration tubular membranes, 90% of water was recovered as permeate with an average flux of about 150 L/m^2h (Jonsson and Wimmerstedt, 1985). Tardif and Hull (1997) and

Elefsiniotis et al. (1997) used different combinations of ultrafiltration and biological treatment to treat simulated white water of a closed-system mechanical newsprint mill. The effect of high temperature on the performance of ultrafiltration and/or biological treatment was also evaluated. They found that the performance of the membrane bioreactor was very stable under varied experimental conditions and was capable of removing virtually 100% of resin and fatty acid, 72 to 84% of dissolved chemical oxygen demand and 18 to 37% of total dissolved solids. Elefsiniotis et al. (1997) also observed flux decline during the treatment of white water with two negatively charged polyethersulfone ultrafiltration membranes with MWCO of 10,000 and 100, 000 Daltons, respectively.

Since 1994, paper machine white water at the Metsa-Serla Kirkniemi mill in Finland has been treated by a cross-rotational (CR) filter using an ultrafiltration membrane (Manttari et al., 1997). Also in Finland, a pilot test with a CR filter and a spiral-wound nanofiltration module was carried out in Varkaus (Enso Gutzeit Oy, now Enso Oy). Different commercial ultrafiltration, nanofiltration and reverse osmosis membranes were tested to treat effluent, which consisted of water from a thermomechanical pulp plant and a paper machine (Manttari et al., 1997). In the ultrafiltration experiments it was found that the resulting permeates were practically free from lignin residuals, anionic trash and turbidity. The reduction in the total carbon, COD and inorganic matter was between 50 and 60%. Even better reductions were achieved from the experiments with nanofiltration membranes. The permeabilities of nanofiltration membranes were between 3 to 13 $L/m^2h.bar$. The permeabilities with RO membranes were below 2.5 $L/m^2h.bar$.

2.1.3. Coating plant effluent

Effluents from a coating plant can upset the operation of the effluent treatment plant. Therefore, the treatment of coating plant effluent would not only recover the coating

chemicals but would also help in improving the operation of a combined effluent treatment plant. Paper coatings are composed of pigments, binders and flow modifiers. Typically a mill wastes 3 to 5% of the daily coating chemicals (Tardy et al., 1992). For a large mill producing 1000 tons/day of light weight coated paper, the lost material would be nearly 12 tons/day (Tardy et al., 1992). Ultrafiltration of coating plant effluent has three advantages. First, no coating effluent is released. Second, the concentrated effluent can be recycled. Third, the permeate can be used as a wash water.

Pichon et al. (1992) demonstrated that ultrafiltration was technically and economically feasible for coating plant effluent treatment. Coating chemicals recovered from ultrafiltration retained their original properties as no chemical had been added and also no chemical had been removed except water. No changes in coated paper properties were observed while coated with the coating colors having 20% recovered chemicals from ultrafiltration of coating waste (Tardy et al., 1992). Coating effluent was successfully concentrated from 10 to 60% by ultrafiltration (Woerner and Short, 1991). Stridsberg et al. (1992) achieved a high flux of 200 L/m^2h at a working pressure of 20 to 28 psig (138 to 193 kPa) while concentrating coating plant effluent form 0.5 to 46% in a CR-filter system. Jonsson et al. (1996 a&b) used a plate and frame module with the rotor (CR) between the membranes in order to reduce fouling. Membranes of different MWCO and of different materials were tested to evaluate the effect of different coating emulsion compositions.

2.1.4. Other potential uses

Other potential uses of membranes in the pulp and paper industry are as follows.

- Water removal by reverse osmosis (RO) from black liquor (spent cooking liquor from chemical pulping) prior to evaporation, in order to reduce steam cost or to expand evaporation capacity (Pepper and Tingle, 1983)

- Recovery and purification of valuable by-products by fractionation with ultrafiltration (Anon., 1982)
- Zero effluent mechanical pulp mills using ultrafiltration and reverse osmosis technology (Jantumen et al., 1992; Paleologou et al., 1994)
- Incremental Kraft recovery capacity and caustic soda production through the electrolysis of a fraction of black liquor (Cloutier et al., 1993)
- Production of bleaching chemicals using bipolar membrane electrolysis (Joshi and Basu, 1973; Paleologou et al., 1992)

From the literature review on membrane applications for white water and coating plant effluent and the fouling problem associated with these applications, the following can be summarized:

- There is not a great deal of literature available on membrane applications for these waste water treatments, as these applications are relatively new.
- In almost all the reported research work, commercially available membranes were used and tested for these applications. Membrane performance under different operational variables was reported. In most cases, the flux was not large enough to be economically feasible for a full scale plant. There were no adequate explanations on the membrane performance. Few attempts were made to correlate membrane performance to the membrane morphology, probably because of the grossly inadequate knowledge of the membrane morphology used in these studies.
- Almost all the studies reported flux decline due to fouling during the application. However, there were hardly any efforts to understand the mechanism of fouling. Only a few attempts were made to reduce the fouling. Efforts were, rather, focused on membrane cleaning after use. In some cases mechanical devices were used to reduce the fouling by high shear force. An understanding of the interactions between feed solute(s) and the

membrane is very important to predict the membrane performance. Therefore, to establish a correlation between membrane performance and membrane, it is essential to know the physico-chemical nature of the membrane.

- Knowing that membrane characterization and studies on fouling are important, the following sections of the literature review are devoted to them.

2.2. Membrane morphology

The flux and rejection characteristics of the asymmetric ultrafiltration membranes are determined by the morphology of the skin layer. The flux mainly depends on the pore density while selectivity depends on the pore size. The porous sublayer acts mainly as a mechanical support. In order to predict the selectivity of a membrane with a significant confidence, it is necessary to know not only the mean pore size but also the pore size distribution. Molecular weight cut-off (MWCO) and the mean pore size alone are not sufficient to predict the membrane selectivity. There are several well established techniques for the determination of pore size and pore size distribution. They include the bubble point technique, mercury porosimetry, the microscopic technique, solute transport, permporometry and thermoporometry. Most of the above mentioned techniques are explained in detail in a recent review article (Nakao, 1994). It was noted that, apart from the mean pore size and the pore size distribution, roughness of the skin layer seems to have a positive effect on permeate flux (Hirose et al., 1996).

2.2.1. Membrane characterization by solute transport technique

There have been a number of studies in which the relationship between the solute separation and the size of the solute has been examined in an attempt to obtain information about the pore size distribution of the membrane. Michaels (1980) found that the sieving coefficient versus solute size plot fits to a log-normal probability distribution curve for a variety of

ultrafiltration membranes, including both biological and synthetic membranes. Kassotis et al. (1985) used dextrans to measure the rejection coefficient of polyacrylonitrile membranes in order to find the pore size distribution. Aimar et al. (1990) measured the rejection coefficients of membranes with dextrans and the data were fitted to a log-normal pore size distribution. Leypoldt (1987) presented the mathematical limitation in determining the pore size distribution from the solute separation. Studies (Zeman and Wales, 1981; Aimar et al., 1990) suggested that the solute separation was dependent on the ratio of solute molecular size to the pore size, as initially suggested by Paine and Scherr (1975). However, in several other studies (Cooper and Van Derveer, 1979; Michaels, 1980; Ishiguro et al., 1996), the dependence of solute separation on the solute size, that results from the steric and the hydrodynamic interactions between the solute and pore, was not considered.

2.2.2. Membrane characterization by microscopic techniques

Since the invention of the atomic force microscope (AFM), this instrument has been applied extensively for studying microfiltration and ultrafiltration membranes (Dietz et al., 1991, 1992a&b; Fritzsche et al., 1992a&b, 1993; Chahboun et al., 1992; Bottino et al., 1994; Bessières et al., 1996; Bowen et al., 1996a&b). Recently, the AFM has also been used for characterizing nanofiltration (Bowen et al., 1997) and gas separation (Khulbe et al., 1996a&b) membranes. AFM can image non-conducting samples both in air and in liquid. AFM has also eliminated the tedious process of sample preparation as is required by a scanning electron microscope (SEM) and by a transmission electron microscope (TEM). Heavy metal coating required in SEM and TEM might give some artifacts. High beam energy as required in SEM for high resolution tends to damage polymeric membranes.

With various microscopic tools available, one can determine many characteristic parameters of membrane such as surface morphology, pore sizes and their distribution, pore density,

surface porosity, cross-sectional structure and so on. Fritzsche et al. (1992a, 1993) and Chahboun et al. (1992) made a comparative study of different microscopic tools while studying ultrafiltration membranes. Average pore diameters obtained from SEM were smaller than those obtained by AFM (Fritzsche et al., 1992a). This diminuation of the pore sizes was a result of sample preparation, including heavy metal coating, for the SEM image. AFM was used to study the characteristics of the various membranes of different MWCO and also of different materials. It was found that the mean pore sizes ranged from 12.6 to 26.2 nm while pore densities were between 88 to 482 pores/μm^2 (Dietz et al., 1992a). However, it should be noted that AFM images are distorted by convolution between pore shape and cantilever tip shape and therefore the quantitative determination of pore size from an AFM image is not always straightforward. Kim et al. (1990) used a high resolution FESEM (field emission scanning electron microscope) for studying various ultrafiltration membranes. Surface characterization was performed by image analysis on an electron micrograph. The surface porosity was found to be between 4 to 15% depending upon the membrane. Pore density was between 100 to 1000 pores/μm^2.

2.3. Membrane fouling and flux decline

One of the most important reasons for the failure of the use of membrane processes on a much larger scale, is the flux decline during operation. The causes for flux decline are first, concentration polarization, i.e. accumulation of retained particles at the membrane feed solution boundary; and second, fouling phenomena such as adsorption, pore blocking and deposition of solutes on the membrane surface. The result of both these phenomena is a decreasing driving force for the filtration or an increasing resistance against transport of the permeate. A dynamic membrane is formed over an original membrane by the cake layer formation. In white water and coating plant effluent applications, a cake layer formation takes place on the surface of the membrane (Woerner and Short, 1991).

In a review article, Fane and Fell (1987) discussed the causes of fouling and its control by the adjustment of operating conditions and pretreatment of the feed solution and the membrane. Crozes et al. (1997) also examined the impact of several operating parameters including permeate flux, feed velocity, transmembrane pressure and backwash frequency on fouling. Muralidhara (1991) presented techno-economic implications of membrane fouling and pointed out that membrane replacement cost was the most significant parameter that affected the economics of membrane processing.

2.3.1. Effect of the feed particle size on fouling

Among various parameters, the particle size of the feed solution has a large effect on fouling. Particles with an effective size that is larger than the pores of a membrane are rejected at the surface of the membrane and therefore should not reduce the permeability of the membrane. However, material deposited or adsorbed on the surface of the membrane may create an additional layer of resistance to the permeate flow and the particle size will affect the hydraulic resistance of this layer (Lahoussine-Turcaud et al., 1990).

The particle size plays a role in determining the net deposition of particles on the membrane surface and several mechanisms have been proposed by which particles may be transported away from the surface of the membranes. The diffusion of the particles away from the membrane is predicted to increase with decreasing particle diameter as per the Stokes-Einstein equation for the particle diffusion coefficient. In contrast with Brownian diffusion, the particle flux away from the membrane by lateral migration is predicted to increase with increasing particle diameter since the lift force is proportional to the particle diameter cubed (Green and Belfort, 1980). Several models for back transport have been presented that consider shear-induced transport or scouring of particles deposited on the membrane (Fane,

1984; Leonard and Vassilief, 1984; Cohen and Probstein, 1986; Zydney and Colton, 1986; Davis and Leighton, 1987; Romero and Davis, 1988 & 1991). Although the details of these models may differ, they are all fundamentally based on the concept that the shear force of fluid moving across the membrane initiates particle migration and at a critical point, overcomes the convective force of fluid moving through the membrane.

Brownian diffusion favors the transport of smaller particles (below 0.01 μm) while shear transport increases with the increasing size (above 10 μm). Hence, the membranes are most susceptible to fouling by particles 0.01 to 10 μm in size since the influence of both diffusive forces are small. Fane (1984) verified this observation with the experimental data from a stirred batch filtration of suspended particles varying in size from 0.025 to 20 μm. A minimum permeate flux was found for the particle diameter near 0.1 μm. Lahoussine-Turcaud et al. (1990) also reported that maximum fouling was observed for the particle size of 0.2 μm, while particles greater than 3 μm in size had a little effect on fouling in a cross-flow hollow fiber module. According to them, these particles (0.2 μm) are too large to be transported by Brownian diffusion and are too small to be pulled from the surface by shear forces. They are also too large to penetrate into the pore of an ultrafiltration membrane. When feed solution contains particles of different sizes, permeate flux is usually governed by selective deposition of smaller particles on the membrane surface (Baker et al., 1985). Dharmappa et al. (1992) presented a semi-empirical model to predict the effect of the particle size distribution on permeate flux.

Various experimental works on crossflow ultrafiltration of different colloidal suspensions have been reported (Porter, 1972a; Hunt et al., 1987; Hoogland et al., 1990; Nakao et al., 1990). With a video recording, Mackley and Sherman (1992) measured *in situ* the rate of the

deposition of polyethylene particles (125 to 180 μm) on the membrane surface. They observed that the capture of particles at the surface was controlled by the relative magnitude of convective flow and cross flow velocity. When convective flow dominates, the packing of particles is non-selective and random. However, when cross-flow dominates, the particles are highly selective as to where they finally reside. Various models (Porter, 1972b; Green and Belfort, 1980; Hermia, 1982) have been developed to understand the mechanism of particle deposition on the membrane surface.

2.3.2. Cake layer thickness

Transmembrane pressure, cross-flow velocity, compressibility of the suspended particles, particle size and the concentration of the feed solution have significant effects on the formation of the cake layer (Riesmeier et al., 1987). In cross-flow filtration, depending upon the experimental conditions, cake layer thickness was found to be between 0.4 to 40 μm (Riesmeier et al., 1987) and between 24 to 150 μm (Shimizu et al., 1993) for bacterial cells. In a stirred ultrafiltration experiment with silica solution (particle size ~ 0.016 μm, spherical), the cake layer thickness was found to be about 5 μm for the feed concentration of 1% and 20 μm for the feed concentration of 10% (Chudacek and Fane, 1984). Khatib et al. (1997) found a cake layer thickness of about 7 μm in the ultrafiltration of a lake water.

2.3.3. Cake layer specific resistance

Specific resistance of a cake is a function of void fraction and specific surface area of the particles. Other variables which affect specific cake resistance are operating pressure, cake compressibility, cross-flow velocity and particle size distribution in the cake.

Baker et al. (1985) observed an increase in the specific cake resistance of the cake layer with time and concluded that it was due to an increase in the fine contents in the cake with time. For example, in a crossflow filtration of TiO_2 slurry, fine contents (particle size <1 μm) were found to be 44%, 70% and 90% in the feed solution, in the cake layer after 30 min of run and in the cake layer after 60 min of run, respectively. Once the cake had reached its equilibrium thickness, large particles deposited on the surface were re-entrained into the bulk solution as they had higher back transport diffusion, whereas smaller particles having a lower back transport diffusion were trapped in the deposit; hence their concentration in the deposited cake increased with time. This resulted in the decrease of the cake permeability or increase in specific cake resistance (Dharmappa et al., 1992).

With the increase in crossflow velocity, the specific cake resistance increased while the deposited mass decreased (Baker et al., 1985). The specific cake resistance was found to be higher for a higher feed concentration and pressure (Fane, 1984; Chudacek and Fane, 1984). Riesmeier et al. (1987) observed a sharp increase in the mass of the cake layer deposited on the membrane surface at the beginning of the experiment.

Cake layer resistance was much higher than the resistance of the membrane and that of the blocked pore at a given pressure and hence, was the controlling resistance for the permeate flux (Shimizu et al., 1993). During cross-flow filtration with various ceramic membranes, it was observed that cake layer resistance did not change much with pore size (Imasaka et al., 1989), however, resistance due to pore plugging was increased with an increase in pore size (Matsumoto et al., 1988; Imasaka et al., 1989; Shimizu et al., 1990).

2.3.4. Various mechanical ways to reduce fouling

The complete elimination of the foulants layer is not practically possible. However, it may be reduced by applying an electrical field (Wakeman and Tarleton, 1987; Brunner and Okoro, 1989; Silva et al., 1991; Ramamurthy et al., 1995). The application of a suitable polarized electric field primarily reduces cake formation by electrophoretic motion of the particles away from the membrane. The application of the electric field is advantageous in the laminar flow regime in which the removal of the foulant solids from the membrane to the bulk of the solution primarily occurs by diffusion. In turbulent regimes, the benefits could be limited because of the already high eddy diffusion (Ramamurthy et al., 1995).

Recently, a CR (cross-rotational) rotor was used while treating coating plant effluent and white water by a number of researchers (Stridsberg et al., 1992; Nuortila-Jokinen et al., 1995 a&b; Jonsson et al., 1996 a&b; Nuortila-Jokinen and Nystrom, 1996). In the cross-rotational membrane filter, the rotor between the two membranes generates a powerful shear force which scours the membrane and also reduces membrane fouling.

2.4. Membrane modification with coating a layer of sulfonated polyphenylene oxide

Sulfonated polyphenylene oxide (SPPO) membranes were tested for the reverse osmosis application as early as in 1970 (Plummer et al., 1970). The salts separation by SPPO membranes was lower than the cellulose acetate membranes, however, the permeate flux was much higher. Huang and Kim (1984) studied the effect of the porous substitute on the performance of the thin film composite membrane. The SPPO-polysulfone membranes were tested for the purification of Alberta tar sand waste-waters. Hamza et al. (1995) studied the effects of ion exchange capacity of SPPO and solvent used for the casting on the performance of SPPO composite membranes. They observed that the preparation of thin-film composite membranes with high

salt separation and high fluxes was possible by properly adjusting the ion exchange capacity and the solvent used for the preparation of polymer solution for surface coating.

2.5. Various models to predict permeate flux

In order to correlate the operating parameters and feed and membrane characteristics to the performance of ultrafiltration membranes (mainly permeate flux) several models such as the 'gel polarization model' (Michaels, 1968a&b; Porter, 1972b; Fane et al., 1981; Blatt et al., 1970), the 'osmotic pressure model' (Wijmans et al., 1984) and 'boundary layer resistance model' (Wijmans et al., 1985; Van den Berg and Smolders, 1989) have been proposed. Some authors (Chudacek and Fane, 1984; Suki et al. 1986; Shirato et al., 1991) also applied cake filtration theory in ultrafiltration. The above models predict fluxes quite accurately for low molecular weight solutions. However, these models have been found to underestimate the flux in ultrafiltration with solutions containing colloidal particles. This problem has been called the 'flux-paradox' for colloidal suspensions. Rautenbach and Schock (1988) presented a modified model and tested it with colloidal suspensions of clay and also of quartz of mean particle size in the range of 2 to 2.5 μm. The calculated fluxes were still lower than the actual fluxes by one order of magnitude. To explain the flux-paradox problem in ultrafiltration of colloidal suspensions, Green and Belfort (1980) proposed a theory based on lateral migration of the particles across streamlines.

CHAPTER 3

Theoretical

3.1. Membrane characterization based on the solute transport data

3.1.1. Mean pore size and pore size distribution

Solute separation, f, in percent is defined as

$$f = \left(1 - \frac{c_p}{c_f}\right) \times 100 \tag{3.1}$$

where c_p and c_f are the solute concentrations in the permeate and in the bulk of the feed solution, respectively. It is to be noted that the effect of concentration polarization on separation is not considered in Eq. (3.1). When the solute separation (%) of an ultrafiltration membrane is plotted versus the solute diameter on a log-normal probability paper, a straight line is yielded as reported by Michaels (1980). If solute separation correlates with solute diameter according to the log-normal probability function, then this relationship can be expressed as

$$f = \mathrm{erf}(z) = \frac{1}{\sqrt{2\pi}} \int_{-\infty}^{z} e^{-\frac{u^2}{2}} du \tag{3.2}$$

where

$$z = \frac{\ln d_s - \ln \mu_s}{\ln \sigma_g} \tag{3.3}$$

and d_s is the solute diameter, μ_s is the geometric mean diameter of solute at f = 50% and σ_g is the geometric standard deviation about the mean diameter. According to Eqs. (3.2) and (3.3), a straight line in the form of

$$F(f) = A_0 + A_1(\ln d_s) \tag{3.4}$$

will yield between f (solute separation in %) and d_s (solute diameter) on a log-normal probability paper. A_0 and A_1 are the intercept and the slope, respectively. From this log-normal plot, the mean solute size (μ_s) can be calculated as d_s corresponding to f = 50%. σ_g can be determined from the ratio of d_s at f = 84.13% and 50%. By ignoring the dependence of solute separation on the steric and hydrodynamic interaction between solute and pore wall (Cooper and Van Derveer, 1979; Michaels, 1980; Ishiguro et al., 1996), the mean pore size (μ_p) and the geometric standard deviation (σ_p) of the membrane can be considered to be the same as the solute mean size and solute geometric standard deviation. From μ_p and σ_p, the pore size distribution of an ultrafiltration membrane can be expressed by the following probability density function (Youm and Kim, 1991)

$$\frac{df(d_p)}{dd_p} = \frac{1}{d_p \ln\sigma_p \sqrt{2\pi}} \exp\left[-\frac{(\ln d_p - \ln \mu_p)^2}{2(\ln\sigma_p)^2} \right] \tag{3.5}$$

where d_p is the pore size.

3.1.2. Pore density and the surface porosity

The number of pores per unit area, known as the pore density, can be calculated from the permeability data of the membrane using the Hagen-Poiseuille equation. Based on this equation, the solvent flux (J_i) through the pores of diameter d_i can be expressed as

$$J_i = \frac{N_i \pi d_i^4 \Delta p}{128 \eta \delta} \tag{3.6}$$

where N_i is the number of pores (per unit area) having diameter d_i, δ is the length of the pores, η is the solvent viscosity and Δp is the pressure difference across the pores. Total flux J through the membrane can be calculated by adding all the fluxes through the pores of different sizes as

$$J = \sum J_i$$

$$J = \frac{\pi \Delta p}{128 \eta \delta} \left\{ N_1 d_1^4 + N_2 d_2^4 + N_3 d_3^4 + - - - - - - - - \right\}$$

$$J = \frac{\pi \Delta p}{128 \eta \delta} \left\{ f_1 N d_1^4 + f_2 N d_2^4 + f_3 N d_3^4 + - - - - - - - - \right.$$

$$J = \frac{\pi \Delta p N}{128 \eta \delta} \sum_{d_{min}}^{d_{max}} f_i d_i^4 \qquad (3.7)$$

where N is the total number of pores and f_i is the fraction of the number of pores with diameter d_i. From Eq. (3.7), the total number of pores (N) per unit area can be calculated as

$$N = \frac{128 \eta \delta J}{\pi \Delta p \sum_{d_{min}}^{d_{max}} f_i d_i^4} \qquad (3.8)$$

Pore length δ is considered equivalent to the skin layer thickness of the asymmetric ultrafiltration membrane.

Similarly, the expression for surface porosity (S_p), which is defined as the ratio between the area of pores to the total membrane surface area, can be derived as

$$S_p = \left(\frac{N \pi}{4} \sum_{d_{min}}^{d_{max}} f_i d_i^2 \right) \times 100 \qquad (3.9)$$

3.1.3. Stokes radius of polyethylene glycol and polyethylene oxide molecules

The Stokes radius of a macromolecule can be obtained from its diffusivity in solution by using the following Stokes-Einstein equation

$$D = \frac{kT}{6\pi\eta a} \tag{3.10}$$

where D is the diffusivity, k is Boltzmann's constant, η is the solvent viscosity and a is the Stokes radius. The diffusivity can also be calculated by the following equation (Hsieh et al., 1979a)

$$D = \frac{2.5\times10^{6}\,kT}{\{\eta(M[\eta])^{1/3}\}} \tag{3.11}$$

where M and $[\eta]$ are the molecular weight and the intrinsic viscosity of the polymer, respectively. By combining Eqs. (3.10) and (3.11) we obtain

$$a = 2.122\times10^{-8}\left(M[\eta]\right)^{1/3} \tag{3.12}$$

where a is in cm, M is in g/mol and $[\eta]$ is in dL/g. The intrinsic viscosity of a polyethylene glycol (PEG) and a polyethylene oxide (PEO) of known molecular weight can be calculated from the following equations

For PEG (Meireles et al., 1995) $$[\eta] = 4.9\times10^{-4}M^{0.672} \tag{3.13}$$

For PEO (Nabi, 1968) $$[\eta] = 1.192\times10^{-4}M^{0.76} \tag{3.14}$$

Intrinsic viscosities of PEGs of various molecular weights calculated from the empirical Eq. (3.13) are in very good agreement with the values determined experimentally by Hsieh et al. (1979a&b). Intrinsic viscosity values for some of the PEG molecules are also given by Bessières et al. (1996), and they are also in very good agreement with the values calculated from the empirical Eq. (3.13). By substituting the expression for $[\eta]$ in Eq. (3.12), we obtain

For PEG $$a = 16.73 \times 10^{-10} M^{0.557} \quad (3.15)$$

For PEO $$a = 10.44 \times 10^{-10} M^{0.587} \quad (3.16)$$

From Eqs. (3.15) and (3.16), Stokes radii of PEG and PEO molecules can be obtained (in cm) from their molecular weights (in g/mol).

3.2. Membrane characterization by atomic force microscopy

3.2.1. Mean pore size and pore size distribution

Pore sizes were measured by visual inspection of line profiles of different pores from various AFM images of different areas of the same membrane. Pore sizes measured by AFM were arranged in ascending order and were assigned median ranks. Median ranks are calculated from the following formula (Lipson and Sheth, 1973)

$$\text{Median or 50\% rank} = \frac{j - 0.3}{n + 0.4} \times 100 \quad (3.17)$$

where, j = order number of the pore when arranged in ascending order

n = total number of pores measured

To obtain a cumulative distribution function graph, these median ranks are plotted on the ordinate against pore sizes arranged in an increasing order on the abscissa. This plot will yield a straight line on a log-normal probability paper if pore sizes have a log-normal distribution. From this graph, values of mean pore size (μ_p) and geometric standard deviation (σ_p) can be calculated as explained in the earlier section.

3.2.2. Surface roughness

Differences in the membrane surface morphology can be expressed in term of various roughness parameters such as the mean roughness (R_a), the root mean square of Z data (R_q),

and the mean difference in the height between the five highest peaks and the five lowest valleys (R_z). All these parameters can be measured by an AFM.

The mean roughness is the mean value of surface relative to the center plane, the plane for which the volume enclosed by the image above and below this plane are equal, and is calculated as

$$R_a = \frac{1}{L_x L_y} \int_0^{L_x} \int_0^{L_y} |f(x,y)| dxdy \tag{3.18}$$

where f(x, y) is the surface relative to the center plane and L_x and L_y are the dimensions of the surface.

The root mean square of Z values (R_q) is the standard deviation of the Z values within the given area and is calculated as

$$R_q = \sqrt{\frac{\Sigma\left(Z_i - Z_{avg}\right)^2}{N_p}} \tag{3.19}$$

where Z_i is the current Z value, Z_{avg} is the average of the Z values within the given area, and N_p is the number of points within a given area.

The average difference in height (R_z) between the five highest peaks and five lowest valleys is calculated relative to the mean plane, which is a plane about which the image data has a minimum variance.

3.3. Fouling

3.3.1. Calculation of the resistances to the permeate flow

Fouling is caused by the plugging of membrane pores by solute species or by their adsorption on the surface of the membrane or by a cake layer formation over the membrane. In white water and coating plant effluent applications, a cake layer formation takes place on the surface of the membrane. The fouling restricts the permeate flow through the membrane.

3.3.1.1. Resistance model

The resistance model has been used extensively in various membrane separation techniques since it was proposed by Henis and Tripodi (1980 & 1981) for gas separation. According to the model developed by Henis and Tripodi, the resistances from each component barrier layer to the permeate flow could be combined mathematically. Therefore, various resistances could be connected in series or in parallel or in combination depending upon their positions relative to the flow of permeate.

According to the resistance model, a membrane can be considered as a combination of different segments each having a specific resistance to the permeating fluid. These resistances are analogous to the resistance of the flow of electricity in an electric circuit. An asymmetric membrane may be divided into a very thin and dense skin layer and a highly porous sublayer. The skin layer can be further divided in two regions: membrane matrix and pores. In Figure 3.1, R_m and R_p are the resistances due to membrane matrix and membrane pores respectively. Resistance due to the porous sublayer is very small and, therefore, is neglected.

It is evident from Figure 3.1 that resistance due to the membrane matrix (R_m) and that due to the membrane's unplugged (R_p) or plugged (R'_p) pores are in parallel. However, several

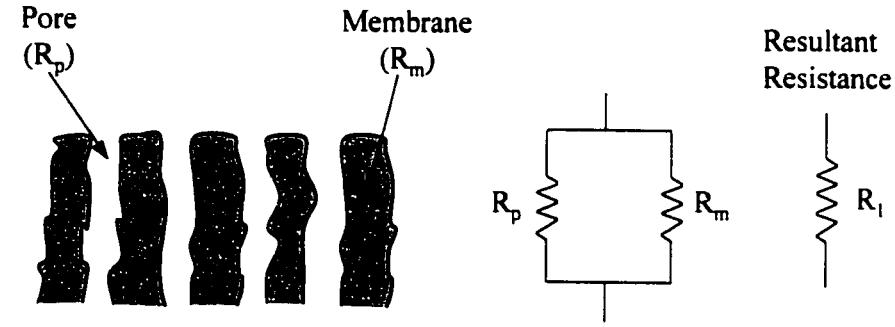

(a) Virgin membrane

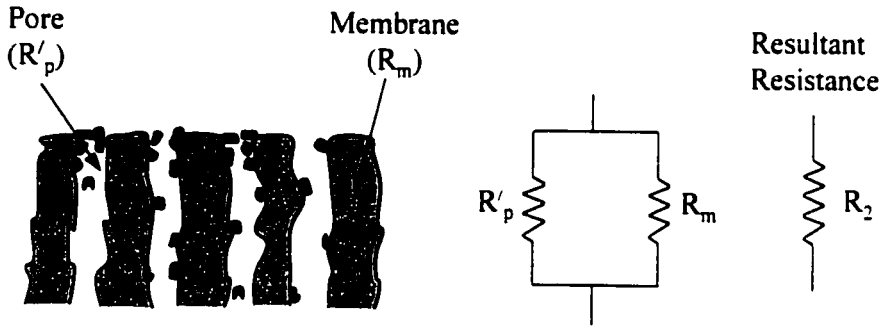

(b) Fouled membrane

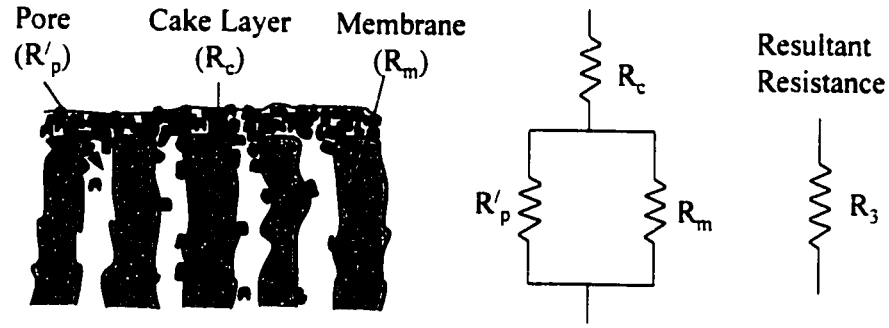

(c) membrane with cake layer

Figure 3.1. Representation of various resistances in (a) virgin membrane, (b) fouled membrane and (c) membrane with a cake layer

authors (Matsumoto et al., 1988; Imasaka et al., 1989; Shimizu et al., 1990 & 1993; Jonsson, 1993; Ramamurthy et al., 1995; Dal-Cin et al., 1996) have considered these resistances in series, which is incorrect.

For the virgin membrane (Figure 3.1a), the resultant resistance R_1 can be written as

$$R_1 = \frac{R_m R_p}{R_m + R_p} \tag{3.20}$$

Similarly for the fouled membrane (Figure 3.1b), the resultant resistance R_2 can be written as

$$R_2 = \frac{R_m R_p'}{R_m + R_p'} \tag{3.21}$$

In Eqs. (3.20) and (3.21), it is considered that the membrane resistance (R_m) does not change during the experiment. After 24 hours of ultrafiltration experiment with clay, or clay and SBR solution, the total resistance R_3 (Figure 3.1c) can be given as

$$R_3 = \frac{R_m R_p'}{R_m + R_p'} + R_c \tag{3.22}$$

where R_c is the resistance due to cake layer. Knowing R_1, R_2 and R_3 experimentally, it was attempted to obtain the component resistances R_m, R_p, R_p' and R_c. However Eqs. (3.20) to (3.22) could not be solved simultaneously for the above four unknowns. Therefore, the following procedure was adopted to find the relative value of these unknown parameters.

The values of R_1, R_2 and R_3 can be calculated from the experimental data. Solvent permeation flux in a pressure driven membrane can be expressed in terms of total resistance as

$$J_s = \frac{\Delta p}{\eta R} \tag{3.23}$$

where

J_S = solvent (water) permeation flux ($m^3/m^2.s$),

Δp = operating pressure, (Pa, i.e. $kg/m.s^2$),

η = solvent (water) viscosity (kg/m.s), and

R = total resistance to the permeate flow (m^{-1})

Eq. (3.23) can be rewritten as

$$R = \frac{\Delta p}{\eta J_s} \tag{3.24}$$

The values of R_1, R_2 and R_3 can be calculated as

$$R_1 = \frac{\Delta p}{\eta J_w} \tag{3.25}$$

$$R_2 = \frac{\Delta p}{\eta J_{wf}} \tag{3.26}$$

$$R_3 = \frac{\Delta p}{\eta J_{p_{24}}} \tag{3.27}$$

where J_w and J_{wf} are the pure water permeation flux of the virgin and the fouled membrane while $J_{p_{24}}$ is the product flux after 24 hours of ultrafiltration experiment with clay or clay and SBR solution.

Eqs. (3.20) and (3.21) can be rewritten in terms of R_m as

$$R_m = \frac{R_p R_1}{R_p - R_1} \tag{3.28}$$

$$R_m = \frac{R'_p R_2}{R'_p - R_2} \tag{3.29}$$

Equating Eqs. (3.28) and (3.29)

$$\frac{R_p' R_2}{R_p' - R_2} = \frac{R_p R_1}{R_p - R_1} \tag{3.30}$$

On simplifying, Eq. (3.30) yields

$$\frac{1}{R_p'} = \frac{1}{R_p} - \frac{1}{\frac{R_1 R_2}{R_2 - R_1}} \tag{3.31}$$

Since R_2 is more than R_1 (total resistance of fouled membrane is more than the total resistance of virgin membrane), then the following conclusions can be drawn form Eq. (3.31)

$$R_p' > R_p \tag{3.32}$$

and $$R_p < \frac{R_1 R_2}{R_2 - R_1} \qquad \text{(for positive } R_p'\text{)} \tag{3.33}$$

The following are also true from Eqs. (3.20) and (3.21),

$$R_p > R_1 \tag{3.34}$$

$$R_m > R_2 \tag{3.35}$$

and $$R_p' > R_2 \tag{3.36}$$

Eq. (3.20) can be rewritten as

$$R_m = R_1\left(\frac{R_m}{R_p} + 1\right) \tag{3.37}$$

From Eqs. (3.35) and (3.37)

$$R_1\left(\frac{R_m}{R_p} + 1\right) > R_2$$

or $$\frac{R_m}{R_p} > \left(\frac{R_2}{R_1} - 1\right) \tag{3.38}$$

Therefore, the following conditions should be fulfilled while solving Eqs. (3.20) to (3.22).

1. $$R_1 < R_p < \frac{R_1 R_2}{R_2 - R_1} \tag{3.39}$$

2. $$R_m > R_2 \tag{3.35}$$

3. $$R'_p > R_2 \tag{3.36}$$

4. $$\frac{R_m}{R_p} > \left(\frac{R_2}{R_1} - 1\right) \tag{3.38}$$

Eq. (3.39) indicates the range of the value of R_p. Therefore, Eqs. (3.20) to (3.22) will be solved for three unknowns, i.e., R_m, R'_p and R_c, assuming a value of R_p within the range given by Eq. (3.39). Furthermore, R_c can be calculated as

$$R_c = R_3 - R_2 \tag{3.40}$$

3.3.2 Concentration polarization and gel layer concentration

For ultrafiltration, the macromolecular solutes and colloidal species are usually present and contribute little to osmotic pressure. However, the concentration of solute at the membrane surface (c_m) is much higher than that in the bulk feed (c_f) due to concentration polarization. Flux reduction phenomenon due to concentration polarization has been discussed by many researchers (Brain, 1965; Michaels, 1968a&b; Kozinski and Lightfoot, 1972). A boundary layer model for crossflow filtration is shown in Figure 3.2, where δ_{bl} is the boundary layer thickness over which the concentration changes from c_f to c_m. Solute is transported to the membrane surface by the convective flow of permeant and this is balanced by diffusion back to the bulk (Belfort and Nagata, 1985);

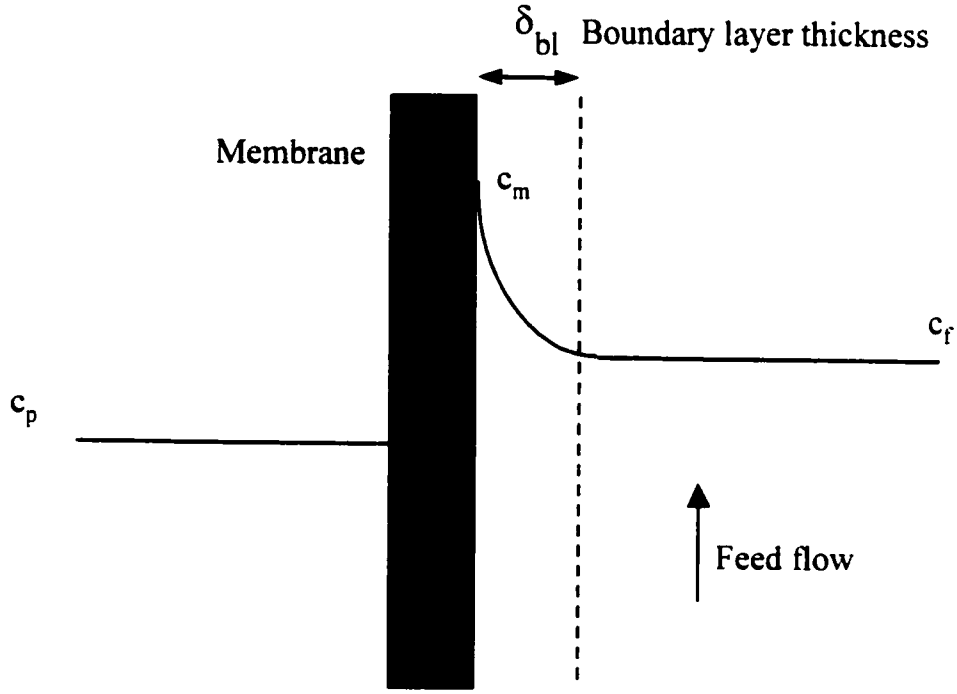

Figure 3.2. Boundary layer formation in ultrafiltration

$$J_s(c - c_p) = D\frac{dc}{dx} \tag{3.41}$$

where J_s is the permeate flux, c_p is the solute concentration in the permeate and D is the diffusivity. Integrating Eq. (3.41) and inserting the following boundary conditions:

at $x = 0, \quad c = c_f$

and at $x = \delta_{bl}, \quad c = c_m$

we obtain

$$J_s = \frac{D}{\delta_{bl}} \ln \frac{c_m - c_p}{c_f - c_p} \tag{3.42}$$

or

$$J_s = k \ln \frac{c_m - c_p}{c_f - c_p} \tag{3.43}$$

where k is the mass transfer coefficient and is equal to D/δ_{bl}. As the flux increases with increasing applied pressure, the value of c_m will increase. As c_m reaches the solubility limit, further increase will cause a precipitate or thixotropic gel to be deposited on the membrane surface. A further increase in the pressure will not increase the flux. For nearly 100% separation (i.e. c_p is very small) the limiting flux J_∞ can be approximated as (Porter, 1972b)

$$J_\infty = k \ln\left(\frac{c_g}{c_f}\right) \tag{3.44}$$

where c_g is the gel concentration which is mainly a function of the solute-solvent system and the operating temperature and is independent of the membrane characteristic, feed concentration, flow conditions and operating pressure. Since the gel concentration is assumed to be constant, Eq. (3.44) predicts a linear plot for J_s versus $\ln c_f$ with a slope equal to -k (mass transfer coefficient) and extrapolation of $J_s = 0$ will yield the value of c_g.

Chapter 4

Methodology and Experimental

4.1. Materials and membrane making

Polyethersulfone (PES, Victrex 4100P) supplied by Imperial Chemical Industries was used for the preparation of ultrafiltration (UF) membranes. Polyethersulfone has been used extensively for making ultrafiltration membranes because of its superior mechanical and thermal stability (T_g-225^{0}C). Asymmetric membranes were made by the phase inversion technique using casting solutions of different concentrations (10, 12, 15 and 20 wt.%) of PES in N-methylpyrrolidone (NMP) solvent. Polyvinylpyrrolidone (PVP), a nonsolvent additive, was added to increase the membrane flux and to enable membrane casting with lower PES concentrations. The ratio of PES and PVP in the casting solutions was kept at 1:1 by weight (Lafrenière et al., 1987). Membranes were cast by pouring the casting solution onto a glass plate at room temperature and spreading it with a casting rod at a uniform speed. The wet thickness (gap between the glass plate and the casting rod) of all the membranes was maintained at 0.33 mm. Immediately after casting, the glass plate was immersed into a gelation bath with ice cold water at about 4^{0}C and kept there for 40 minutes (Lafrenière et al., 1987). Membranes were stored in distilled water in 'never dried state' until used. These laboratory made ultrafiltration membranes were designated as 10U, 12U, 15U and 20U. The first two digits in the above nomenclature indicate the PES concentration in the casting solution while the 'U' indicates that the membranes were unmodified. Some of the

membranes made above (never dried state) were further immersed in a glycerol solution of 30 wt.% for 24 hours prior to air drying at room temperature for a couple of days. These membranes were designated as 10UD, 12UD, 15UD and 20UD. The first two digits and 'U' were explained above, while 'D' means that the membranes were dried after glycerol treatment.

4.1.1. Membrane modification

In order to reduce the fouling, the membranes were coated with a thin layer of the sulfonated polyphenylene oxide (SPPO) polymer. Negatively charged SPPO layer will reduce the clay, a major constituent in the feed solution, deposition on the membrane surface by rejecting the negatively charged clay particles.

4.1.1.1. Preparation of sulfonated poly(2,6-dimethyl-1,4-phenylene oxide) polymer

Following the method outlined by Plummer et al. (1970), a 10 wt.% solution of poly(2,6-dimethyl-1,4-phenylene oxide) (PPO, General Electric Co.) was prepared by dissolving PPO (intrinsic viscosity - 0.46 dL/g) in chloroform. To obtain the ion exchange capacity (IEC) of 2.0 meq/g of dry powder (Hamza et al., 1995), a stoichiometric amount of chlorosulfonic acid (Appendix A) was added dropwise to the PPO solution. The solution was then vigorously stirred and allowed to react for about 30 minutes. An inert environment was maintained in the reaction vessel by a nitrogen blanket. The sulfonation reaction is illustrated in Figure 4.1. As the reaction progressed, sulfonated poly(2,6-dimethyl-1,4-phenylene oxide) (SPPO), insoluble in chloroform, precipitated from the solution. The precipitate (SPPO) thus prepared was then dissolved in methanol, poured in a glass dish, and allowed to dry overnight. The resulting dry SPPO film was cut into small pieces and washed thoroughly with distilled water until the pH of the wash water became higher than 4.0. The washing process of SPPO pieces

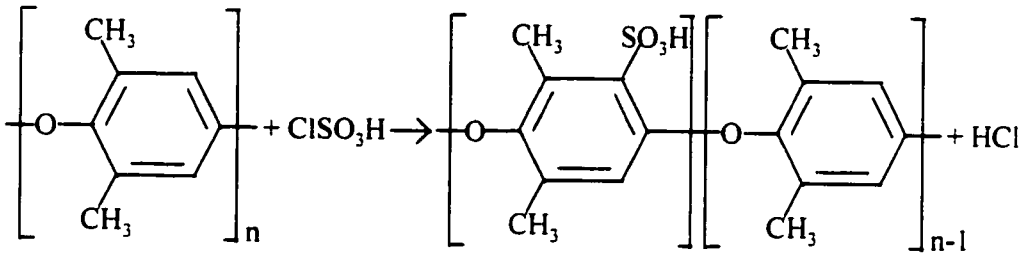

Figure 4.1. Sulfonation reaction of polyphenylene oxide (PPO) with chlorosulfonic acid

took several days. The SPPO was then vacuum dried at room temperature for two days. The polymer so prepared was in hydrogen form (SPPOH). The exact IEC value of the SPPO polymer was determined using acid-base titration (Appendix A).

4.1.1.2. Preparation of modified membranes

The SPPO polymer thus prepared was dissolved in methanol (Hamza et al., 1995) to make 1 wt.% solution. One and a half mL of this SPPO solution was poured and spread over the skin side of the unmodified dried membrane (UD) of 5.6 cm in diameter. The excess solution was drained by holding the membrane vertically, leaving a thin layer of SPPO solution over the membrane surface. The SPPO coated membranes were then dried overnight prior to use. These membranes were designated as 10S, 12S, 15S and 20S, where 'S' stands for sulfonated modified (SPPO coated) membranes.

4.2. Preparation of feed solution for testing membrane performance

White water from the paper machine and effluent from the coating plant vary considerably from mill to mill and also from time to time in the same mill. Therefore, simulated feed solutions were prepared in the laboratory to ensure a constant feed condition. As coating plant effluent mainly consists of pigments (e. g. clay, $CaCO_3$, TiO_2 etc.) and binders (e. g. latex, starch etc.), feed solutions for ultrafiltration experiments were prepared by mixing clay (Ultra Cote, Engelhard, particle size ~ 80-82% < 2 μm) and Styrene Butadiene Rubber (SBR, a latex, CP620NA, Dow Chemicals, particle size ~ 175 nm, 50% w/w emulsion). The ratio of clay to SBR was kept at 100/15 by weight (Skowronski and Lepoutre, 1986), a typical ratio of the pigments and the binders in a coating emulsion. Feed solution containing clay and SBR is also a fairly good representation of white water, as fillers and some kind of strength additives are the main components in it. Different feed concentrations were used to study the permeate flux and solute separation for the membranes made in the laboratory. Experiments

were also conducted when only clay or SBR was present in the feed solution. In some experiments, NaCl (200 ppm) was added to the feed solution containing clay, or clay and SBR.

4.3. Ultrafiltration experiment

4.3.1. Ultrafiltration system and operating parameters

Ultrafiltration experiments were conducted by using laboratory cross-flow test cells each with an effective area of 13.2 cm^2, details of which were described elsewhere (Sourirajan and Matsuura, 1985). A sketch of the permeation cell is given in Figure 4.2. Six cells were connected in series as shown in the schematic layout of the ultrafiltration system (Figure 4.3). Feed solution from the feed tank was pumped by a constant discharge pump to the inlet of the first permeation cell. An accumulator was installed in the pump delivery line to reduce pulsation in the pressure. Since the pump was a constant discharge type, a bypass line was provided to vary feed flow in the system whenever required. As permeation cells were connected in series, the retentate of the first cell became the feed to the second cell and so on. As permeate flow was very small compared to feed flow, the characteristics of the feed solution to all the cells were virtually the same. A pressure regulator was installed at the outlet of the last cell to regulate the pressure in the system. For recording inlet and outlet pressures across all six permeation cells, two pressure gauges were installed as shown in Figure 4.3.

All the experiments were conducted at room temperature. All the operating pressure data (except pressure difference), which are mentioned in this thesis, are the gauge pressure. The inlet pressure at the first cell was maintained at 365 kPa (53 psi) while the pressure at the outlet of the last cell was around 324 kPa (47 psi) with a total pressure drop of 41 kPa across

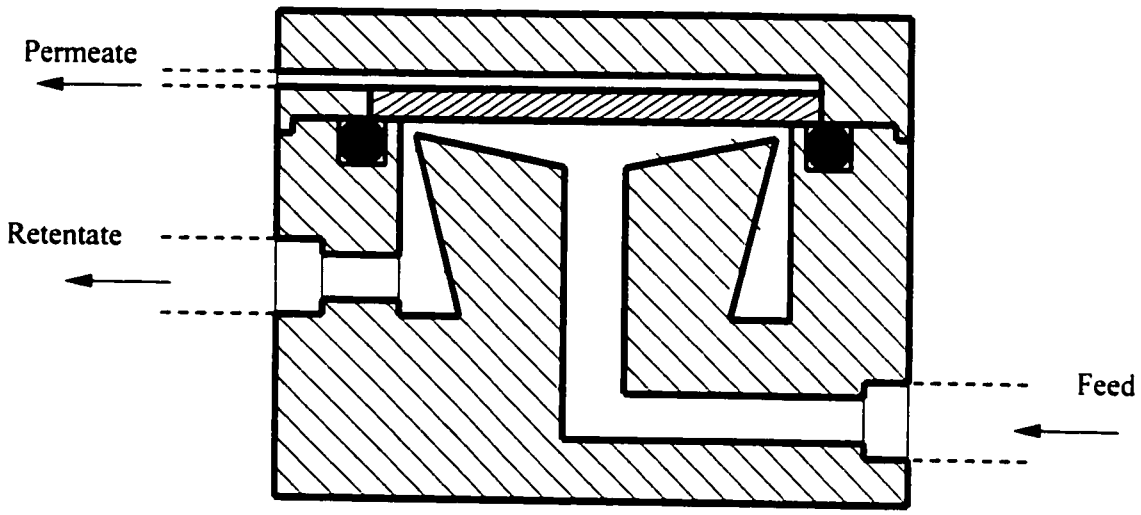

Figure 4.2. Cross-sectional sketch of laboratory cross-flow permeation cell for a flat ultrafiltration membrane

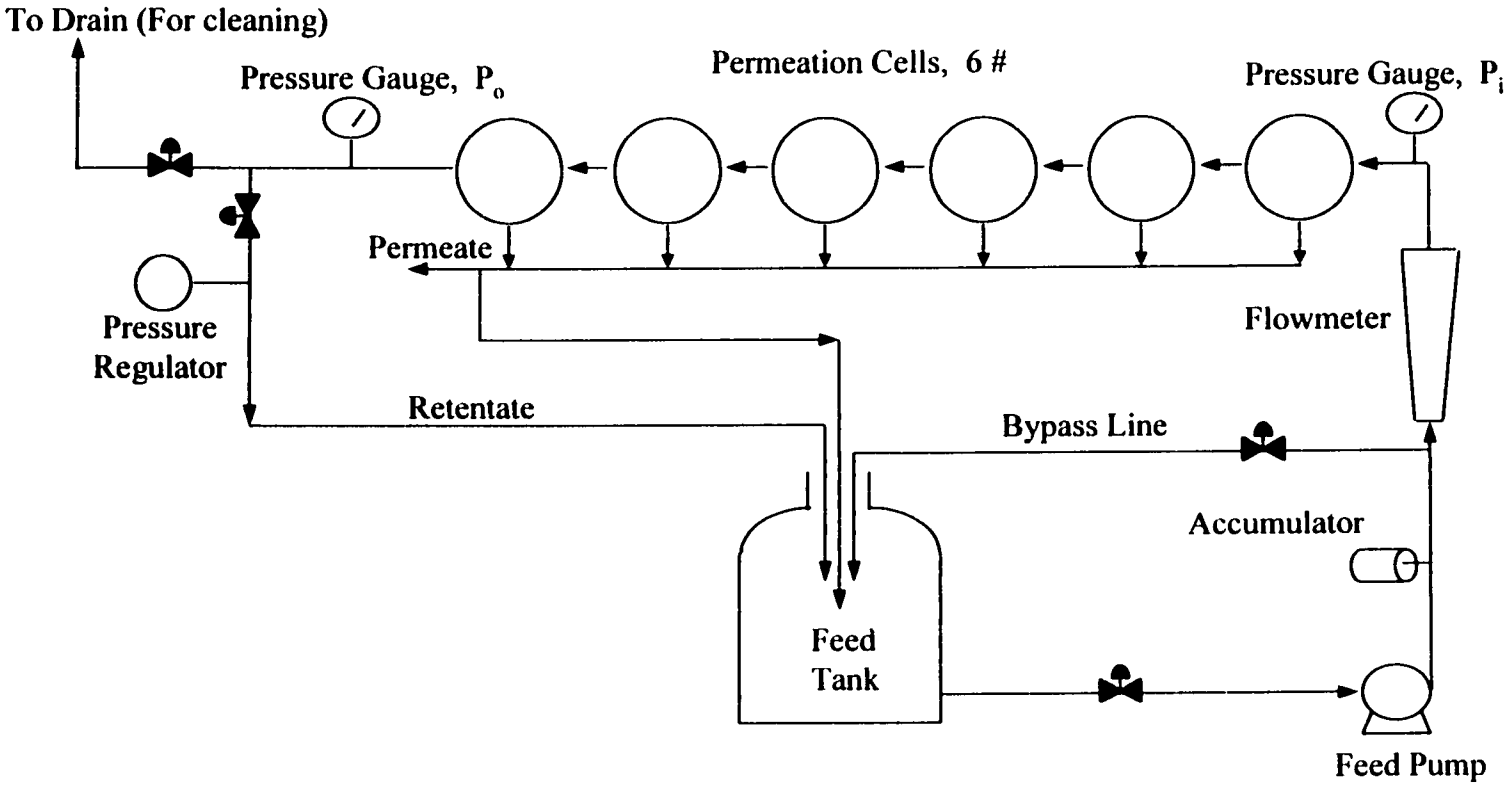

Figure 4.3. Schematic layout of the ultrafiltration system

the six cells. Equal pressure drop of about 7 kPa (~1 psi) was considered across each cell. Fluxes were corrected to 345 kPa (50 psi) for each cell assuming a linear relationship (confirmed in a separate experiment, Appendix B) between pressure and flux in the pressure range from 300 to 400 kPa. Each membrane was compacted at 552 kPa (80 psi) for 5 hours, unless otherwise mentioned, prior to any measurement. The feed solution was circulated through the feed chamber of the permeation cell at a flow rate of 2650 mL/min. For each experiment, both the pure water permeation flux (PWP) and the permeate flux (PF) in the presence of solute were measured in L/m^2h (or m^3/m^2s),. The permeate flux was also measured at various intervals during the experiment. Both PWP and PF were converted to the values at 25^0C by using the density and viscosity data of water (Appendix C).

4.3.2. Ultrafiltration experiment with clay or clay and SBR

Ultrafiltration experiments were conducted with various constant feed concentrations and also with increasing feed concentrations. In the experiment with constant feed concentration, both permeate and retentate were recycled to the feed reservoir. In the varying feed concentration experiment, the feed concentration was gradually increased by collecting the permeate in a separate vessel.

Total solids (clay + SBR) in the feed and permeate samples were determined by weighing the solid residue after heating the sample at 105^0C for 8 hours. Ash content (i.e., clay content) was measured after burning the sample at 925^0C for 8 hours (CPPA Standard, G.11, 1996). SBR content in the feed and in the permeate were measured in terms of total organic carbon (TOC) by using a carbon analyzer (DC-190, Folio Instruments).

The NaCl concentration, when NaCl was present in the feed solution, was measured in terms of conductivity. For the value of the conductivity due to NaCl in the clay solution, the value

of conductivity in the clay solution before adding NaCl was subtracted from the value of the conductivity of the solution after adding NaCl.

4.4. Membrane characterization by solute transport

For membrane characterization, polyethylene glycol (PEG, molecular weight up to 35,000) and polyethylene oxide (PEO, molecular weight of 100,000 and 200,000) were used as solutes in the feed solution. The feed solute concentration was kept at 200 ppm by weight while PEG or PEO was used. Membrane characterization by solute transport is discussed in detail in Chapter 3.

4.4.1. Virgin membrane characterization

In the ultrafiltration experiments for PEG/PEO separation, the molecular weight of either PEG or PEO was increased progressively. The ultrafiltration system was thoroughly flushed with distilled water between experiments with different molecular weight solutes of PEG/PEO. The PEG/PEO contents in the feed and permeate were measured in terms of the total organic carbon (TOC) by using a carbon analyzer (DC-190, Folio Instruments).

4.4.2. Fouled membrane characterization

After an ultrafiltration experiment with the feed solution of either clay, or clay and SBR, membranes were flushed with tap water of 45^{0}C for half an hour and then with distilled water for another half an hour at 70 kPa and at a feed flow rate of 4000 mL/min. These membranes are referred to as 'fouled membranes' hereafter. These membranes were characterized in the same way as fresh membranes were characterized.

4.5. Separation

Separations, f (in percent) for clay, SBR, NaCl, PEG and PEO were calculated by the following equation

$$f = \left(1 - \frac{c_p}{c_f}\right) \times 100 \qquad (4.1)$$

where c_p and c_f are the concentrations in the permeate and in the bulk of the feed solution, respectively.

4.6. Microscopic techniques

4.6.1. Atomic force microscope (AFM)

AFM images were obtained by using a Nano Scope III atomic force microscope (Digital Instruments Inc., Santa Barbara, USA) and operating in tapping mode (TM). In tapping mode, a fast oscillating probe is employed for surface imaging and a short and intermittent contact prevents the development of inelastic surface deformation. The vertical separation between the probe tip and the surface is rapidly oscillated such that the probe taps the surface slightly. The discontinuous contact eliminates any lateral forces exerted on the surface by the scanning tip.

A schematic diagram of an AFM utilizing an optical lever technique for sensing cantilever deflection is shown in Figure 4.4. An extremely sharp tip, attached to a cantilever arm, is vibrated and brought near the sample surface. The cantilever oscillation is modified by interactions between the tip and the surface of the sample. Changes in the cantilever oscillation are detected by a split diode photo-detector, which monitors a laser beam reflected off the cantilever. The signal from the photo-detector is sent to a control system which maps the sample surface by adjusting the piezo height to maintain constant vibrational amplitude of the cantilever.

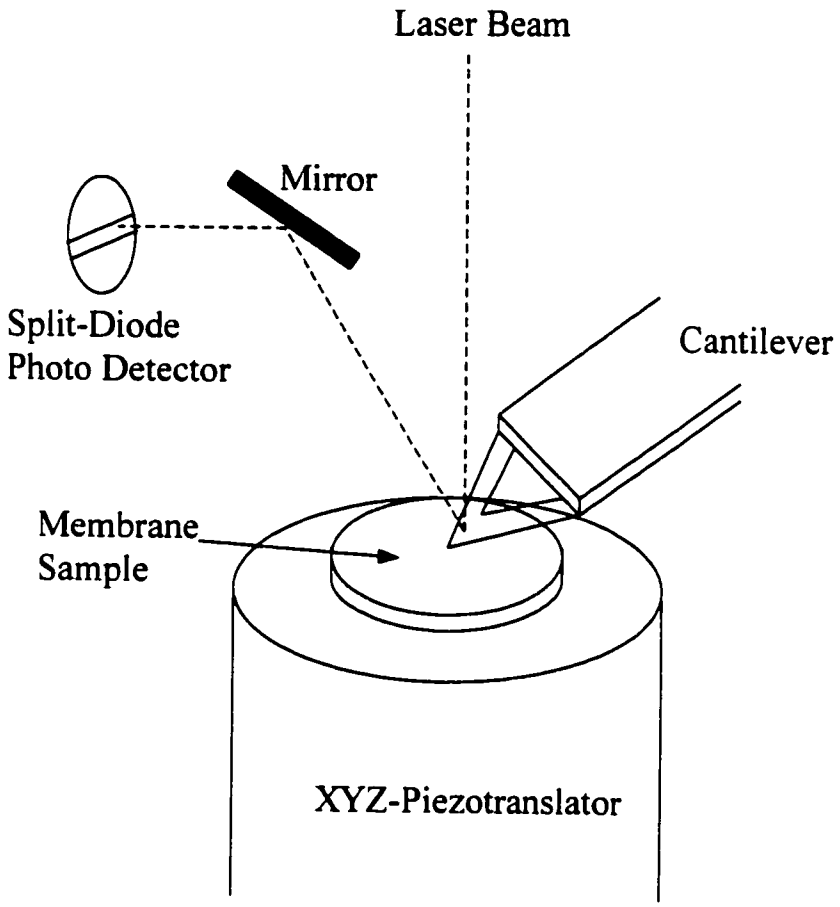

Figure 4.4. Schematic diagram of atomic force microscope for surface imaging

No special sample preparation for AFM imaging was necessary except to attach a small piece (0.5 cm × 0.5 cm) of the membranes to a steel disc sample holder with double-sided tape. The sample thus prepared was ready to use for AFM imaging. AFM images of both unused membranes and membranes with cake layer on them were taken.

4.6.1.1. Pore size measurement from AFM images

The sizes of pores on an AFM image were estimated from a cross-sectional profile of the data along the reference line. An example of the measurement of the pore sizes is shown in Figure 4.5. Because of various shapes (circular, elliptical, slits etc.) of the pores, the sizes were calculated by taking average of the width and length of the pore. The window in the bottom right corner in Figure 4.5 shows the horizontal and vertical distances between cursors. The horizontal distance between the pair of cursors was taken as pore length/width.

4.6.1.2. Roughness parameter measurement from AFM images

Various surface roughness parameters such as mean roughness (R_a), the root mean square of Z data (R_q), and the mean difference in the height between the five highest peaks and the five lowest valleys (R_z) were measured by using an image analysis software supplied with the AFM equipment (Digital Instruments, 1993). Detailed description of these roughness parameters is presented in Chapter 3. Since roughness parameters depend upon the type of probe used and the treatments given to the captured surface data, all the AFM imaging was done with the same type of probe and also the same treatments were given.

4.6.2. Scanning electron microscope (SEM)

Scanning Electron Microscopes at Department of Chemistry, University of Ottawa and also at the Science Technology Center, Carleton University were employed to study the surface and cross-section of both virgin membranes and membranes with cake layer on them.

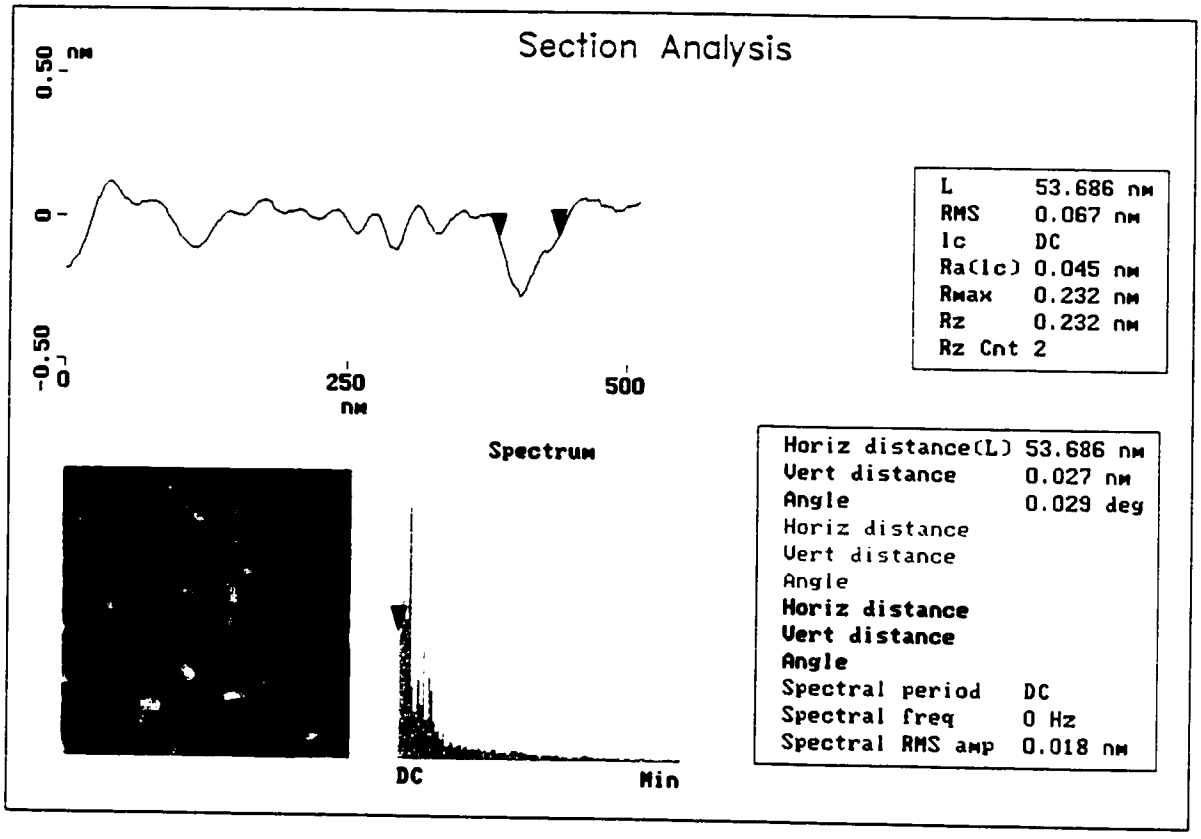

Figure 4.5. Illustration of pore size measurement by an atomic force microscope

4.7. Cake layer study

In the experiment for the study of the cake layer, twelve cells were connected in series as shown in Figure 4.6. These cells were divided into three groups and cell(s) from each group were used for the specific purpose as explained in the following section.

Group A-(Cell #1): Membranes were taken out after different operational times and freeze dried for the measurement of the thickness of the cake layer by SEM and for the study of the surface of the cake layer by SEM and AFM.

Group B-(Cell # 2 to 6): Clay deposited on the membrane surface in each cell was collected in separate beakers to measure the amount of clay deposited at different operational times.

Group C-(Cell # 7 to 12): Clay deposited on the membrane surface in each cell was collected in a common beaker for the particle size analysis.

In the above mentioned experiment, the following procedure was followed.

Ultrafiltration experiments were conducted for 8 different operational times ranging from 5 min to 24 hours (5 min, 15 min, 30 min, 1 hr, 3 hrs, 6 hrs, 21 hrs and 24 hrs) to find out the effect of operational time on the cake layer formation. Therefore, the same experiment was performed 8 times for different operational times. In the above ultrafiltration experiments, a 20UD membrane was used with a feed solution of 0.87% of clay. The following steps were performed in each of the ultrafiltration experiments.

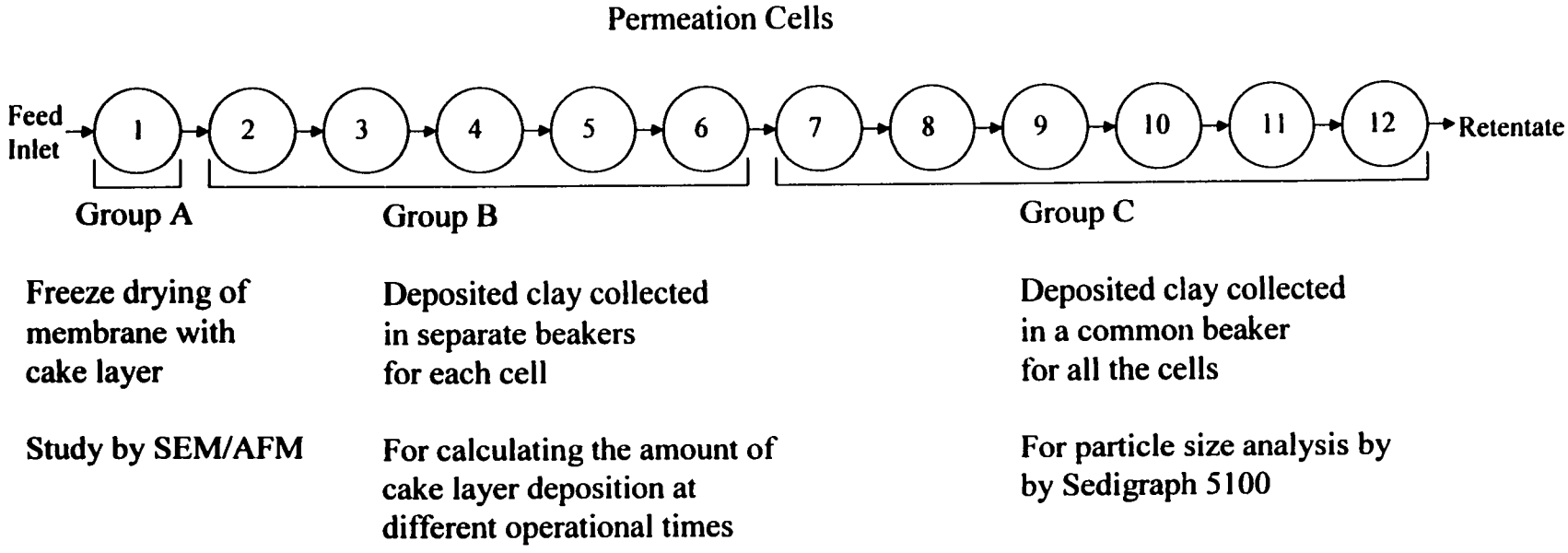

Figure 4.6. Permeation cells arrangement and their utilization in a cake layer study in ultrafiltration experiment with a feed solution of 0.87% of clay

4.7.1. Experiment I: Operational time – 5 min

1. After mounting a membrane coupon (20UD) in each cell, the ultrafiltration system was started and was allowed to run for 5 min.
2. The membrane from cell #1 (Group A) was taken out for freeze drying without washing. Procedure of freeze-drying is explained in section 4.7.3.
3. Membranes from cell #2 to 6 (Group B) were taken out and washed with distilled water to remove the clay deposited on the membrane surface for collection. Clay obtained from each membrane surfaces was collected in separate beakers. Care was taken to collect the clay only from the effective area of the membrane.
4. Membranes from cell # 7 to 12 (Group C) were taken out and washed with distilled water to remove the clay deposited on the membrane surface. The clay obtained from all the membranes surface was collected in a common beaker. The clay solution thus obtained was continuously stirred by a magnetic stirrer to inhibit agglomeration of clay particles.
5. New membrane coupons were mounted in the cells.

4.7.2. Experiment II: Operational time – 15 min

After mounting new membrane coupons in the cells, the system was started and the pump was turned off after 15 min of operation. Steps 2 to 5 as described in 'Experiment I' (Section 4.7.1.) were repeated. Clay deposited on the surface of membranes in cell #2 to 6 was again collected in separate beakers (not those were used in 'Experiment I'). However clay from membranes in cell # 7 to 12 was collected in the same beaker used in the 'Experiment I' for collecting clay from membranes from cell #7 to 12.

The same steps as described in 'Experiments I & II' (Section 4.7.1. & 4.7.2.) were repeated for the different operational times.

4.7.3. Freeze drying of membrane with cake layer

To preserve the structure of cake layer existing in the wet stage (while in the operation), the membranes were immersed in liquid nitrogen immediately after they were taken out from cell #1. The frozen membranes with cake layer were subsequently freeze-dried by sublimation at a very low temperature (-30^{0}C) and under vacuum (<1 mm of Hg). Freeze drying of membranes took several days.

4.7.4. Air drying of membrane with cake layer

The clay layer deposited on the membrane surface came off during freeze drying of the membranes. Also almost all the membranes cracked, probably due to severe thermal shock (liquid nitrogen temperature -196^{0}C). The cake layer which came off from the membrane surface was too fragile to be used for the study by SEM/AFM. Therefore, instead of freeze drying, membranes were dried at room temperature (~22^{0}C) after they were taken out from the cell.

4.7.5. Measurement of the mass of the clay collected from the membrane surface

The amount of clay collected in each beaker (total 40 beakers: 5 in each experiment for a total of 8 experiments) from the membranes in cell #2 to 6 for eight different operational times was determined by weighing the solid residue after heating the sample (in beaker) at 105^{0}C for 8 hours.

4.7.6. Particle size analysis of clay by Sedigraph 5100

Particle size analysis (PSA) of the clay deposited on the membrane surface as well as the clay used in the feed solution for ultrafiltration experiments was performed by Sedigraph 5100 (Micrometritics Instrument Corporation, Norcross, USA) available at the Department of Chemistry, University of Ottawa. The Sedigraph 5100 uses the principle of sedimentation

(details are given in Appendix D) in order to determine the diameter of particles in a suspension.

A magnetic stirrer continuously stirred the clay solution obtained in a beaker by washing the membranes that were taken from cell # 7 to 12 after ultrafiltration. Water from the clay solution was evaporated at about 40^0C to make the concentration sufficiently high for the particle size analysis by the Sedigraph 5100. It took several days to achieve the desired concentration of about 4%.

For the particle size analysis of clay in the feed solution of the ultrafiltration experiment, about 1.5 g of the clay was added to 40 mL of 0.05% sodium metaphosphate solution. The clay solution was sonified to disperse all the clay particles. One drop of Photoflow (Kodak) was added to prevent bubble formation.

The clay solution was poured into the sample mixing chamber of the Sedigraph. Bubble detection was set to low and pump speed was set to high. X-ray intensity was kept at normal. A 0.05% sodium metaphosphate solution was used as both the background liquid and as dispersant. The solvent parameters for pure water were employed for the software data treatment. A clay (kaolin) density of 2.66 g/cm^3 was used, as measured and reported by Tunney (1995). The particle size analysis was performed at temperatures ranging from 30 to 40^0C. The measurement was repeated three times for each sample.

PART II

Results and Discussion

Definitions

The definitions of the terms that are used in Part II are as follows.

Virgin (or fresh or unused) membrane:

Membrane **not** used for the ultrafiltration experiment with the feed solution containing clay and/or SBR.

Fouled membrane:

Membrane used for the ultrafiltration experiment with the feed solution containing clay and/or SBR and then **cleaned** with water.

Used membrane:

Membrane used for the ultrafiltration experiment with the feed solution containing clay and/or SBR and was **not** cleaned after use.

Cake layer:

Foulants layer deposited on the membrane surface during ultrafiltration experiment.

Final permeate flux:

Permeate flux after 24 hours of ultrafiltration experiment with the feed solution containing clay and/or SBR.

Final sodium chloride separation:

Sodium chloride separation after 24 hours of ultrafiltration experiment with the feed solution containing sodium chloride along with clay and/or SBR.

CHAPTER 5

Virgin Membrane Characterization

In this chapter, results on characterization of virgin membranes are presented while results on fouled membrane characterization are discussed in Chapter 10. Four series of virgin membranes (20 series, 15 series, 12 series and 10 series) were studied and each series had three membranes (U, UD and S). In total, therefore, 12 different membranes were studied. PEG/PEO separation data from which mean pore size and pore size distribution are determined are averages of three data points from three different coupons taken from the same sheet of the membrane.

5.1. Membrane characterization based on solute transport data

5.1.1. Mean pore size and pore size distribution

Pore sizes and their distribution of the membranes were calculated from the transport data with PEG and PEO solutes of various molecular weights. PEG and PEO did not significantly foul the membrane, as the permeate flux of the membrane when the solutes were present in the feed was very close to the pure water permeation flux. A straight line was obtained with a reasonably high correlation coefficient ($r^2 \geq 0.90$) while plotting the percent separation of the PEG/PEO solutes on the ordinate vs their diameters on the abscissa of a log-normal probability paper as depicted in Figure 5.1. The values of the geometric mean pore size (μ_p)

and the geometric standard deviation (σ_p) around the mean were determined from Figure 5.1, as described in Chapter 3 and these values are summarized in Table 5.1. Mean pore size was the smallest for the 20 series membranes while it was the largest for the 10 series membranes. There was not much difference between 'U' and 'UD' membranes in term of their μ_p and σ_p. It should be noted that the pure water permeation flux (PWP) (Figure 7.1, Chapter 7) and molecular weight cut-off (MWCO, molecular weight of the solute at which 90% separation can be achieved) (Table 5.1) of these membranes were also very similar. It is also interesting to note that the μ_p of the 20U membrane was the smallest among 'U' membranes; however, its σ_p was the largest. Similarly, μ_ps of 20UD and 20S membranes were smaller and their σ_ps were larger than other 'UD' and 'S' membranes. The geometric standard deviations of 15U, 12U and 10U membranes were very close to each other, although their mean pore sizes were different. The mean pore size for the 10U membrane (MWCO - 98,000 Daltons) was found to be 11.12 nm, which is comparable to the mean pore size of 15.4 nm of a sulfonated polysulfone membrane of the MWCO of 100,000 Daltons calculated by Bessières et al. (1996) from solute transport data. In general, the mean pore size was higher for the membrane having a higher MWCO (Table 5.1). 20U, 20UD and 12S membranes which showed a MWCO of about 20,000 Daltons had similar mean pore sizes of 3.24, 3.36 and 3.44 nm, respectively.

When a thin layer of SPPO was coated on the surface of 'UD' membranes, the pore sizes were reduced considerably. This effect is obvious when μ_ps for 20S, 15S and 12S membranes are compared to their corresponding 'UD' membranes from which the former membranes were made. For 10S membrane, the pore size reduction was modest, from 10.38 nm to 7.10 nm.

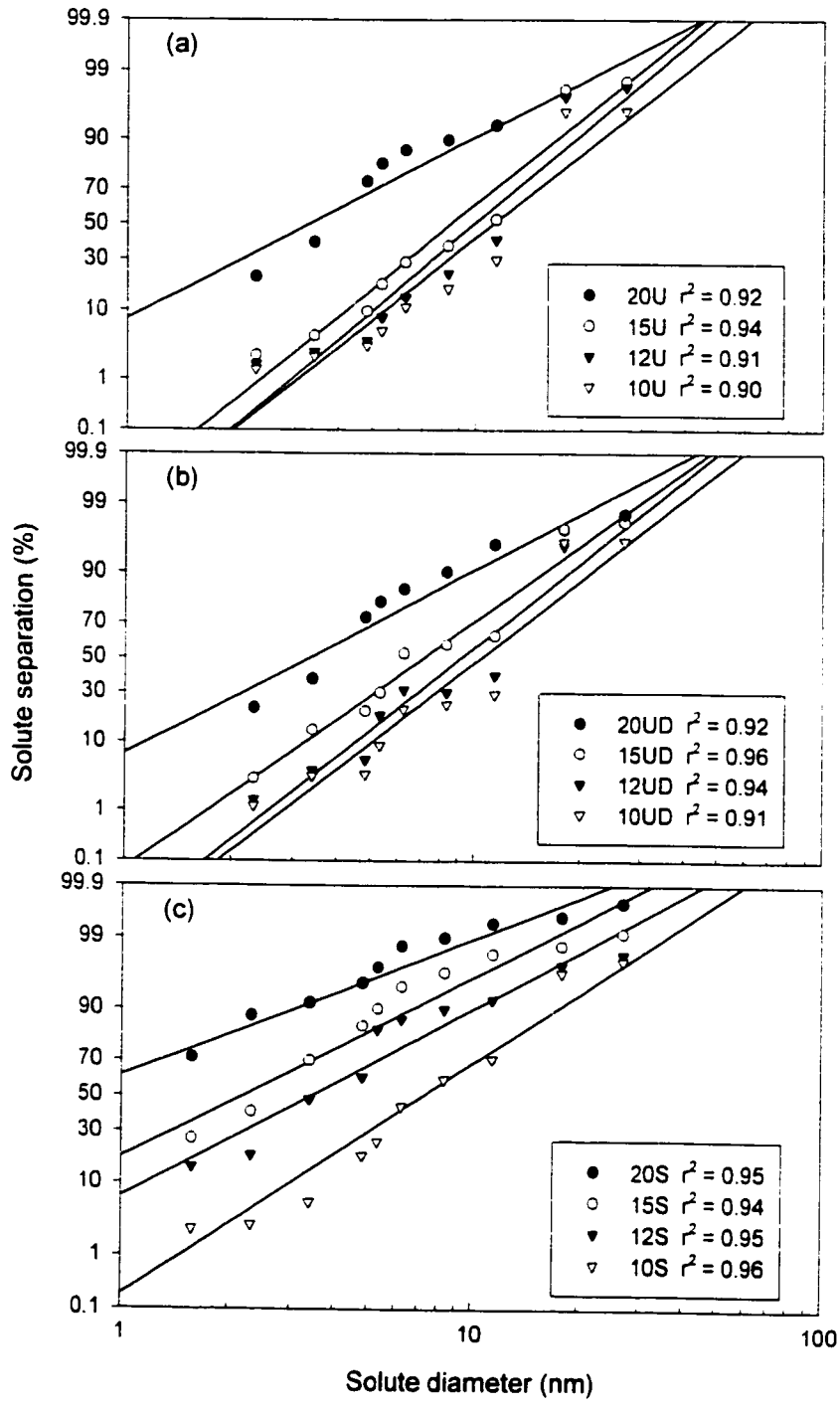

Figure 5.1. Solute separation curves (solute diameter versus their separation) plotted on a log-normal probability paper for (a) 'U' membranes, (b) 'UD' membranes and (c) 'S' membranes

Table 5.1. Geometric mean pore size (μ_p) and geometric standard deviation (σ_p) for various membranes calculated from solute separation data and from AFM images. MWCO values obtained form solute transport data are also shown.

Membrane	From Solute transport			From AFM images	
	MWCO kDa*	Mean pore size μ_p (nm)	Geometric Std. Dev. σ_p	Mean pore size μ_p (nm)	Geometric Std. Dev. σ_p
20U	21	3.24	2.37		
20UD	20	3.36	2.29		
20S	3.5	0.70	3.31		
15U	84	8.43	1.74		
15UD	75	7.18	1.84	25.4	1.57
15S	11	2.19	2.43		
12U	94	9.91	1.68		
12UD	91	9.14	1.74	32.4	1.46
12S	20	3.44	2.32		
10U	98	11.12	1.76		
10UD	94	10.38	1.78	37.6	1.43
10S	71	7.10	2.02	30.5	1.50

* kilodaltons

The cumulative pore size distributions for different membranes are shown in Figure 5.2. It is evident from this figure that there was no significant change in pore size distributions of 'U' and 'UD' membranes. On the other hand, pore size distribution curves were shifted to the left for all the SPPO coated membranes. For example, for 20U and 20UD membranes, only about 50% of the pores were less than 3.4 nm in diameter while for 20S membranes, as much as 90% of the pores were less than 3.4 nm in diameter. Probability density function curves were also generated from Eq. (3.5) by using the values of mean pore size and geometrical standard

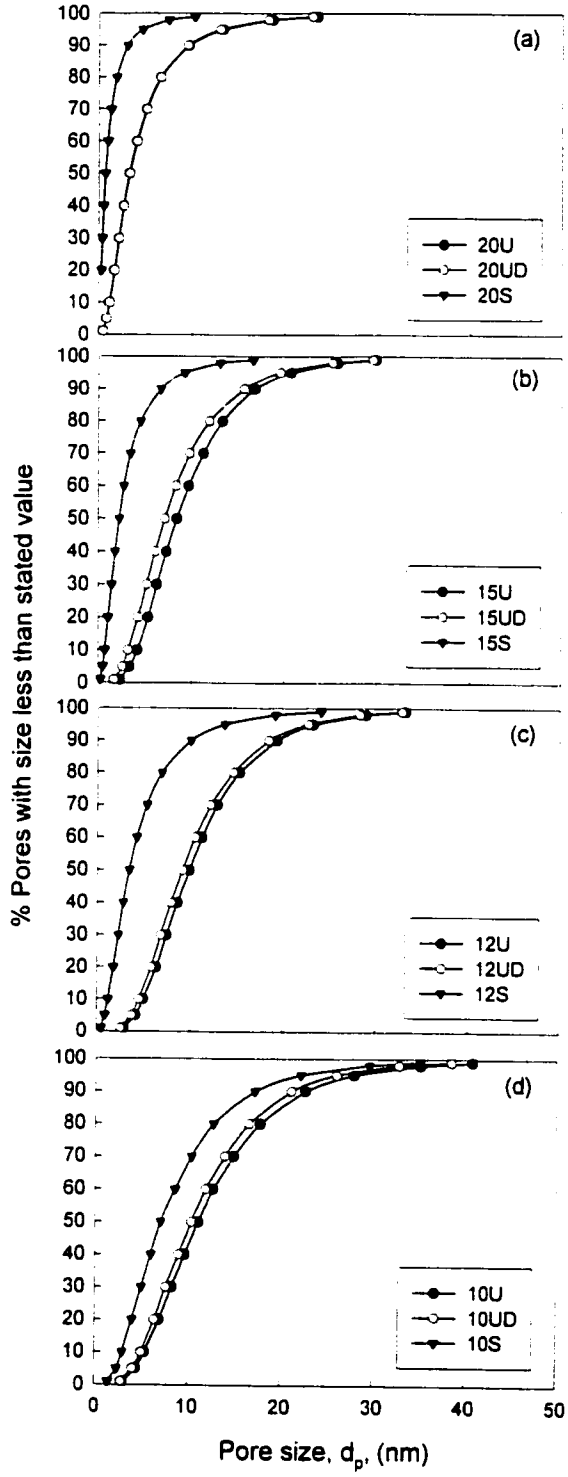

Figure 5.2. Cumulative pore size distribution for various membranes. (a) 20 Series membranes, (b) 15 Series membranes, (c) 12 Series membranes and (d) 10 Series membranes

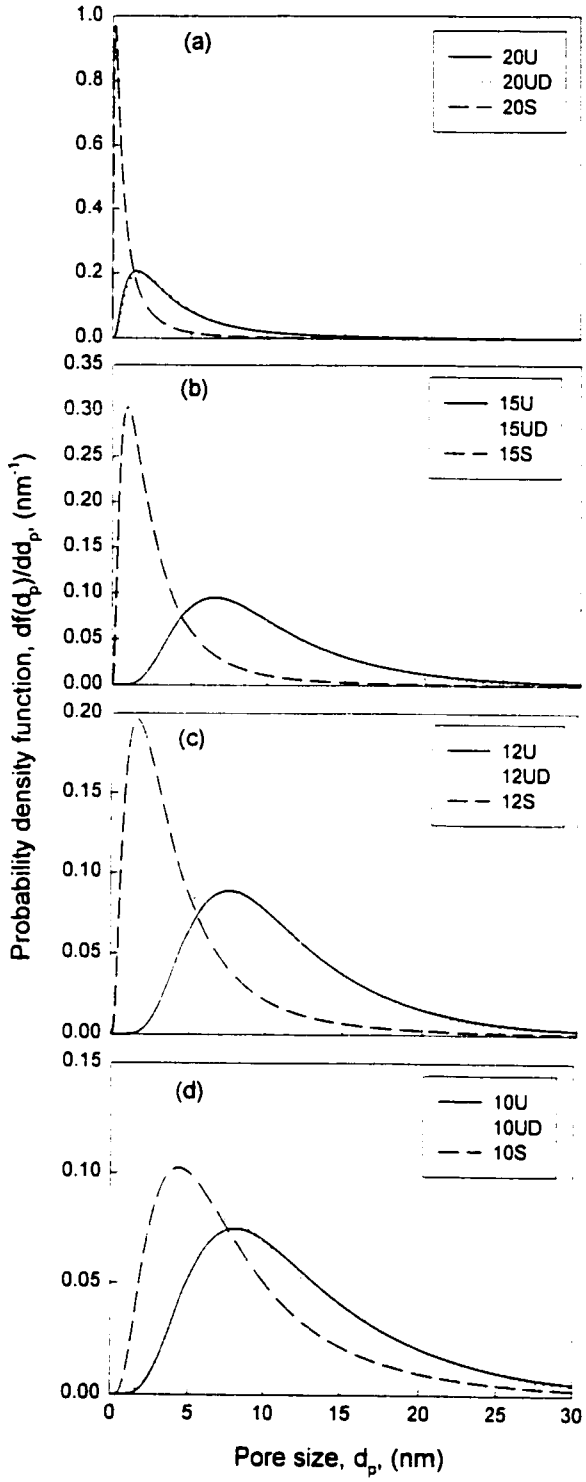

Figure 5.3. Probability density function curves for (a) 20 Series, (b) 15 Series, (c) 12 Series and (d) 10 Series membranes.

deviation for all the membranes under study. As shown in Figure 5.3, the leftward shifts of the probability density function curve for 'S' membranes from 'UD' membranes are noted for all the series.

Michaels (1980) found that σ_ps of different ultrafiltration membranes, both biological and synthetic, were very close to each other (from 1.20 to 1.66). On this basis, it was said that virtually all the membrane ultrafilters, irrespective of their origin, were quite similar in their microstructure. However, membranes prepared in this study showed a wide range of σ_p (1.68 to 3.31). σ_p was found as high as 7.35 for a montmorillonite ceramic membrane (Ishiguro et al., 1996).

5.1.2. Pore density and surface porosity

Pore density and surface porosity were calculated from Eqs. (3.8) and (3.9), respectively and the results are summarized in Table 5.2. For 'U' and 'UD' membranes, the skin layer thickness was taken as 0.2 μm, which was well within the range of the skin layer thickness mentioned by other researchers (Riley et al., 1964; Michaels et al., 1971; Strathmann et al., 1975; Kakuta et al., 1980; Fane et al., 1981) for ultrafiltration membranes made of various materials. The thickness of the SPPO layer coated on 'UD' membranes was calculated from the weight of SPPO coated on the membrane surface of known surface area and it was found to be around 0.2 μm.

Among 'U' membranes, 20U had the highest pore density of 257 pores/μm^2. For 10U membrane, it was as low as 38 pores/μm^2. In general, pore densities of 'UD' membranes were very similar to their corresponding 'U' membranes. However, pore densities of the 'S'

Table 5.2. Pore density and surface porosity of various membranes calculated from the solute transport data and from the AFM images

Membrane	From solute transport		From AFM images	
	Pore density pores/μm^2	Surface porosity (%)	Pore density pores/μm^2	Surface porosity (%)
20U	257	0.84		
20UD	231	0.76		
20S	1291	0.60		
15U	100	1.00		
15UD	122	1.02	136	10.24
15S	447	0.73		
12U	74	0.97		
12UD	84	1.01	103	11.27
12S	170	0.61		
10U	38	0.68		
10UD	51	0.80	91	12.86
10S	49	0.50	95	9.54

membranes, as calculated, were substantially higher than those of both 'U' and 'UD' membranes. Based on the Eq. (3.8), the 20S membrane had as many as 1291 pores/μm^2 while 20UD had only 231 pores/μm^2. It is to be noted that 'S' membranes were made by coating a thin layer of SPPO on 'UD' membranes. To explain the increase in the number of pores in the modified membrane, it is theorized that there are several pores in the coated layer of SPPO over a single pore in the skin layer of uncoated membrane as depicted in Figure 5.4(a). The number of pores in the SPPO layer over a single pore of the skin layer of the uncoated membrane depends upon the pore size on the SPPO layer relative to that on the skin layer of the uncoated membrane. For example, for the series of 20 membranes, there are approximately 6 pores on the SPPO layer over a single pore of the skin layer of the uncoated

membrane. For 10S membrane, however, there was no increase in the number of pores as compared to the 10UD membrane. The mean pore size of 10S membrane was 7.10 nm while it was 10.38 nm for 10UD membrane. Based on the mean pore sizes of 10S and 10UD membranes, no more than one pore can be placed in the SPPO layer over a single pore in the skin layer of the uncoated membrane. From the reduction of the mean pore size of 10S membrane, it can be speculated that the reduction in the size of the bigger pores took place by the coating of a SPPO layer on the pore walls as shown in Figure 5.4(b). Another explanation for the larger number of pores for SPPO-coated membrane could be based on the Hagen-Poiseuille equation itself. The Hagen-Poiseuille equation does not take into account any kind of interaction between the solvent (permeate) and the membrane. When coated with a SPPO layer, the membrane surface becomes hydrophilic, which in turn enhances the water permeation through the membrane. Therefore, the number of pores required should be less than that calculated by the Hagen-Poiseuille equation for a given permeation rate.

Surface porosities of the membranes were between 0.5 to 1% (Table 5.2). It was slightly lower for 'S' membranes as compared to 'UD' membranes. The surface porosity of a XM100A membrane (MWCO-100,000 Daltons) from Amicon was found to be 0.75% by Fane et al. (1981).

5.2. Membrane characterization using atomic force microscope

5.2.1. Mean pore size and pore size distribution

Different pore shapes, including circular, elliptical and slits, were observed in the AFM images of the membrane surface. Pore sizes, therefore, were calculated by taking the average of the width and the length of the pore. AFM images of various unmodified and modified

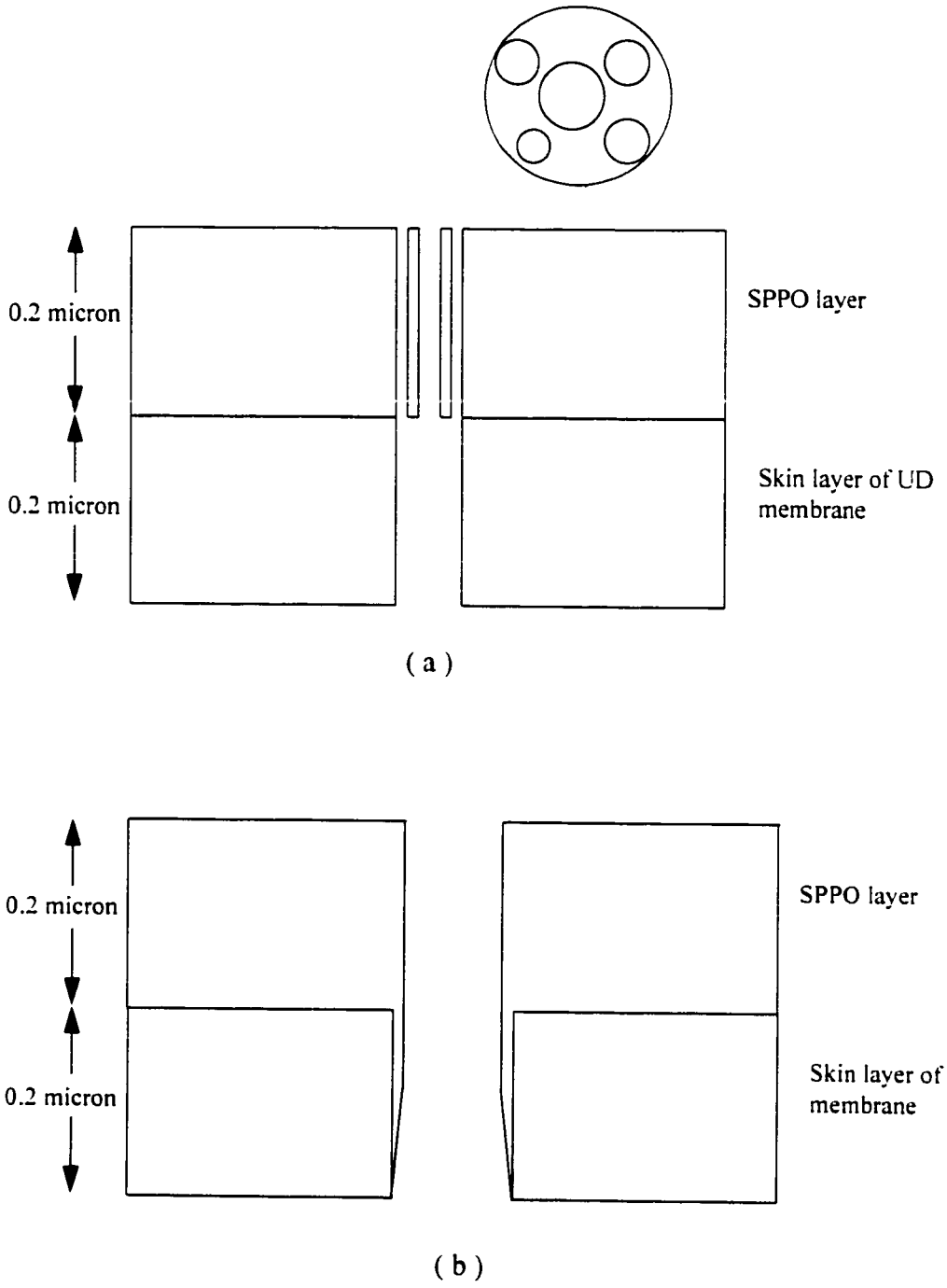

Figure 5.4. Simplistic representation of pore(s) in SPPO layer over a single pore in UD membranes (not to the scale), (a) for smaller pores in UD membrane (like in 20UD). (b) for bigger pores in UD membrane (like in 10UD membrane)

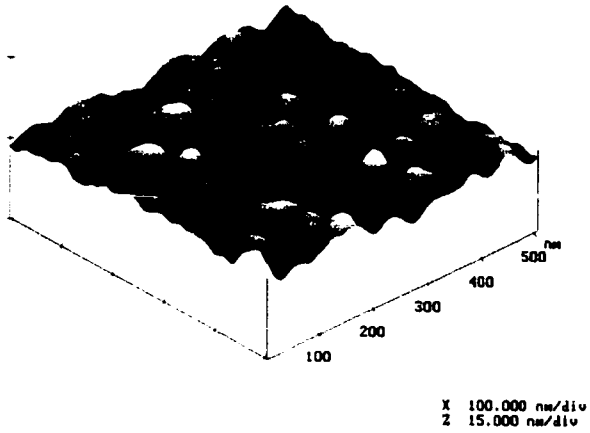

(a) 20UD

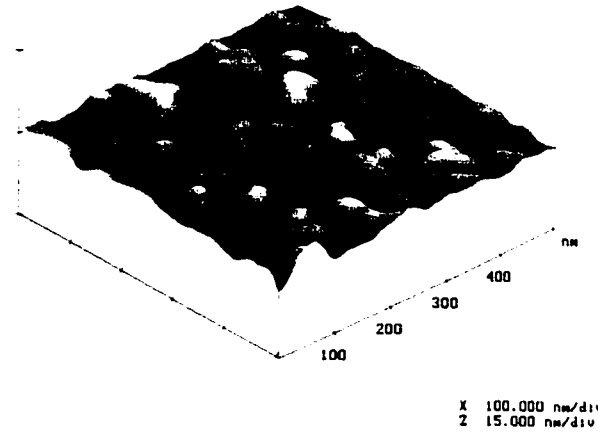

(b) 15UD

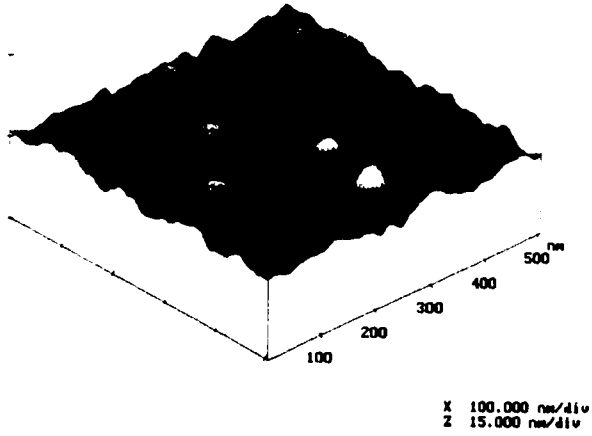

(c) 12UD

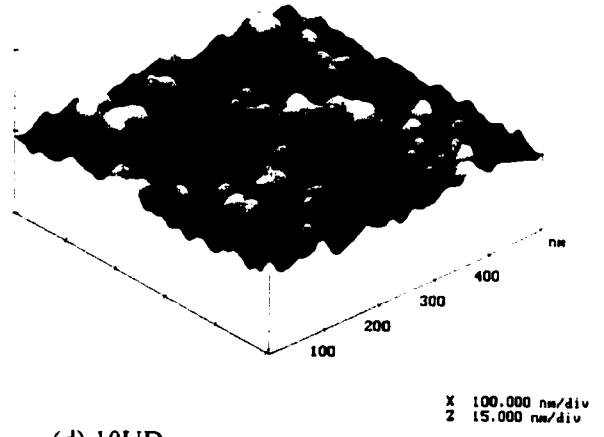

(d) 10UD

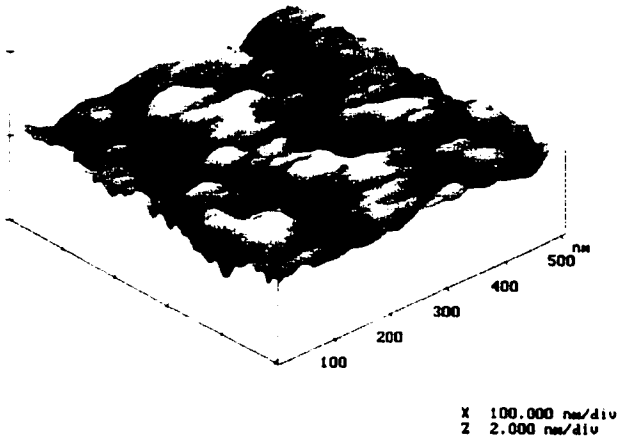

(e) 20S

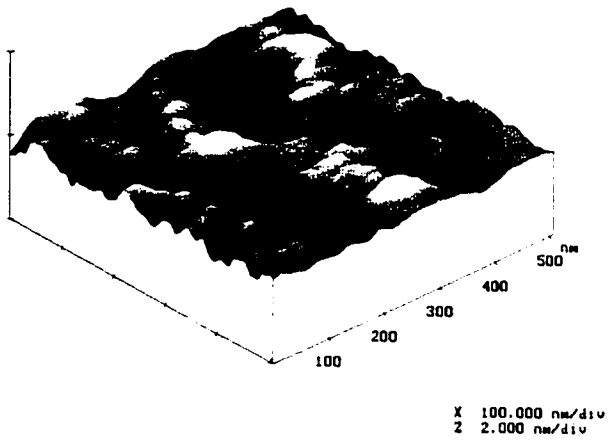

(f) 15S

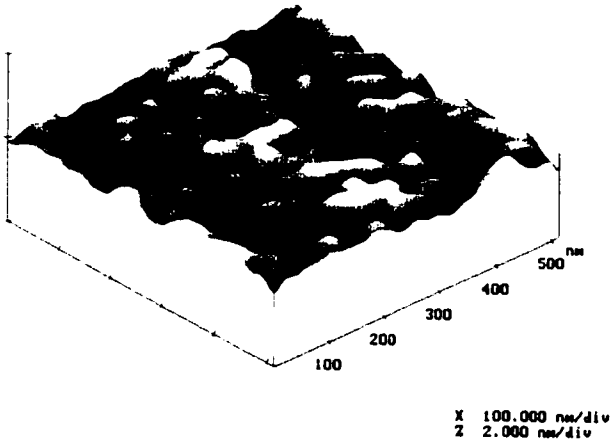

(g) 12S

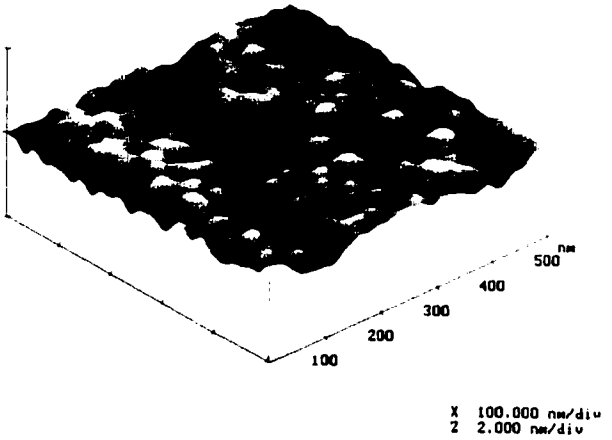

(h) 10S

Figure 5.5. Atomic force microscopic images of the top (skin) side of (a) 20UD membrane, (b) 15UD membrane, (c) 12UD membrane, (d) 10UD membrane, (e) 20S membrane, (f) 15S membrane, (g) 12S membrane and (h) 10S membrane.

membranes are shown in Figure 5.5. It should be noted that the Z-ranges of the AFM images of 'UD' and 'S' membranes are 15 nm and 2 nm, respectively. The bright regions are the highest points while the dark regions are the depressions. For analyzing surface pore characteristics, the AFM image analysis program was used. Pore sizes were measured by visually inspecting line profiles of different pores which were observed on AFM images taken for different areas of the same membrane. Pore sizes of 50 pores measured from the AFM images were plotted against the median ranks, as discussed in Chapter 3, on a log-normal probability paper (Figure 5.6), which yielded a straight line with a very high correlation coefficient ($r^2 \geq 0.97$ for all the membranes). This confirmed that pore sizes had a log-normal distribution. Values of the mean pore size and the geometric standard deviation were calculated from the data plotted on Figure 5.6 and the results are presented in Table 5.1. The 10UD membrane with a MWCO of 94,000 Daltons showed a mean pore size of 37.6 nm. Dietz et al. (1992a) found a mean pore size of 25.2 nm in a DUS-1020 membrane made of polyethersulfone having a MWCO of 100,000 Daltons.

Mean pore sizes measured by the AFM technique were about 3.5 times larger than those calculated from the solute transport data (Table 5.1). Bessières et al. (1996) also observed that AFM gave 2 to 4 times bigger diameters than those obtained from the solute (PEG) transport. According to Bessières et al. (1996), pore sizes obtained from a solute separation correspond to a minimal size of the pore constriction experienced by the solute while passing through the pore. On the other hand, pore sizes measured by AFM correspond to the pore entrances which are of funnel shape and have maximum opening at the entrance. The cumulative pore size distribution curve and probability density function curves were also generated and are shown in Figures 5.7 and 5.8, respectively.

Pore sizes obtained by AFM for 20UD, 20S, 15S and 12S membranes were too large to be assigned actual pore sizes. Pores were indistinct and an amalgamation of a few small pores could easily be misinterpreted as one big pore, resulting in an overestimation of the pore sizes. It was also difficult to distinguish between the pores and the depressions in the membrane surface. Fritzsche et al. (1992a) and Kim et al. (1990) also pointed out that it was not possible to measure the pore sizes of membranes having a MWCO less than 30.000 ~ 40.000 Daltons. However recently, Bowen et al. (1996b) were able to measure the pore sizes of a polyethersulfone ultrafiltration membrane (ES625) having a MWCO of 25.000 Daltons by AFM. The latter membrane had very low surface roughness which made the pore size measurement possible. It is to be noted that the surface smoothness is known to be an important requirement in obtaining high resolution images from the atomic force microscope. The mean pore size of the above membrane was measured to be 5.1 nm (by AFM) which is very comparable to the mean pore sizes of 20U, 20UD and 12S (~3.4 nm obtained from the solute separation data) membranes each with MWCO of about 20.000 Daltons.

5.2.2. Pore density and surface porosity

Pores were counted visually from several AFM images covering an area of 200 nm × 200 nm. Surface porosity was calculated by using Eq. (3.9). Both pore density and surface porosity data are shown in Table 5.2. For 10UD membrane, pore density and surface porosity were 91 pores/μm^2 and 12.86% respectively. These results are in fairly good agreement with the results of Bessières et. al. (1996) (pore density: 70 pores/μm^2, surface porosity: 11.8% of IRIS sulfonated polysulfone membrane with a MWCO of 100,000 Daltons) measured by AFM.

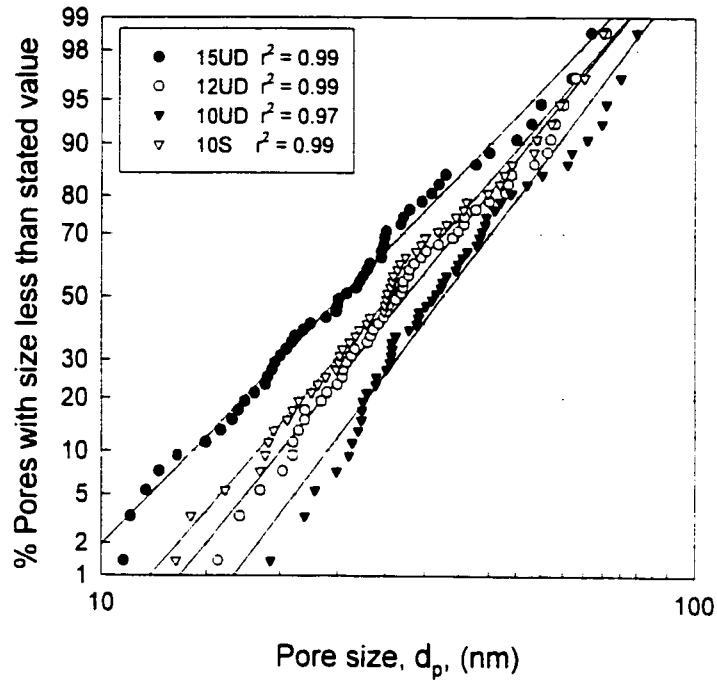

Figure 5.6. Log-normal pore size distributions of the pore sizes measured from the AFM images.

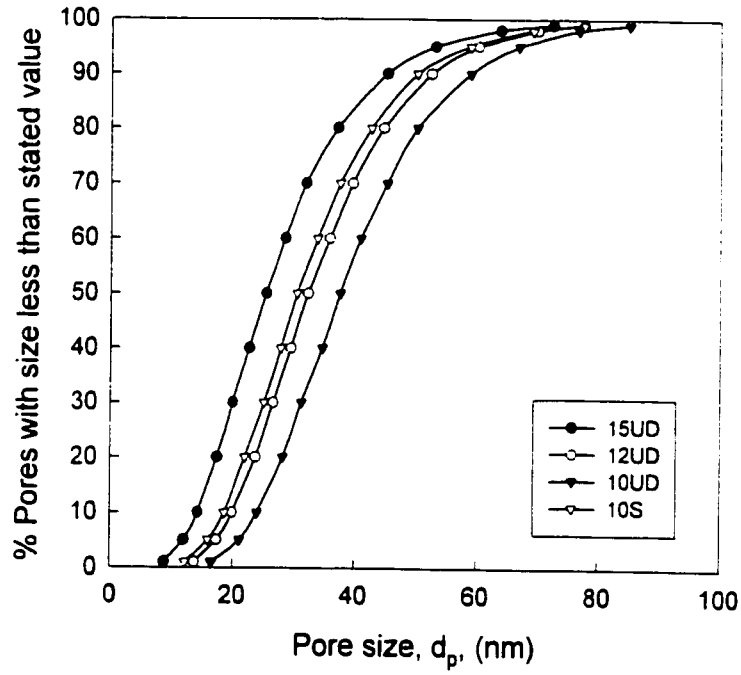

Figure 5.7. Cumulative pore size distributions of the pore sizes measured from the AFM images.

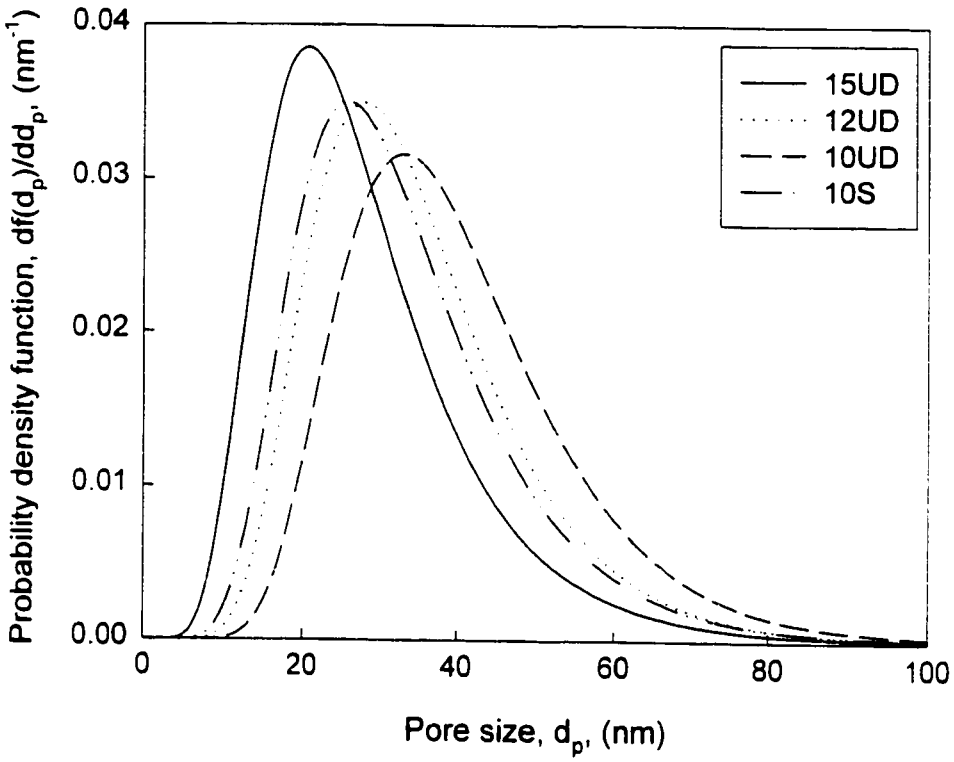

Figure 5.8. Probability density function curves generated for the pore sizes measured from the AFM images.

Surface porosity, calculated from the pore size distribution obtained from the AFM images, was very high compared to the one calculated from the solute transport data. This was mainly because of the bigger pore size obtained from AFM images, as surface porosity is proportional to the square of the pore diameter. However, pore densities measured from AFM images were quite comparable to those calculated form Eq. (3.8) for 15UD and 12UD membranes (Table 5.2).

5.2.3. Surface roughness

Different roughness parameters (R_a, R_q and R_z) were measured by AFM. Several AFM images (500 nm × 500 nm) of different parts of the same membrane were analyzed and mean values of each roughness parameter are reported in Table 5.3. Generally, the roughness parameter of 'UD' membranes became higher when the MWCO became higher. For example, the 10UD membrane had maximum values of R_a, R_q, and R_z among all the uncoated membranes. Membranes of higher MWCO were cast from the solution having lower polymer concentration and therefore will have less tightly packed nodule aggregates in the skin layer, which in turn would contribute to a higher degree of roughness on its surface. The same trend between roughness and MWCO was also observed by other researchers (Fritzsche et al., 1992a; Bessières et al., 1996).

On coating of a thin layer of SPPO on 'UD' membrane surface, the roughness of the membrane surface was reduced. Reduction in surface roughness could be understood on the basis of the filling of the valleys by dilute SPPO solution during the coating of the membrane surface. There was not much difference in the roughness of the various SPPO coated membranes.

Table 5.3. Various roughness parameters measured from the AFM images of 500 nm × 500 nm for different membranes.

Membrane	Roughness parameters		
	R_a (nm)	R_q (nm)	R_z (nm)
20UD	0.68* ± 0.12**	0.86 ± 0.15	5.07 ± 1.32
20S	0.18 ± 0.04	0.23 ± 0.05	1.09 ± 0.16
15UD	0.61 ± 0.07	0.78 ± 0.08	4.03 ± 0.61
15S	0.14 ± 0.07	0.22 ± 0.04	1.06 ± 0.12
12UD	1.02 ± 0.12	1.31 ± 0.17	6.64 ± 0.61
12S	0.06 ± 0.01	0.09 ± 0.02	0.72 ± 0.10
10UD	2.02 ± 0.12	2.40 ± 0.46	14.02 ± 2.77
10S	0.07 ± 0.01	0.09 ± 0.01	0.59 ± 0.07

* mean value ** standard deviation

5.3. Cross-sectional structure of 'UD' membranes

Cross-sectional images of 20UD, 15UD, 12UD and 10UD membranes were taken by scanning electron microscope (SEM) and are shown in Figure 5.9(a-d). The 20UD membrane (Figure 5.9a) has a thick dense portion between the skin layer and finger-like structure. The other three membranes do not have such a thick dense layer. However, all the membranes have finger-like structures.

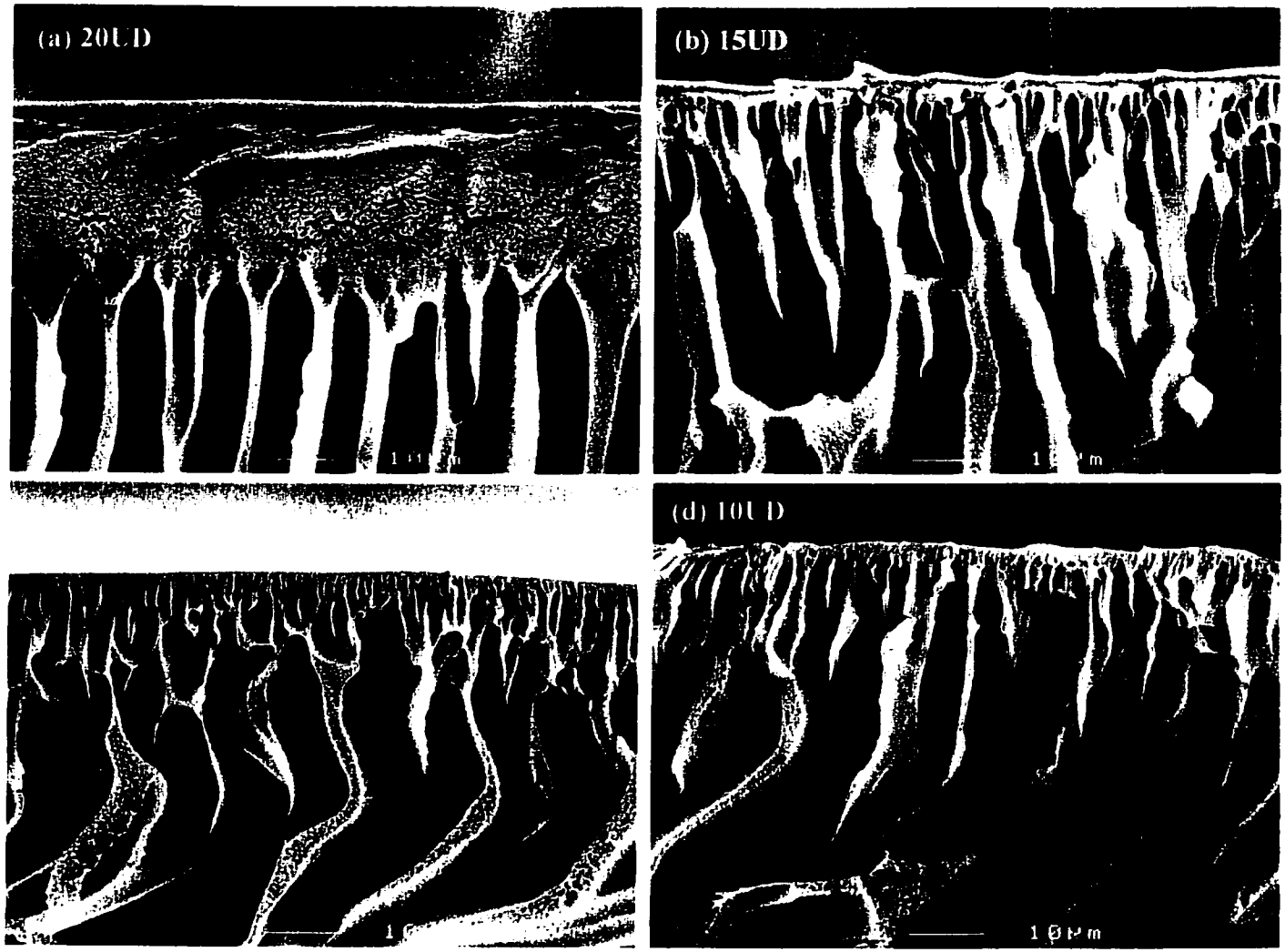

Figure 5.9. SEM picture of the cross-section of (a) 20UD, (b) 15UD, (c) 12UD, and (d) 10UD membranes

5.4. Conclusions

Membranes were characterized by solute transport and AFM. Comparison of the results obtained from these two techniques were made. It was found that the log-normal distribution was very appropriate for describing the pore size distribution both from solute transport and from AFM. There was no significant difference between 'U' (never dried) and 'UD' (after glycerol treatment) membranes in terms of their mean pore sizes, geometric standard deviations, pore densities and surface porosities. However, when a thin layer of SPPO was coated on the surface of the 'UD' membranes, the mean pore sizes were reduced, pore densities were substantially increased and values representing surface roughness were reduced. For all the membranes, mean pore sizes ranged from 0.70 to 11.12 nm, geometric standard deviation ranged from 1.68 to 3.31, pore density ranged from 38 to 1291 pores/μm^2, and surface porosity ranged from 0.50 to 1.02% as calculated from solute transport data. Pore density was the highest for the 20 series membranes and was the least for the 10 series membranes. Mean pore sizes measured by AFM were about 3.5 times larger than those calculated on the basis of data from solute transport experiment. The 20UD membrane had a thicker dense layer on the top compared to other 'UD' membranes. However, all the membranes had finger-like structure.

CHAPTER 6

Performance of Unmodified Membranes (U)

The membrane performance was evaluated in terms of pure water permeation, permeate flux, flux reduction, clay and SBR separation and membrane fouling. All the permeate flux and separation data are the average of three data points from three different coupons taken from the same membrane. Pure water permeation flux data are the average of at least 10 data points. Ultrafiltration experiments were conducted with constant and also with varying feed concentration with time.

6.1. Pure water permeation flux (PWP)

Pure water permeation refers to the water flux through the membrane when the feed is distilled water. As expected, the PWP was higher for the membrane made from a casting solution having lower polymer (PES) concentration. For example, the PWP was the highest for a 10U membrane (1025 L/m^2h) while it was the lowest for a 20U membrane (531 L/m^2h). It is to be noted that the mean pore size of the 10U membrane was the largest while that of the 20U membrane was the smallest. The molecular weight cut-off (MWCO) and geometric mean pore size (μ_p) were determined from the separation data of polyethylene glycol and polyethylene oxide solutes of known molecular sizes and are given in Table 5.1. The MWCO of the membranes ranged from 21 kDa (20U) to 98 kDa (10U) and their and μ_ps values ranged from 3.24 nm (20U) to 11.12 nm (10U). The PWP data for all four membranes (10U,

12U, 15U and 20U) are shown in Figure 6.1. A linear relationship between the PES concentration in the casting solution and the PWP of the membrane was found, with a very high correlation coefficient (Figure 6.2). The following regression equation was established

$$y = 1539.13 - 50.02x \qquad (r^2 = 0.997) \qquad (6.1)$$

where y is the PWP in L/m^2h and x is the PES concentration (%wt) in the casting solution. However, it should be noted that Eq. (6.1) is specific to our study and should not be considered as a general equation for predicting pure water permeation of a membrane made from a casting solution of a known PES concentration. It should also be noted that the casting solution used for making membranes in this study also contained polyvinylpyrrolidone.

6.2. Permeate flux and flux reduction

Different membranes had different pure water permeation fluxes. Therefore, to normalize the data, the flux reduction was calculated from the permeate flux and the pure water permeation flux by using the following equation

$$Fr_t = \left(1 - \frac{J_{p_t}}{J_w}\right) \times 100 \qquad (6.2)$$

where Fr_t and J_{p_t} are the flux reduction and the permeate flux respectively at time t after the start of the ultrafiltration experiment, and J_w is the pure water permeation flux measured immediately before the ultrafiltration experiment.

6.2.1. Performance of the membranes with constant feed concentration

Feed solutions with different concentrations (0.1, 1, 10, 20 and 30 wt%) of clay and SBR (clay : SBR = 100 : 15) were used to test the performance of the membranes. Constant feed

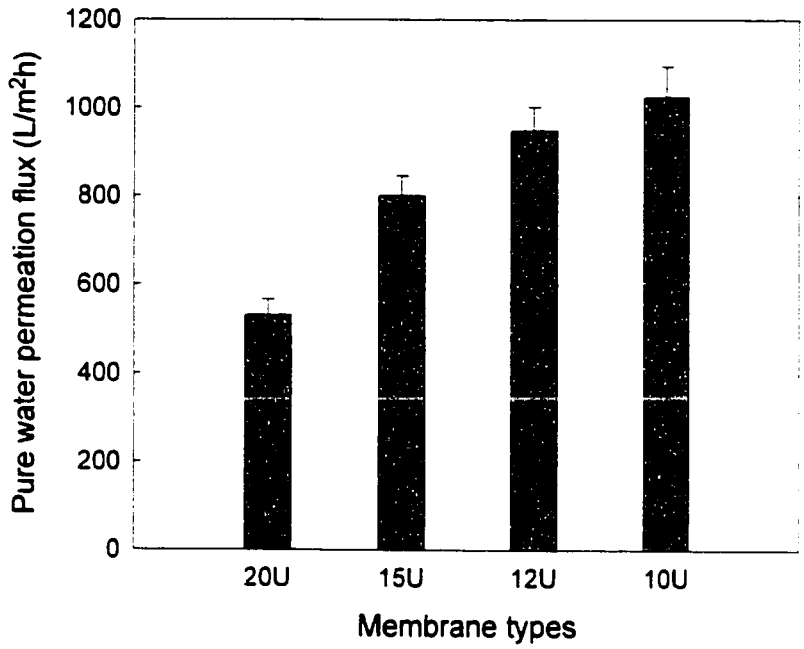

Figure 6.1. Comparison of pure water permeation fluxes for all 'U' membranes tested (Error bars indicate 95% confidence interval.), Operating pressure – 345 kPa

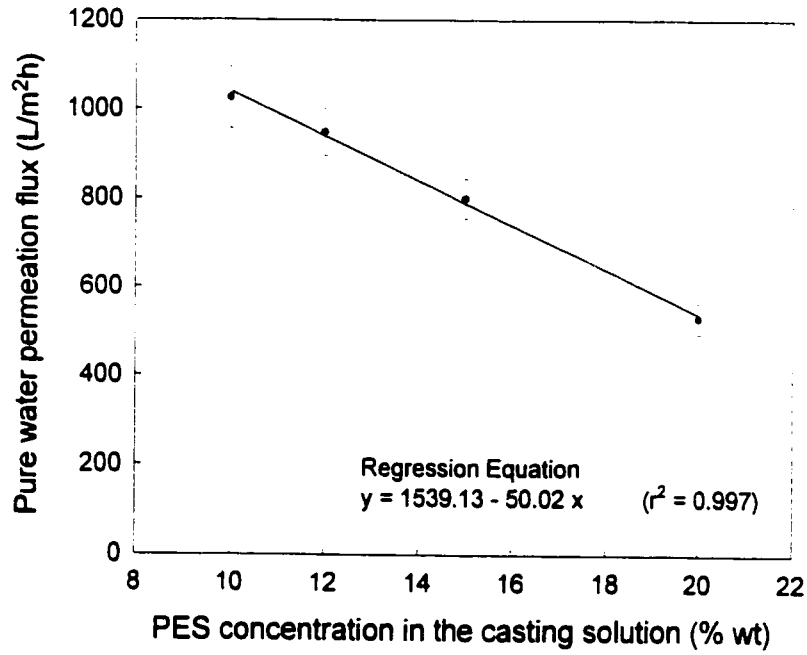

Figure 6.2. Polymer (PES) concentration in casting solutions versus pure water permeation fluxes of 'U' membranes (Error bars indicate 95% confidence interval.)
Operating pressure – 345 kPa

concentration was maintained by recycling both the permeate and retentate to the feed reservoir. Permeate fluxes for the membranes over a period of 24 hours are shown in Figure 6.3(a-e) for different feed concentrations. The reduction of the permeate flux is obvious when compared with the pure water permeation flux given in Figure 6.1. Although pure water permeations were quite different, the final fluxes after 24 hours of operation were similar for all the membranes studied at a given feed concentration. For all the membranes, final permeate fluxes ranged from 168 to 224 L/m^2h and from 18 to 30 L/m^2h for 0.1 and 30% feed concentration, respectively. With respect to the 20U membrane, the final permeate flux at the end of 24 hours of operation was 206 L/m^2h for 0.1% feed concentration and was only 18 L/m^2h for 30% feed concentration. It is important to mention that no attempt was made to clean the membranes during the experiments.

Flux reductions for 20U and 12U membranes at different feed concentrations are given in Figure 6.4(a & b) as a function of operating time. It can be seen from Figure 6.4 that the flux reduction was the highest for the highest feed concentration (30%) while it was the lowest for the lowest feed concentration (0.1%) for every membrane. For the feed concentrations of 10%, 20% and 30%, the initial flux reduction in the first 15 minutes (the data corresponding to the shortest operating time shown in Figure 6.4) was 90-95% and there was little change in flux reduction thereafter. Comparing the flux reduction of different membranes, the flux reduction became more as the membrane pore size increased. For example, with the feed solution of 0.1% of clay and SBR, flux reductions after 24 hours of operation were 58%, 73%, 79% and 84% for 20U, 15U, 12U and 10U membranes, respectively. Therefore, it can be concluded that the membranes become more susceptible to fouling as the pore size of the membrane increases. The fouling is probably due to the blocking of the pores and cake layer formation on the membrane surface.

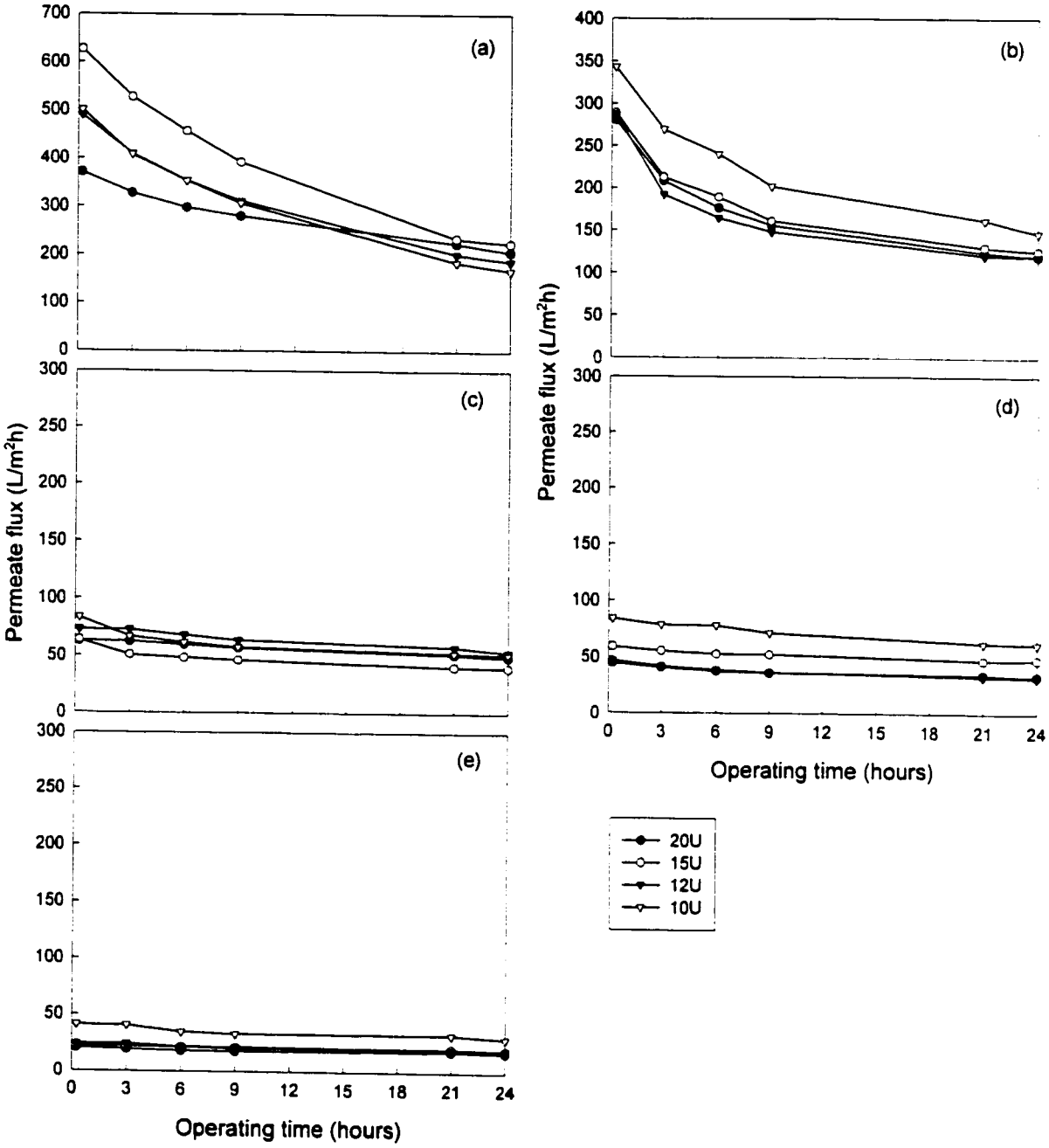

Figure 6.3. Permeate fluxes over a period of 24 hours of operation for all 'U' membranes Feed concentration - (a) 0.1%, (b) 1%, (c) 10%, (d) 20% and (e) 30% of clay and SBR, (Clay/SBR = 100/15), Operating pressure – 345 kPa

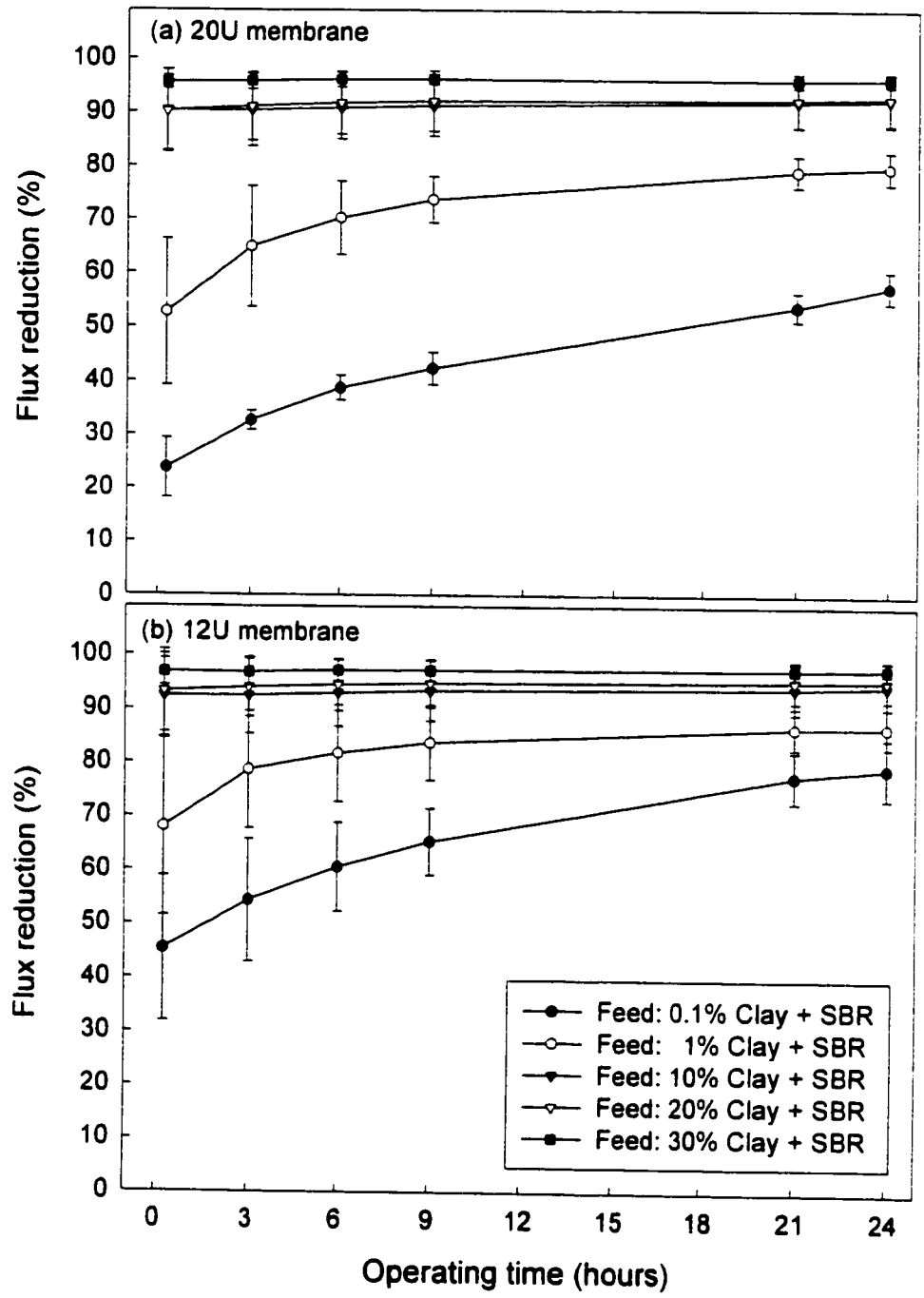

Figure 6.4. Flux reduction with time with various feed concentrations (0.1%, 1%, 10%, 20% and 30% of clay and SBR, clay/SBR = 100/15) (Error bars indicate 95% confidence interval.) Membrane – (a) 20U, and (b) 12U, Operating pressure – 345 kPa

The experiments mentioned above were conducted with the feed solution having both clay and SBR. Experiments were also conducted with the feed solutions containing either clay or SBR. Figure 6.5 shows the permeate fluxes for different membranes when the feed solution contained 0.87% of clay. The latter clay concentration is equivalent to the concentration of clay in 1% (clay + SBR) solution. Permeate fluxes were higher for the feed solution with 0.87% of clay (Figure 6.5) than that with 1% of clay and SBR (Figure 6.3b). For instance, after 24 hours of operation, permeate fluxes ranged from 168 to 188 L/m^2h for the feed solution with 0.87% of clay and from 119 to 147 L/m^2h for the feed solution with 1% of clay and SBR. Permeate fluxes for the feed solution with 0.13% of SBR were between 214 to 273 L/m^2h as shown in Figure 6.6.

Figure 6.7 compares the fluxes of the 15U membrane for different feed solutions (1% of clay and SBR, 0.87% of clay, and 0.13% of SBR). There are two things that are evident from this figure. First, the flux decline in first 15 min was more for 0.87% of clay solution than that for 0.13% of SBR solution. Second, a further flux decline (slope of the curve) was more for 0.13% of SBR solution. It indicates that the clay contributed more to initial flux decline while the SBR contributed more to the continuous flux decline. The same phenomenon was also observed with other membranes (20U, 15U and 10U).

Experiment with 0.87% of clay solution was continued for an extended period of time (~26 days) in order to determine the long term effect on permeate flux. As can be seen from Figure 6.8, there was a sharp flux decline during the first day for all the membranes. Then, the flux decline was gradually reduced. Once the cake layer thickness reaches its maximum under experimental hydrodynamic conditions, a further flux decline could be attributed to the continuous compaction of the cake layer and to the increase in the specific cake layer resistance. The final permeate flux after 26 days was around 50 L/m^2h.

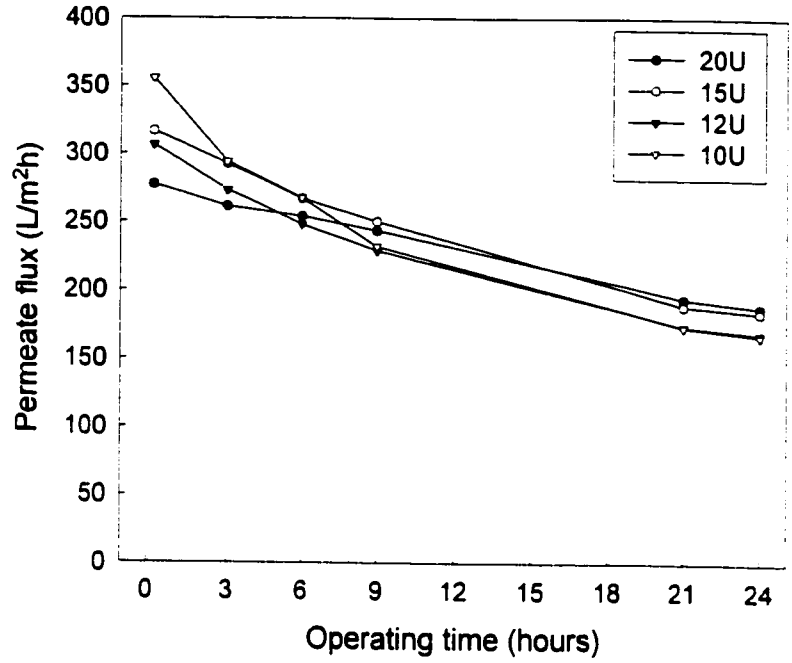

Figure 6.5. Permeate fluxes over a period of 24 hours of operation for all 'U' membranes
Feed concentration – 0.87% of clay, Operating pressure – 345 kPa

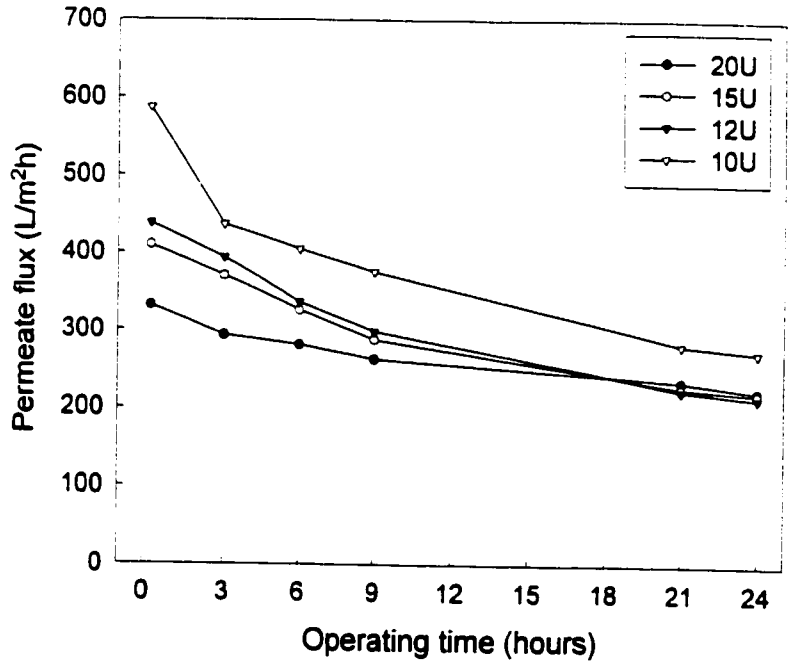

Figure 6.6. Permeate fluxes over a period of 24 hours of operation for all 'U' membranes
Feed concentration – 0.13% of SBR, Operating pressure – 345 kPa

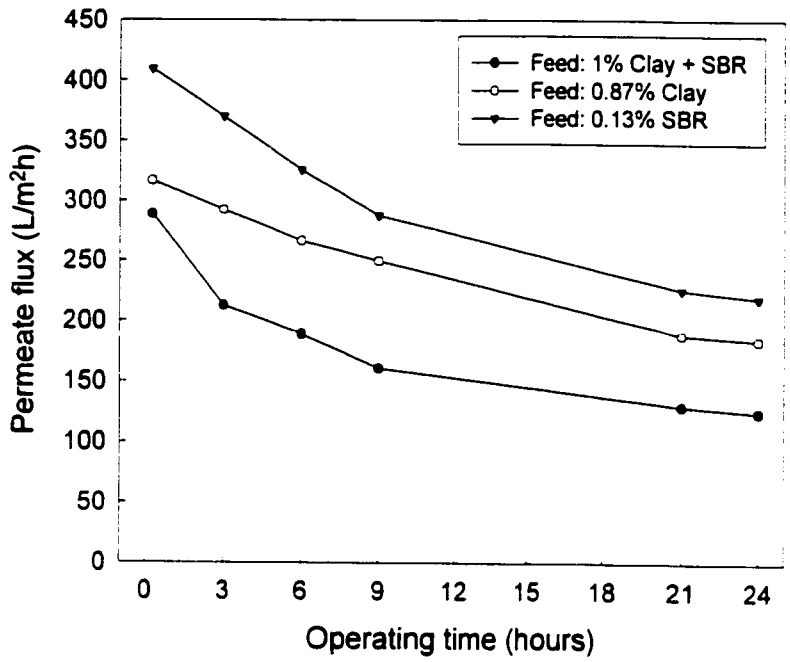

Figure 6.7. Comparison of permeate fluxes with various feed concentrations (1% of clay and SBR, 0.87% of clay, 0.13% of SBR) for 15U membrane, Operating pressure – 345 kPa

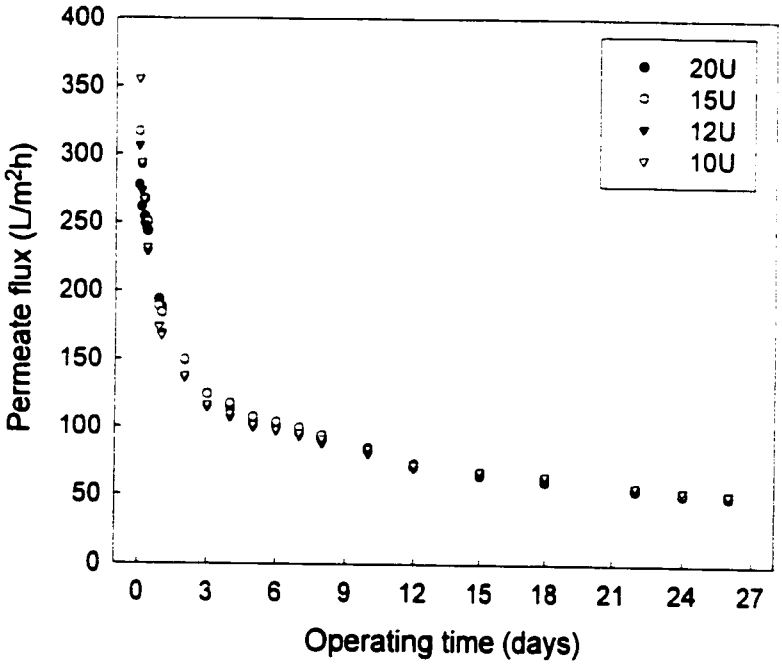

Figure 6.8. Permeate fluxes over an extended period of time for all 'U' membranes Feed concentration – 0.87% of clay, Operating pressure – 345 kPa

6.2.2. Performance of the membranes with increasing feed concentration

Feed solution containing 1% of clay and SBR was concentrated by collecting permeate in a separate tank until the feed concentration became 30%. The experiment was started with 110 L of feed solution and continued until about 4 L of feed solution was left. The permeate fluxes versus operating time are presented in Figure 6.9. The flux decline was very steep in the beginning and leveled off later. Final permeate fluxes after about 120 hours of operation were very low (~10-12 L/m^2h) and similar for all the four membranes. A similar experiment was also performed with a starting feed solution containing 1% clay (without SBR). The changes in the permeate fluxes with time during this experiment are shown in Figure 6.10. In the latter experiment, it took only 60 hours to reach about 30% concentration from the initial 1%, while in the experiment with clay and SBR it took 120 hours. Final permeate fluxes were 10-12 L/m^2h (Figure 6.9) when SBR was present in the feed while they were 44-55 L/m^2h (Figure 6.10) in the absence of SBR. This can be understood by considering SBR as a binding material which enhances the clay deposition on the membrane surface. The presence of SBR also makes the clay layer more dense and thus increases the resistance to the flow of the permeate.

6.3. Fouling

Initial flux reduction was very steep for all the membranes studied. Flux reduction could be attributed to the following two effects.

1. Partial or complete pore blocking
2. Cake layer formation over the membrane

As soon as an experiment was started, pore blocking and cake layer formation over the membrane occurred. It was speculated that pore blocking took place in the initial stage of the experiment, followed by a clay layer formation. It was observed that the final fluxes for all

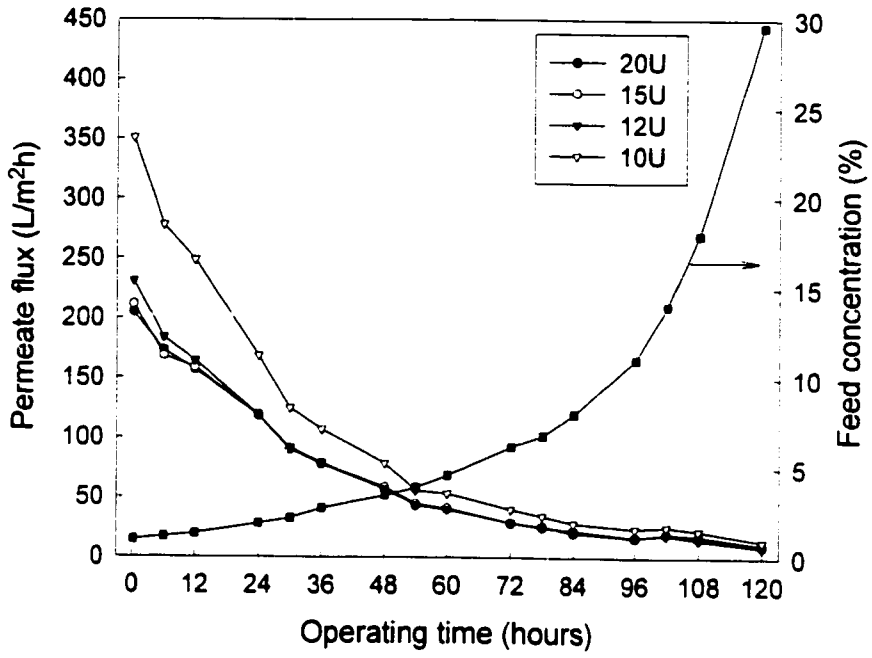

Figure 6.9. Permeate fluxes versus time for all 'U' membranes
Initial feed concentration - 1% of clay and SBR, Operating pressure – 345 kPa

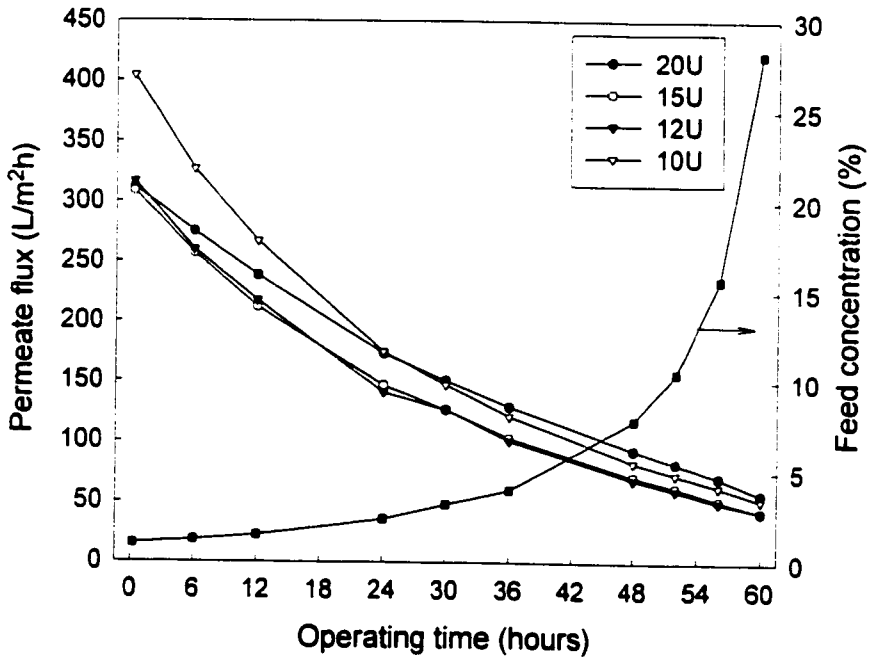

Figure 6.10. Permeate fluxes versus time for all 'U' membranes
Initial feed concentration - 1% of clay (no SBR), Operating pressure – 345 kPa

the four membranes used were similar for a given feed concentration. This indicated that the total resistances (combined resistances of the blocked pore, the cake layer and the membrane) were similar for all the membranes used. As resistance due to the polymeric membrane was higher for less porous membranes such as 20U, the fouling resistance (resistance due to blocked pores and cake layer) was lower for this membrane (20U) compared to the more porous membranes such as 10U and 12U. Fouling resistance was also very high compared to that of the membrane and hence controlled the permeate flux. Nuortila-Jokinen et al. (1995a) also found that the permeate flux after some time of operation was almost independent of membrane types (molecular weight cut-off point and pore size). They attributed the flux reduction to the adsorption of the foulants on the membrane surface and to the plugging of membrane pores.

Scanning electron micrographs in Figure 6.11(a-d) show the cross-sectional image of the 20U membrane used in various experiments with constant feed concentrations. The micrographs clearly reveal a distinct layer of foulants on the membrane surface. The thickness and density of the foulants layer seem to increase with the feed (clay + SBR) concentration.

6.4. Clay and SBR separation

Separation for clay particles was nearly equal to 100%, as no traces of clay particles were found in the permeate. The SBR concentration in the permeate was dependent on the feed concentration, although its separation was very high (more than 98%, Table 6.1) for all the membranes studied and for all the feed solutions tested. These results are in agreement with that of Woerner and Short (1991). High separation could be expected because of the large particle sizes of both clay and SBR compared to the size of the pores of the membranes used in this study.

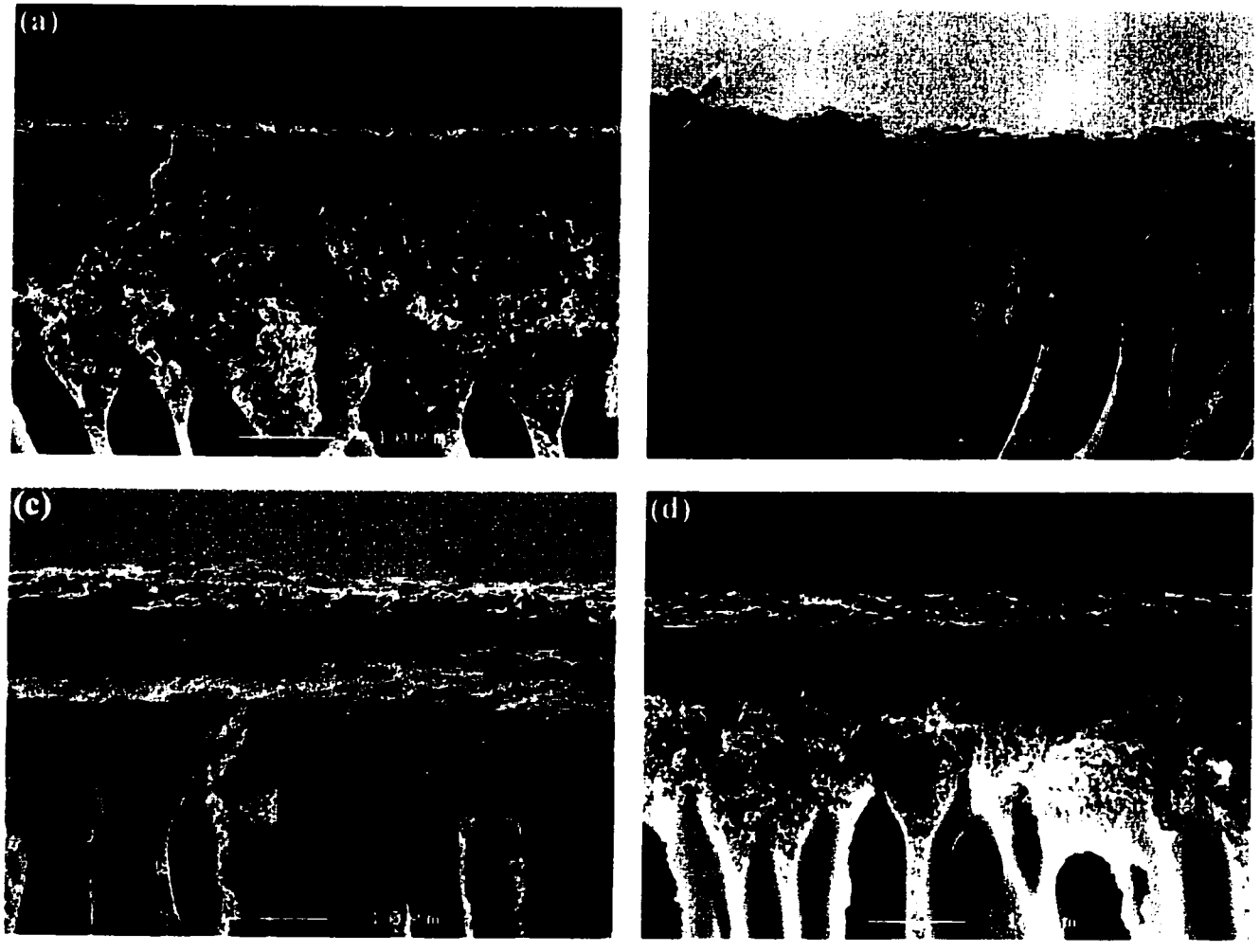

Figure 6.11. Scanning electron microscopic images of the cross-section of 20U membranes after 24 hours of operation with (a) 0.1%, (b) 1%, (c) 20%, and (d) 30% feed concentration of clay and SBR (Clay/SBR = 100/15)

Table 6.1. SBR separation for various feed concentrations including both clay and SBR

Memb -rane	Feed[1] - 0.1% c_f[2] = 105.4 ppm		Feed – 1% c_f = 1054 ppm		Feed - 10% c_f = 10540 ppm		Feed - 20% c_f = 21080 ppm		Feed - 30% c_f = 31620 ppm	
	c_p[2] (ppm)	f (%)	c_p (ppm)	f (%)	c_p (ppm)	f (%)	c_p (ppm)	f (%)	c_p (ppm)	f (%)
20U	2.1	98.0	4.3	99.6	19.4	99.8	40.3	99.8	123.5	99.9
15U	2.0	98.1	4.3	99.6	52.3	99.5	59.8	99.7	134.9	99.6
12U	1.6	98.4	4.9	99.5	28.9	99.7	75.6	99.6	192.7	99.4
10U	1.9	98.2	5.1	99.5	60.2	99.4	75.8	99.6	160.8	99.5

[1] Feed concentration includes both clay and SBR (ratio 100/15).

[2] C_f and C_p are TOCs representing SBR concentration in the feed and permeate respectively.

6.5. Conclusions

Ultrafiltration is a very promising method to treat white water and coating plant effluent in order to recover valuable chemicals and to reuse the water. Water recovered from ultrafiltration was clean as recovery of chemicals (clay and SBR) was nearly 100%. The major drawback of the process for these applications was the flux decline over time due to fouling. A very sharp flux reduction was observed immediately after the start of the experiment for all the membranes studied. Flux reduction was attributed to the additional resistance due to fouling (because of the pore blocking and the cake layer formation on the membrane surface). The thickness and density of the cake layer on the membrane surface seemed to increase with the feed concentration. The flux was considerably higher when SBR was not present in the feed solution. The final permeate flux was dependent on the feed concentration but was almost independent of the characteristics of the membrane used in this study. The flux reduction was higher for the membranes having bigger pores.

CHAPTER 7

Comparison of the Performance of Unmodified (U), Glycerol Treated (UD) and SPPO Coated (S) Membranes

In this chapter a comparison is made in the performance of unmodified wet (U), glycerol treated dried (UD) and sulfonated (SPPO-coated) modified (S) membranes. Comparison in terms of membrane characteristic parameters is presented in Chapter 5. Pure water permeation data for 'U', 'UD' and 'S' membranes are the averages of at least 10 data points. All the permeate fluxes and separation data are the averages of three data points from three different coupons taken form the same membrane.

7.1. Comparison of pure water permeation flux

Pure water permeation flux (PWP) data for all the membranes studied are shown in Figure 7.1. It is evident from this figure that the PWP was substantially reduced when the membrane was coated with SPPO. The PWP reduction after SPPO coating was more pronounced with the membranes having smaller pore sizes such as 20UD and 15UD. The MWCO and mean pore sizes of the SPPO-coated membranes were significantly smaller compared to those of the unmodified membranes (Table 5.1). Therefore, the reduction in the PWP was mainly due to reduction in the pore sizes.

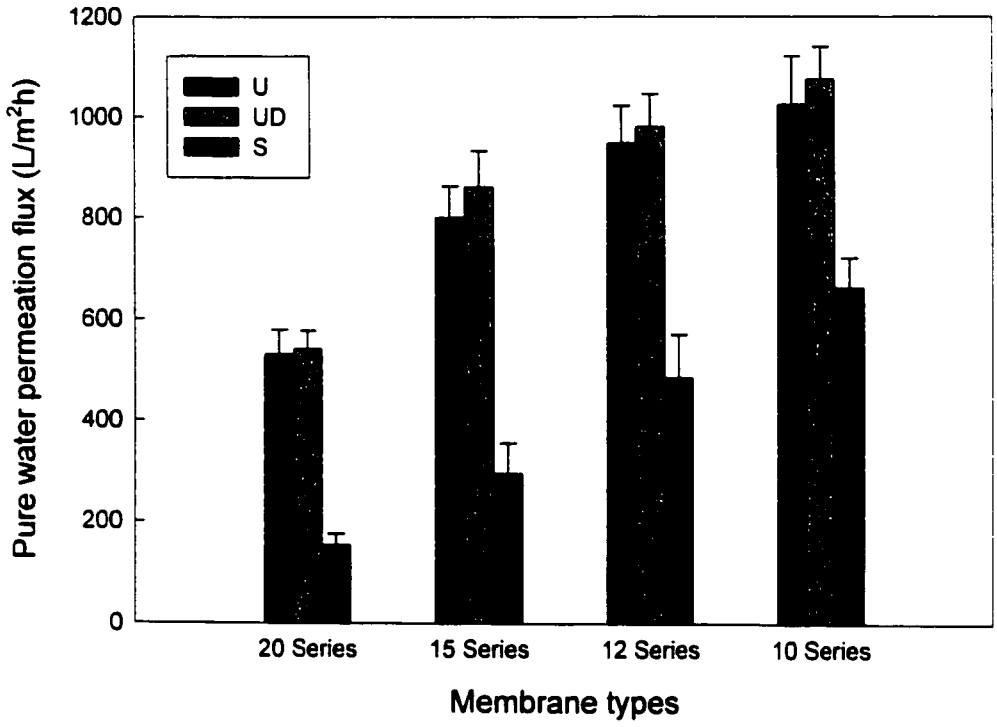

Figure 7.1. Comparison of pure water permeation flux of unmodified and modified membranes (Error bars indicate 95% confidence interval)

Unlike SPPO coated membranes, there was no reduction in the PWP of unmodified dried membranes (UD) compared to unmodified wet membranes (U) (Figure 7.1). It was even slightly higher. Usually membranes show lower PWP when dried as pores collapse during the drying process. However, when membranes were treated with glycerol solution, the water in the pore was replaced by glycerol which stayed in the pores even after air drying of the membranes, because of its high boiling point. Glycerol in the pores did not let the pores collapse since it worked as a pore filler. The MWCO and mean pore sizes of 'UD' membranes were very similar to their respective 'U' membranes (Table 5.1).

7.2. Comparison of the permeate flux and flux reduction

Three different feed concentrations (1 and 0.1% of clay + SBR, and 0.87% of clay only) were used to study the performance of the modified and unmodified membranes.

7.2.1. With 1% feed solution of clay and SBR

The permeate flux and flux reduction with 1% feed solution of clay and SBR are shown in Figures 7.2(a-d). The flux reduction was calculated using Eq. (6.2) as discussed in Chapter 6. Although the PWP of the SPPO coated membranes was quite low compared to the unmodified membranes, permeate fluxes were only slightly lower. In some cases, for example, 15S and 12S, permeate fluxes were even higher than those of their respective unmodified membranes. Flux reduction was the lowest for SPPO coated membranes compared to unmodified membranes for all the four series. For instance, the flux reduction after 24 hours of operation was 44% and 80% for 20S and 20UD membrane, respectively. With SPPO coated membranes, clay particles were rejected because of the repulsion force between the negatively charged membrane surface (sulfonate substituent) and the clay particles which were also negatively charged. Rejection of clay particles reduced the fouling

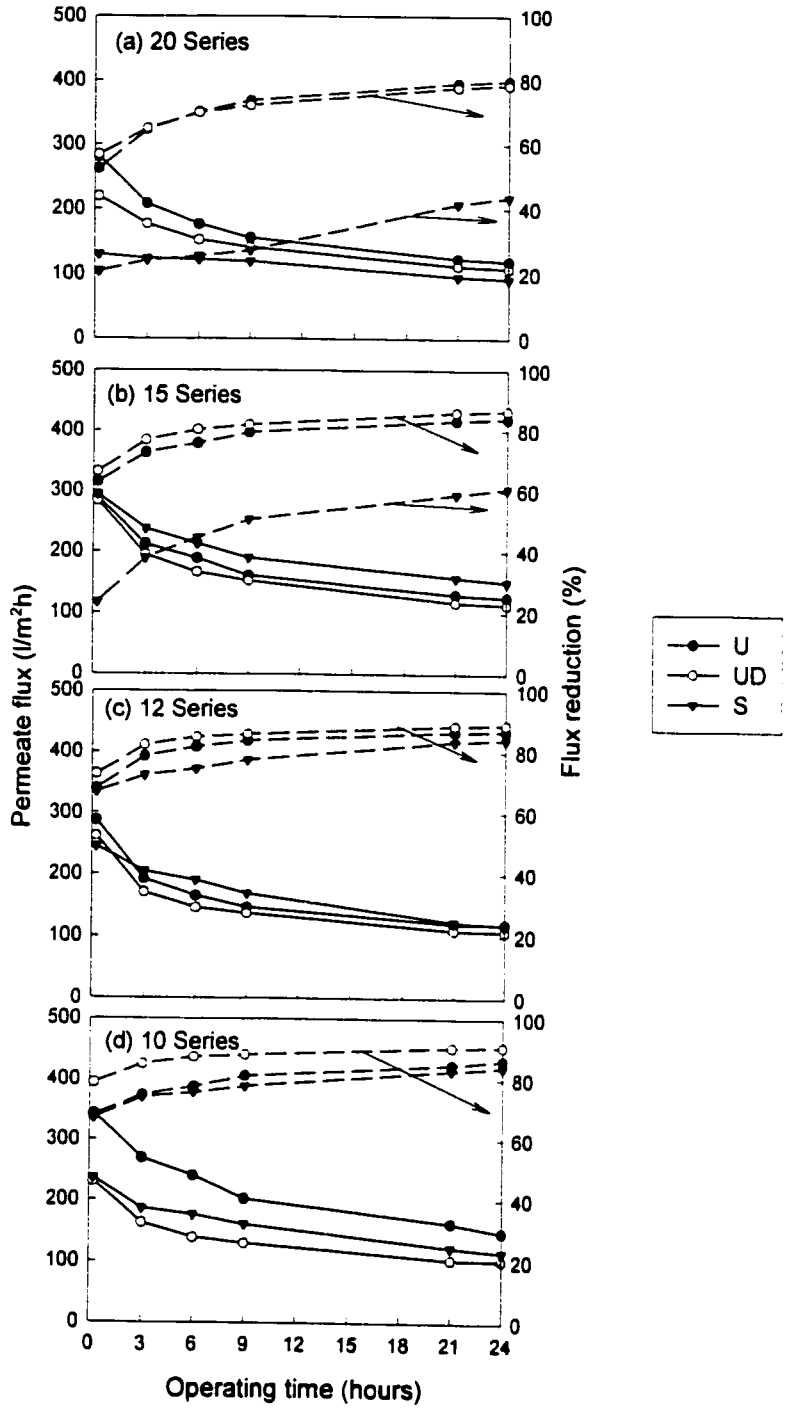

Figure 7.2. Permeate flux and flux reduction with time for different membranes, (a) 20 Series, (b) 15 Series, (c) 12 Series and (d) 10 Series
Feed concentration – 1% of clay and SBR (clay/SBR = 100/15), Operating pressure - 345 kPa

on the membrane surface, resulting in higher permeate fluxes. Permeate fluxes after 24 hours of operation were in the range of 90 L/m^2h (for 20S) to 150 L/m^2h (for 15S).

7.2.2. With 0.1% feed solution of clay and SBR

Because of the high flux reduction immediately after the start of the experiment with 1% feed solution, it was speculated that there was instant pore blocking and cake formation on the membrane surface for all the membranes used, including SPPO coated membranes. Once a cake layer is formed on the membrane surface, the repulsion force between the SPPO layer and clay particles is not very effective as it is hindered by the cake layer. In order to reduce the cake formation on the membrane surface, experiments were conducted with a lower feed concentration, e.g. 0.1% of clay and SBR.

The Permeate flux and flux reduction with time with 0.1% feed solution of clay and SBR are shown in Figure 7.3 (a-d). Permeate fluxes were substantially higher with 0.1% feed concentration compared to those with 1% feed concentration for most of the membranes. For SPPO coated membranes, the flux reductions in the first 15 minutes with 0.1% feed concentration were only 2 to 9% compared to 21 to 67% for 1% feed concentration. It is believed that, at 0.1% feed concentration, the cake formation was not very prominent and clay particles were rejected more effectively because of the repulsion between the SPPO coated membrane surface and clay particles. However, it should be noted that the lower flux reduction is ascribed not only to the stronger repulsive force, but also to the lower concentration of the feed solution. For example, with respect to 20UD membranes, the flux reduction in the first 15 minutes was 38% for 0.1% feed concentration compared to 57% for 1% feed concentration. With respect to the 20S membrane, the flux reduction in first the 15

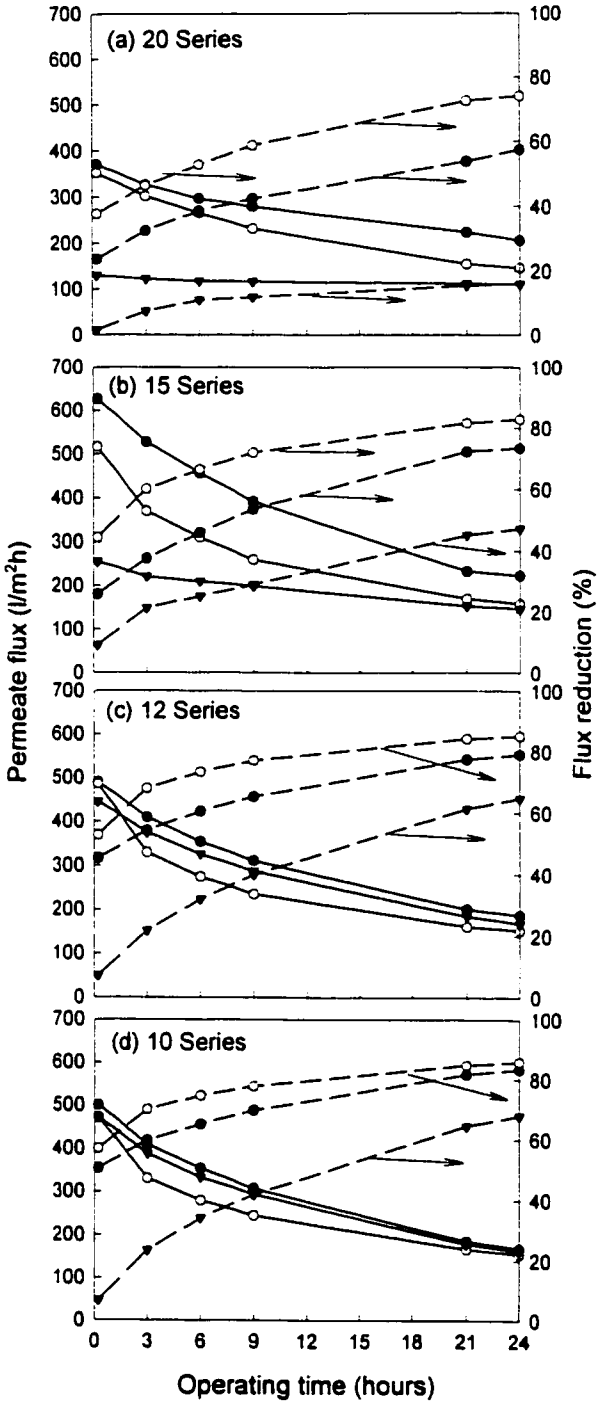

Figure 7.3. Permeate flux and flux reduction with time for different membranes, (a) 20 Series, (b) 15 Series, (c) 12 Series and (d) 10 Series
Feed concentration - 0.1% of clay and SBR (clay/SBR = 100/15),
Operating pressure - 345 kPa

minutes was only 2% for 0.1% feed concentration compared to 21% for 1% feed concentration. It is very evident from Figure 7.3 that the flux reductions were lower when the membranes were coated with SPPO. Permeate fluxes after 24 hours of operation were around 150 L/m^{2}h for most of the 'S' membranes.

7.2.3. With 0.87% feed solution of clay

SBR is a neutral polymer and it is speculated that it forms a thin layer on the surface of the clay particles when present in the clay solution. In a separate electrophoresis experiment, it was found that the mobility of the clay particles towards the cathode was reduced when SBR was added to the clay solution. The thin layer of SBR on clay particles would reduce the charge density on the particles which, in turn, would result in the reduction of the repulsion force between the sulfonated membrane surface and the clay particles.

Experiments were conducted with the feed solution which included clay particles only. The amount of clay in the feed solution was kept at 0.87% which was equivalent to the amount of clay present in the 1% feed solution involving both clay and SBR. Results of these experiments are presented in Figures 7.4(a-d). Flux reduction was the lowest with SPPO coated membranes. However, it is not clear that the lower flux reduction was because of higher repulsive force between the sulfonated membrane surface and the clay particles, or because of the lesser degree of fouling in the absence of SBR. It is to be noted that an increase in the permeate flux was also observed with the unmodified membranes when SBR was not present in the feed solutions. For example, for 20UD membrane, permeate flux was 109 L/m^{2}h for the feed solution of 1% clay and SBR. Permeate flux was increased to 140 L/m^{2}h when the feed solution contained only 0.87% of clay. As unmodified membranes did not have any charges, the only possible reason for the higher flux was the decrease in fouling in the absence of SBR.

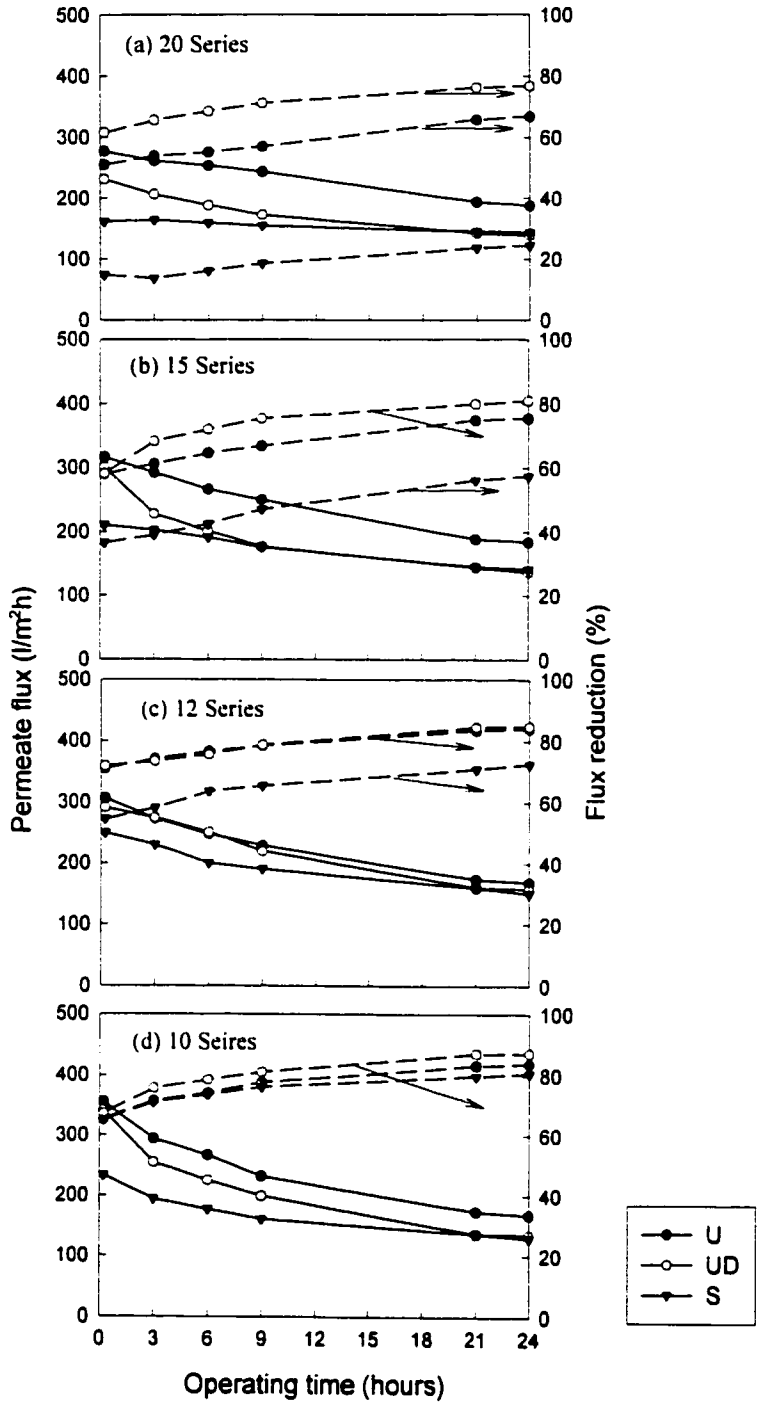

Figure 7.4. Permeate flux and flux reduction with time for different membranes, (a) 20 Series, (b) 15 Series, (c) 12 Series and (d) 10 Series
Feed concentration – 0.87% of clay, Operating pressure – 345 kPa

In the case of sulfonated membranes, the higher flux could be due to 1) more repulsion between clay particles (having no SBR layer on them) and the negatively charged sulfonated membrane surface; and 2) less fouling in the absence of SBR.

From Figures 7.2, 7.3 and 7.4, it can be concluded that the flux reduction for unmodified dried membranes (UD) was slightly higher than that for unmodified wet membranes (U), although differences were not significant. Therefore, it can be stated that the performance of the glycerol treated dried membrane (UD) was similar to that of the unmodified wet membrane (U).

Figure 7.5 shows the comparison of the permeate fluxes of 20UD and 12S membranes for different feed concentrations. It should be noted that 20UD and 12S membranes are alike in terms of their MWCO (20,000 Daltons each), mean pore sizes (3.36 nm and 3.44 nm, respectively) and geometrical standard deviations (2.29 and 2.32, respectively) (Table 5.1). The only difference is that 12S membrane is negatively charged as it is coated with a thin layer of SPPO polymer. Permeate fluxes for the 12S membrane were higher compared to the 20UD membrane for all the three feed solutions. This indicates that charged SPPO coated membranes have higher fluxes compared to the uncharged ultrafiltration membrane of similar mean pore size and pore size distribution. Figure 7.6 shows the flux reductions for 20 series membranes for all three feed solutions. Flux reductions with SPPO coated membranes for all the feed solutions were always lower compared to the unmodified membrane. The flux reduction of the 20S membrane with a 1% feed solution was lower than the flux reduction of 20U membrane with even a 0.1% feed solution.

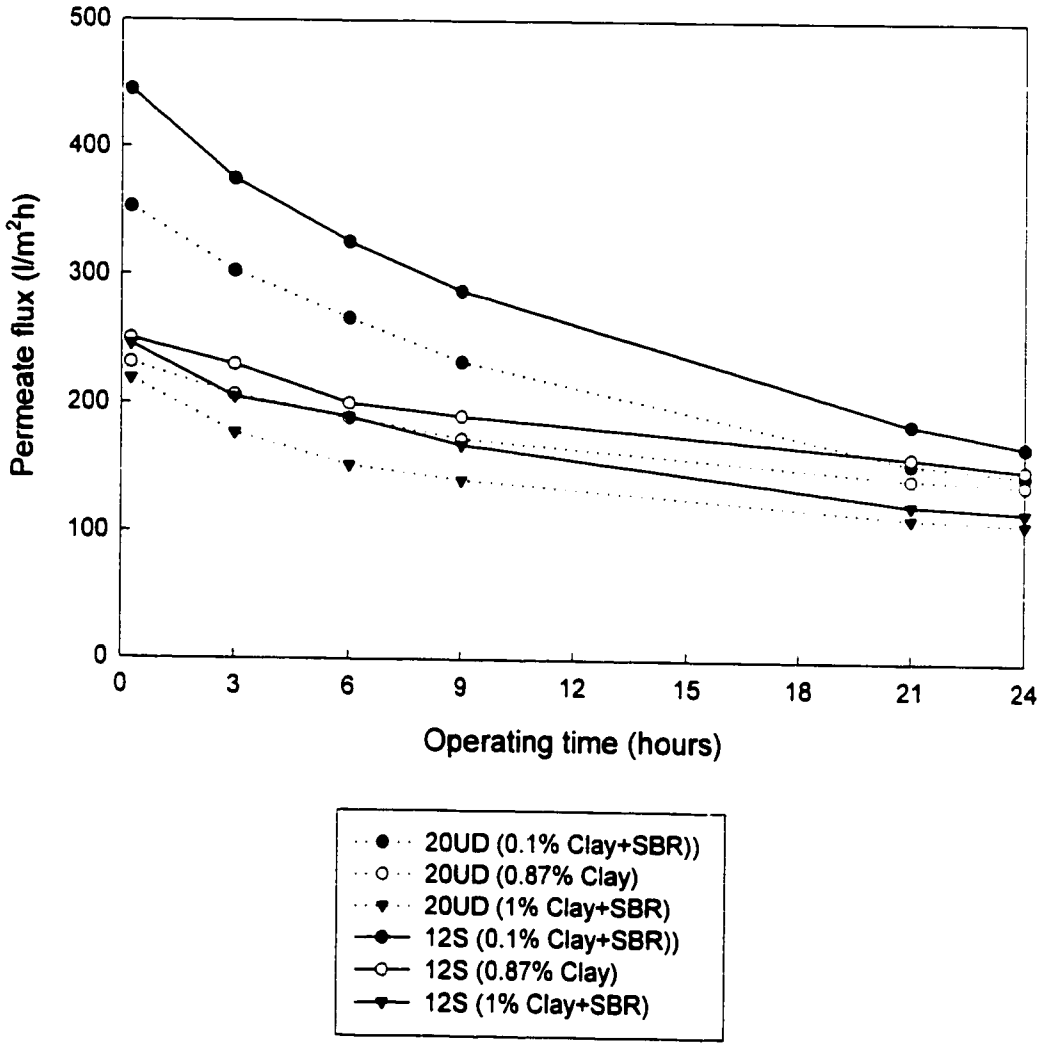

Figure 7.5. Comparison of permeate flux of unmodified (20UD) and SPPO coated (12S) membranes for different feed concentrations

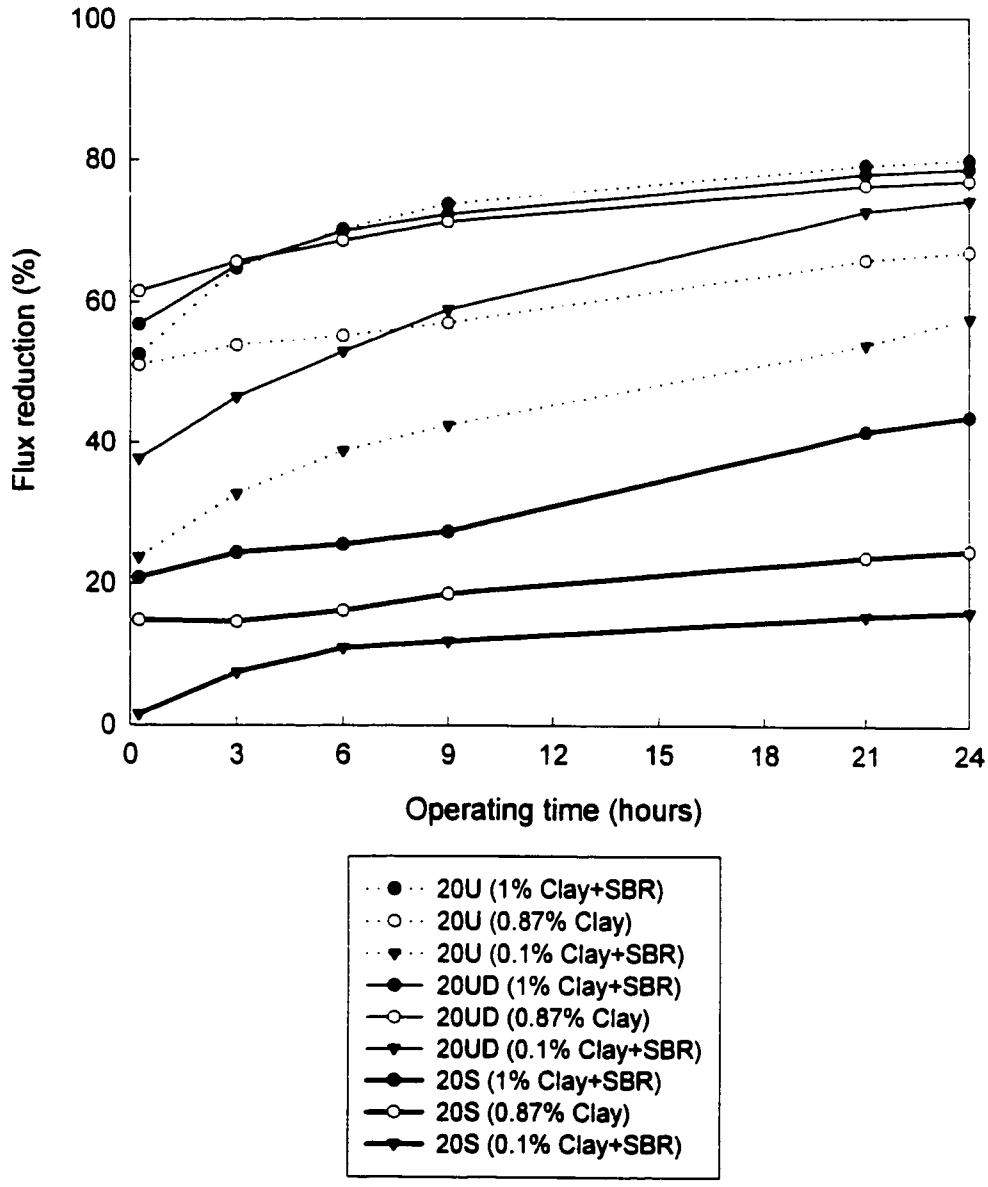

Figure 7.6. Comparison of flux reduction of 20 Series membranes for different feed concentrations

7.3. Fouling

7.3.1. Fouling resistance

The fouling restricts the permeate flow through the membrane. A very sharp flux reduction was observed in the beginning of the experiment for all the membranes used, including SPPO coated membranes. A dynamic membrane was formed over an original membrane by the cake layer formation. The cake layer exhibited very high resistance to the permeate flow. Resistance to the permeate flow can be divided into the following two components.

1. Resistance contributed by the polymeric membrane (R_m), and
2. Resistance contributed by fouling (R_f)

It is to be noted that a simplistic approach, different from the one discussed in Chapter 3, is adopted to calculate the values of R_f and R_m. Since the membranes were not cleaned after use, it was not possible to calculate the resistance due to pore blocking. Instead, the total resistance due to fouling (R_f) was calculated. The following was the approach used to calculate the value of R_m and R_f.

$$J_w = \frac{\Delta p}{\eta R_m} \tag{7.1}$$

$$J_{p_{24}} = \frac{\Delta p}{\eta (R_m + R_f)} \tag{7.2}$$

On rearranging Eqs. (7.1) and (7.2), we obtain

$$R_m = \frac{\Delta p}{\eta J_w} \tag{7.3}$$

$$R_f = \frac{\Delta p}{\eta}\left(\frac{1}{J_{p_{24}}} - \frac{1}{J_w}\right) \tag{7.4}$$

where Δp, η, J_w, and $J_{p_{24}}$ are the operating pressure, water viscosity, pure water permeation flux and product flux after 24 hours of operation, respectively. The values of the resistances

contributed by the membrane (R_m) and by fouling (R_f) after 24 hours of operation were calculated from Eqs. (7.3) and (7.4) for different membranes with various feed solutions, and the results are tabulated in Table 7.1. The table shows that the resistance due to fouling (R_f) is lower for most of the SPPO coated membranes compared to the unmodified membranes. This leads to a conclusion that fouling was reduced when the membrane was coated with SPPO. It is also evident from this table that R_f for all the membranes was lower with the feed concentration of 0.1% compared to that with the feed concentration of 1%. For example, R_f values of the 20U, 20UD and 20S membranes were 3.87×10^{12} m^{-1}, 7.01×10^{12} m^{-1} and 2.00×10^{12} m^{-1}, respectively, corresponding to the feed concentration of 0.1%, while they were 9.27×10^{12} m^{-1}, 10.00×10^{12} m^{-1} and 6.55×10^{12} m^{-1} respectively at a feed concentration of 1%. It confirms that the fouling was higher for the higher feed concentration.

Comparing the resistances contributed by the membrane (R_m) and by fouling (R_f), R_f is substantially higher for most of the membranes except 20S and 15S and hence is the controlling factor to the permeate flow. This is also confirmed by the permeate flux data as they were very similar for different membranes at a given feed concentration. Nuortila-Jokinen et al. (1995a) also found that the permeate flux was independent of membrane types (MWCO and pore size).

7.3.2. Cross-sectional images of used membranes

SEM pictures of the used membranes (Figure 7.7) show that a substantial amount of cake layer was deposited even onto the SPPO coated membranes when the feed solution contained 1% of clay and SBR. However, no cake layer was observed on the 20S membrane when the feed solution contained 0.1% of clay and SBR.

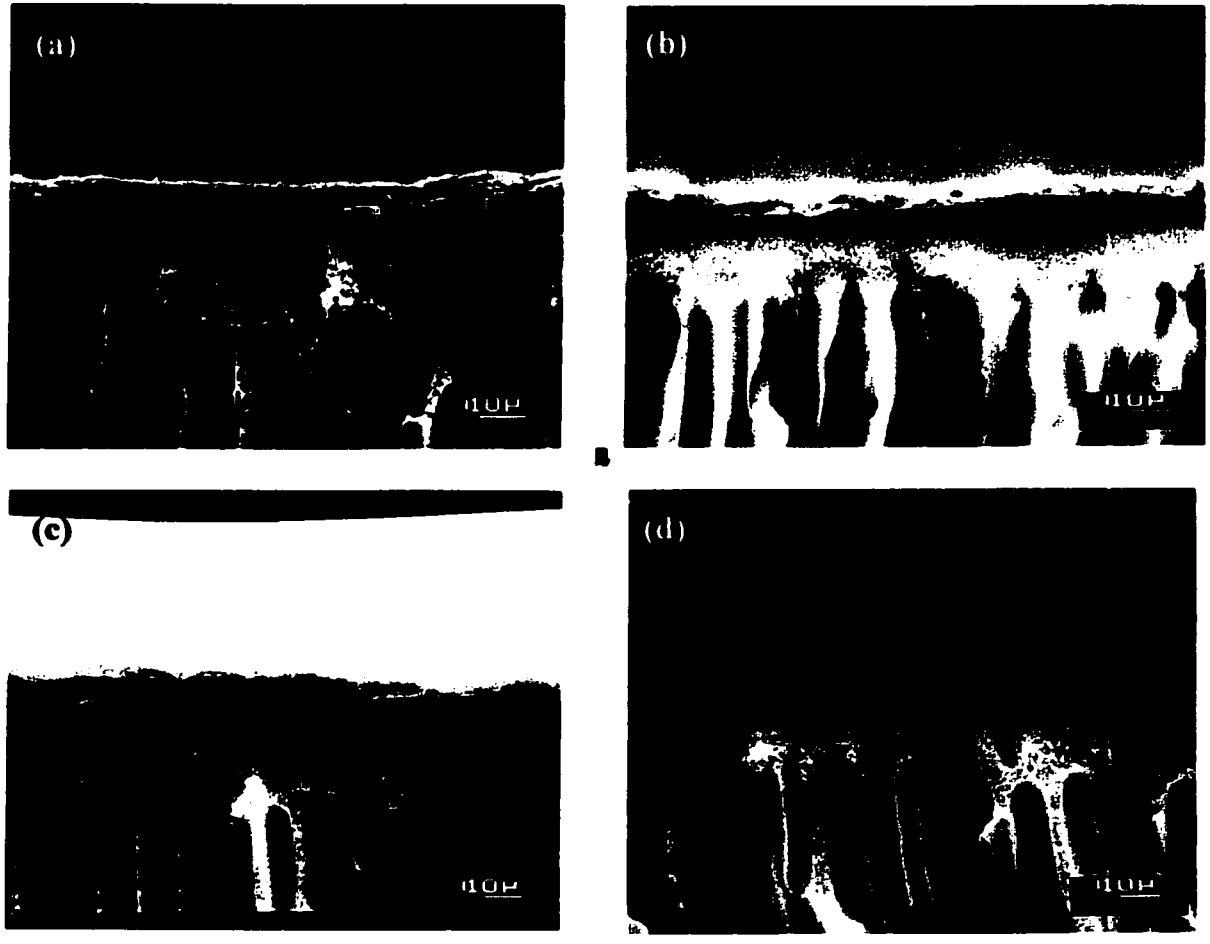

Figure 7.7. Cross-sectional SEM pictures of the fouled membranes used for ultrafiltration experiment. (a)20UD, Feed conc. – 1%, (b) 20S, Feed conc. – 1,% (c) 20UD, Feed conc. – 0.1%, and (d) 20S, Feed conc. – 0.1%. Feed solution contained clay and SBR.

Table 7.1. Resistances to the permeate flow of unmodified and modified membranes for various feed concentrations

Membrane	Feed -1% of clay+SBR		Feed -0.1% of clay+SBR		Feed -0.87% of clay	
	Resistance (m^{-1})		Resistance (m^{-1})		Resistance (m^{-1})	
	$R_m \times 10^{-12}$	$R_f \times 10^{-12}$	$R_m \times 10^{-12}$	$R_f \times 10^{-12}$	$R_m \times 10^{-12}$	$R_f \times 10^{-12}$
20U	2.35	9.27	2.85	3.87	2.45	4.94
20UD	2.74	10.00	2.45	7.01	2.31	7.60
20S	8.46	6.55	10.50	2.00	7.29	2.37
15U	1.78	6.32	1.64	4.55	1.84	5.70
15UD	1.64	10.06	1.50	7.20	1.93	8.23
15S	3.62	5.61	4.93	4.44	4.18	5.65
12U	1.54	10.10	1.55	5.86	1.31	6.91
12UD	1.44	11.50	1.35	7.74	1.34	7.44
12S	1.87	9.90	2.90	5.33	2.52	6.67
10U	1.29	8.16	1.37	6.89	1.35	6.94
10UD	1.27	12.40	1.26	7.67	1.33	9.00
10S	1.92	10.20	2.74	5.82	2.07	8.64

7.4. Clay and SBR separation

No traces of clay were found in the permeate for all the membranes studied. Separation of SBR was more than 94% in all the experiments as given in Table 7.2. Separation of SBR was almost independent of the membrane used. These results are in good agreement with those of Woerner and Short (1991).

Table 7.2. SBR Content (in terms of Total Organic Carbon, TOC) in the feed and in the permeate for the feed solutions of 1% and 0.1% of Clay and SBR

Membrane Types	Feed Solution – 1%			Feed Solution - 0.1%		
	Feed TOC (ppm)	Permeate TOC (ppm)	Separation f (%)	Feed TOC (ppm)	Permeate TOC (ppm)	Separation f (%)
20U	1054	4.30	99.6	105.4	2.13	98.0
20UD	1054	4.36	99.6	105.4	2.32	97.8
20S	1054	4.25	99.6	105.4	5.10	95.2
15U	1054	4.33	99.6	105.4	2.02	98.1
15UD	1054	3.72	99.7	105.4	2.53	97.6
15S	1054	3.92	99.6	105.4	6.19	94.1
12U	1054	4.91	99.5	105.4	1.64	98.4
12UD	1054	4.50	99.6	105.4	3.84	96.4
12S	1054	4.97	99.5	105.4	6.08	94.2
10U	1054	5.13	99.5	105.4	1.88	98.2
10UD	1054	4.42	99.6	105.4	2.65	97.5
10S	1054	5.11	99.5	105.4	4.94	95.3

7.5. Conclusions

Pure water permeation of ultrafiltration membranes made of polyethersulfone was substantially reduced when a thin layer of SPPO material was coated on their surface. A very sharp flux reduction was observed immediately after the start of the experiment for most of the membranes including SPPO coated membranes. However, the flux reduction was lower for the SPPO coated membranes. The permeate flux became higher when SBR was not present in the feed. No significant differences were found in the performance of never-dried wet membranes and glycerol-treated dried membranes.

Cake formation was quite substantial on the membrane surface, including the SPPO coated membranes. The resistance to the permeate flow due to fouling was quite high compared to that of the membrane. The resistance of the fouling was, however, lower for the SPPO coated membranes compared to the unmodified membranes. No traces of clay were found in the permeate water. The SBR separation was higher than 94%.

CHAPTER 8

Fouling Study: I. Cake Formation

8.1. Fouling study

The following ultrafiltration experiments were conducted with 'UD' and 'S' membranes of all four series. Experiments were performed at an operating pressure of 345 kPa.

1. **Membrane – UD:** Ultrafiltration experiment with a feed solution containing 1% of clay and SBR (Clay/SBR = 100/15) and 200 ppm of sodium chloride
2. **Membrane – UD:** Ultrafiltration experiment with a feed solution containing 0.87% of clay and 200 ppm of sodium chloride
3. **Membrane – S:** Ultrafiltration experiment with a feed solution containing 0.87% of clay and 200 ppm of sodium chloride

In each experiment, fresh membranes were used. Membranes which were freshly mounted on the permeation cells are referred to as 'virgin membranes'. After compacting at 552 kPa for 5 hours, the pure water permeation rate was measured for each membrane. First, sodium chloride separation was performed with each virgin membrane at the operating pressure of 345 kPa and a feed concentration of 200 ppm of NaCl. Then, a separation experiment was performed with the feed solution containing either 0.87% of clay and 200 ppm of NaCl, or 1% of clay and SBR and 200 ppm of NaCl. The above experiment was performed for 24

hours, and during this time the feed and the permeate were recycled to the feed tank. Feed and permeate samples were collected from time to time and the sodium chloride concentration was determined as per the procedure described in Chapter 4. Thus, the sodium chloride separation could be obtained by Eq. (4.1) as a function of operating time. The permeate flux was also measured as a function of time. The data of sodium chloride separation and permeate flux after 24 hours of ultrafiltration experiment are called hereafter as 'final NaCl (or sodium chloride or salt) separation' and 'final permeate flux', respectively. The membranes were then flushed with tap water of 45^0C for half an hour and then with distilled water for another half an hour at 70 kPa and at a feed flow rate of 4000 mL/min. Membranes after cleaning are referred to hereafter as 'fouled membranes'. Sodium chloride separation of the fouled membranes was also determined in the same way as for virgin membranes. Pure water permeation of the fouled membranes was also measured.

8.1.1. Resistances to the permeate flow

As discussed in the theoretical section (Chapter 3), it was not possible to calculate the absolute values of R_m, R_p, R'_p and R_c. In order to make the calculation possible, the value of R_p should be assumed between R_1 and $R_1R_2/(R_2-R_1)$, as per Eq. (3.39). Therefore R_p was chosen as the average of R_1 and $R_1R_2/(R_2-R_1)$ and the values of R_m, R'_p and R_c were obtained. The results are given in Table 8.1. The following inferences can be made from the value of the resistances presented in Table 8.1.

Table 8.1. Values of the resistances due to membrane matrix (R_m), due to pores (R_p), due to pores after partial plugging (R'_p) and due to cake layer (R_c) after ultrafiltration experiment for 24 hours

Membrane code	Feed solution	R_m $\times 10^{-12}$ (m^{-1})	R_p $\times 10^{-12}$ (m^{-1})	R'_p $\times 10^{-12}$ (m^{-1})	$(R'_p - R_p)$ $\times 10^{-12}$ (m^{-1})	R_c $\times 10^{-12}$ (m^{-1})	R_p/R_m
20UD	1*	4.76	6.55	17.87	11.32	17.90	1.38
20UD	2**	4.64	7.84	20.33	12.48	13.78	1.69
20S	2	6.63	-	-	-	10.33	
15UD	1	4.53	2.68	9.90	7.21	15.78	0.59
15UD	2	3.63	2.96	9.55	6.59	14.20	0.81
15S	2	5.94	24.13	54.19	30.06	10.66	4.07
12UD	1	4.37	2.47	9.31	6.84	19.18	0.56
12UD	2	3.52	2.24	8.00	5.76	15.88	0.64
12S	2	4.40	11.36	27.12	15.76	16.77	2.58
10UD	1	4.01	1.93	7.86	5.93	17.00	0.48
10UD	2	2.90	1.91	6.73	4.82	14.95	0.66
10S	2	5.25	4.94	15.14	10.19	13.11	0.94

1* 1% of clay and SBR (clay/SBR = 100/15) + 200 ppm of NaCl
2** 0.87% of clay + 200 ppm of NaCl

1. The cake layer resistance (R_c) was higher when SBR was present in the feed solution for all the membranes studied.
2. R_c was lower for 'S' membranes compared to 'UD' membranes. Therefore, it can be stated that 'S' membranes did not have as much cake layer formation as 'UD' membranes had. It should be noted that the value of R_c was independent of the value of R_p (assumed).

3. Both R_p and R'_p were higher for the membranes which had smaller pore sizes such as 20 series and 15 series membranes. This is understandable since smaller pores have higher resistance to the flow of permeate. Pore resistance (R_p) increased substantially upon coating of a thin SPPO layer on 'UD' membranes. In other words, 'S' membranes have higher pore resistance than 'UD' membranes. For example, R_p increased from 2.96×10^{12} m^{-1} to 24.13×10^{12} m^{-1} for 15 series, from 2.24×10^{12} m^{-1} to 11.36×10^{12} m^{-1} for 12 series and from 1.91×10^{12} m^{-1} to 4.94×10^{12} m^{-1} for 10 series membranes.
4. The ratio of R_p/R_m was higher for 'S' membranes compared to 'UD' membranes, indicating that on coating, the increase in R_p was higher than the increase in R_m. Also, this ratio was higher for the membranes having smaller pore sizes.

Although R_m and R'_p depended on the value chosen for R_p between R_1 and $R_1R_2/(R_2 - R_1)$, the above mentioned trends remained the same.

8.1.2. Sodium chloride separation versus operating time

8.1.2.1. 'UD' membranes

As expected, the sodium chloride separations of virgin 'UD' membranes were very low (2.3 to 5.5%) (Figure 8.1). However, when separation experiments were carried out with the feed solution containing 0.87% of clay and 200 ppm of NaCl, NaCl separation increased steeply within 5 min of operation. For example, NaCl separation went up to 26.8% for 20UD, 28.9% for 15UD, 25.5% for 12UD and 26.2% for 10UD after 5 min (Figure 8.2). NaCl separation was even higher when the feed solutions contained both clay and SBR. For instance, NaCl separations were 42.6% for 20UD, 39.6% for 15UD, 34.7% for 12UD and 31.4% for 10UD

8.1(a). 20 Series

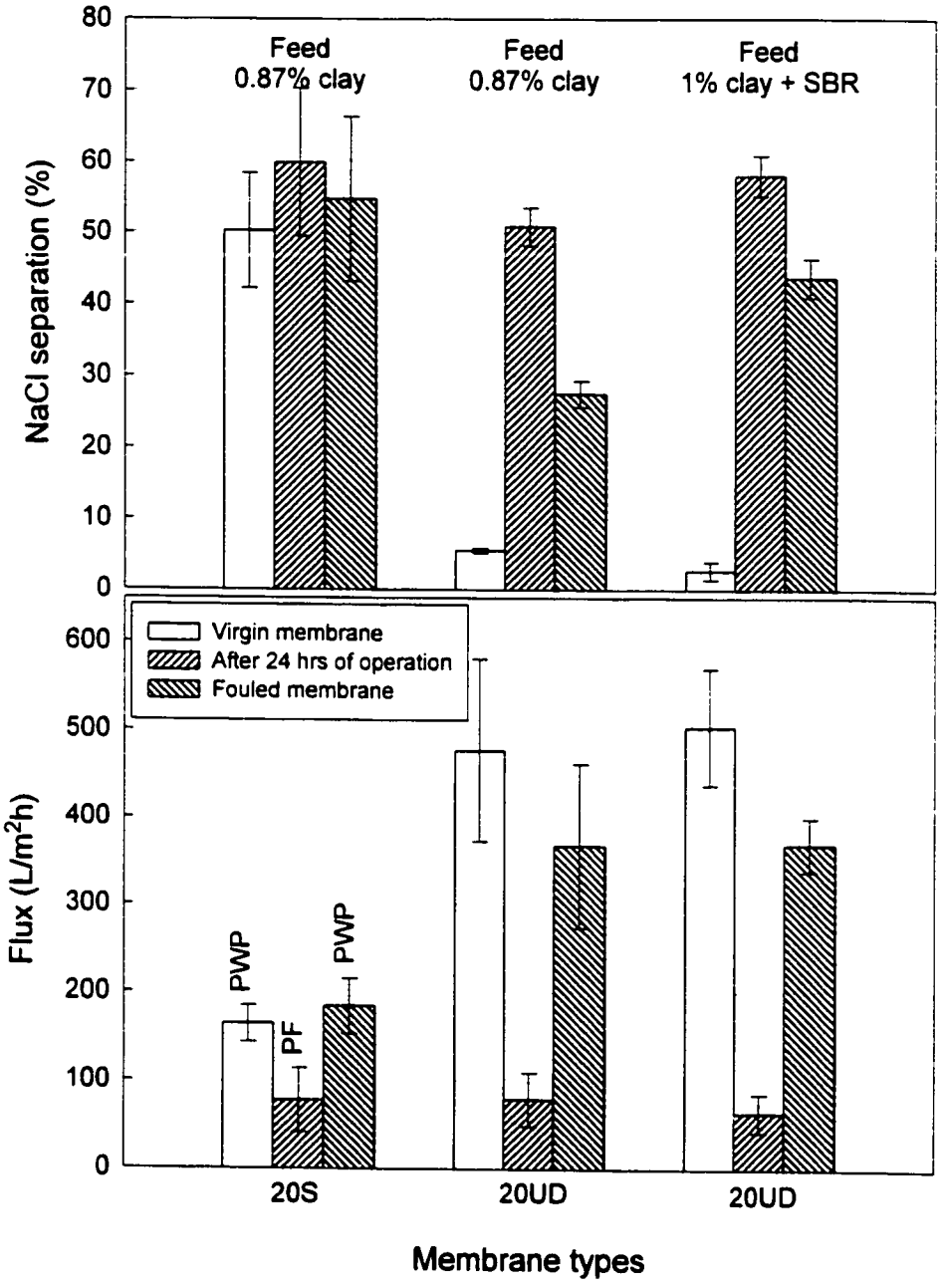

8.1(b). 15 Series

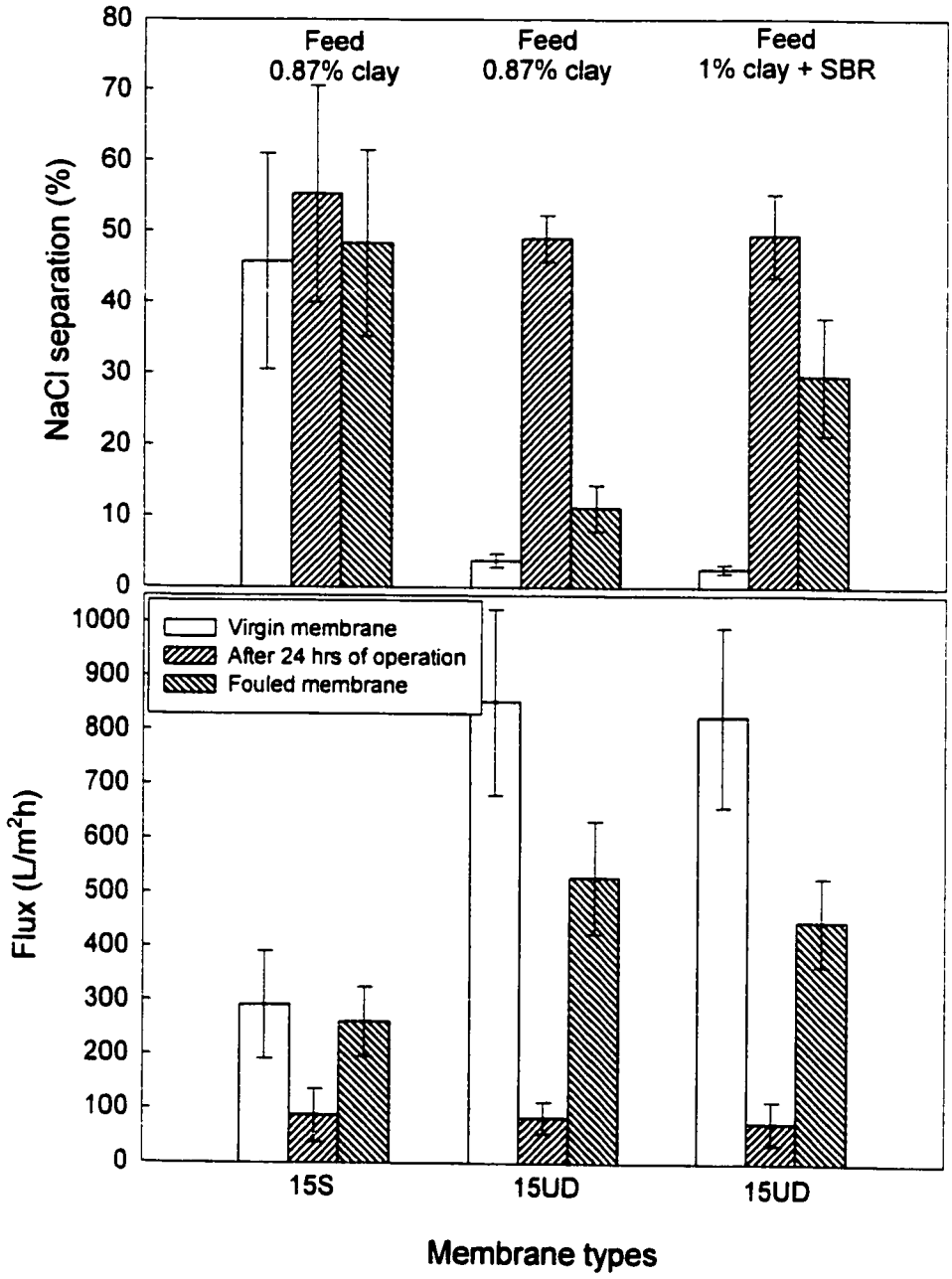

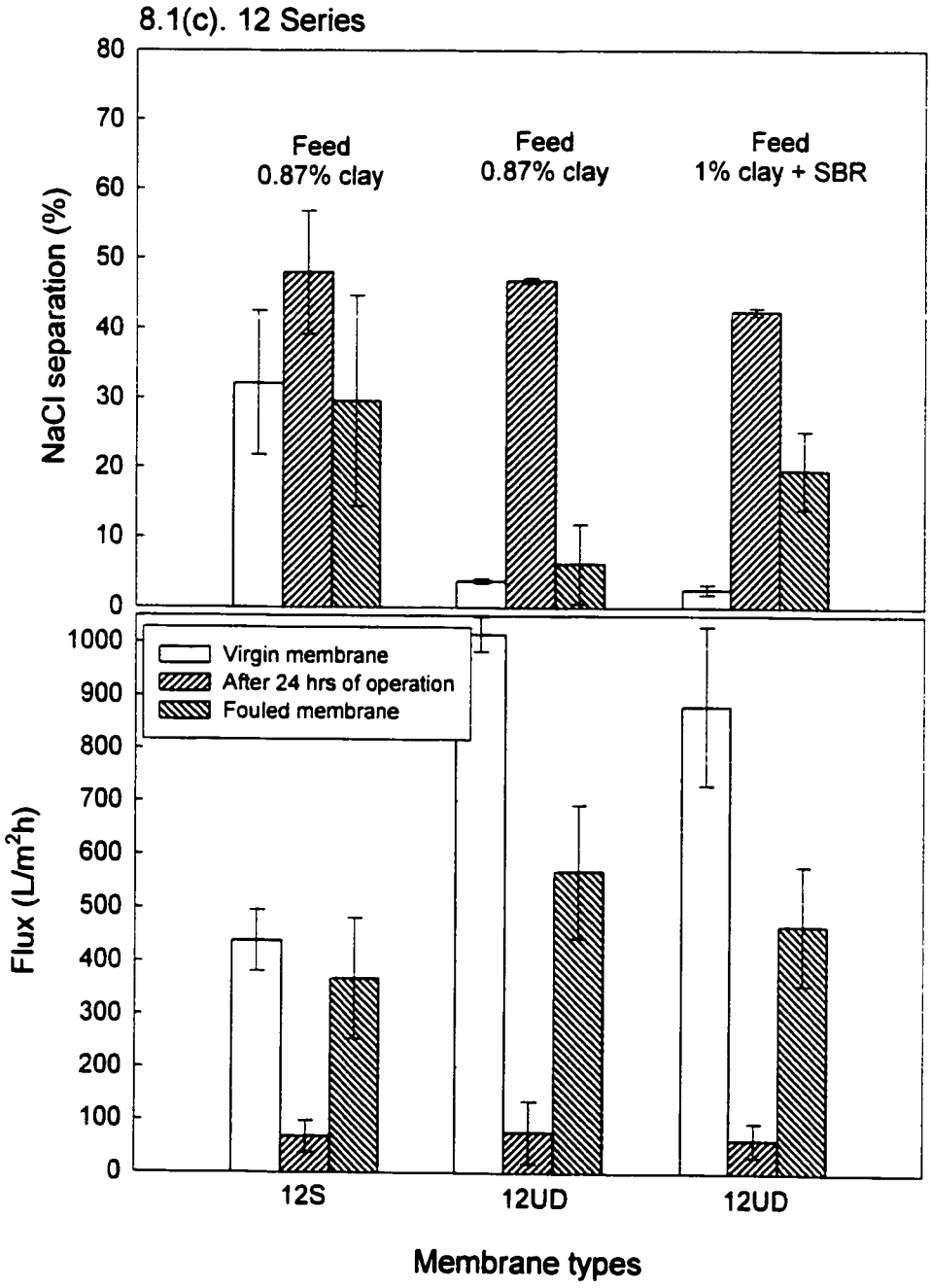
8.1(c). 12 Series
NaCl separation (%)
Feed
0.87% clay
Feed
0.87% clay
Feed
1% clay + SBR
Virgin membrane
After 24 hrs of operation
Fouled membrane
Flux (L/m2h)
12S
12UD
12UD
Membrane types

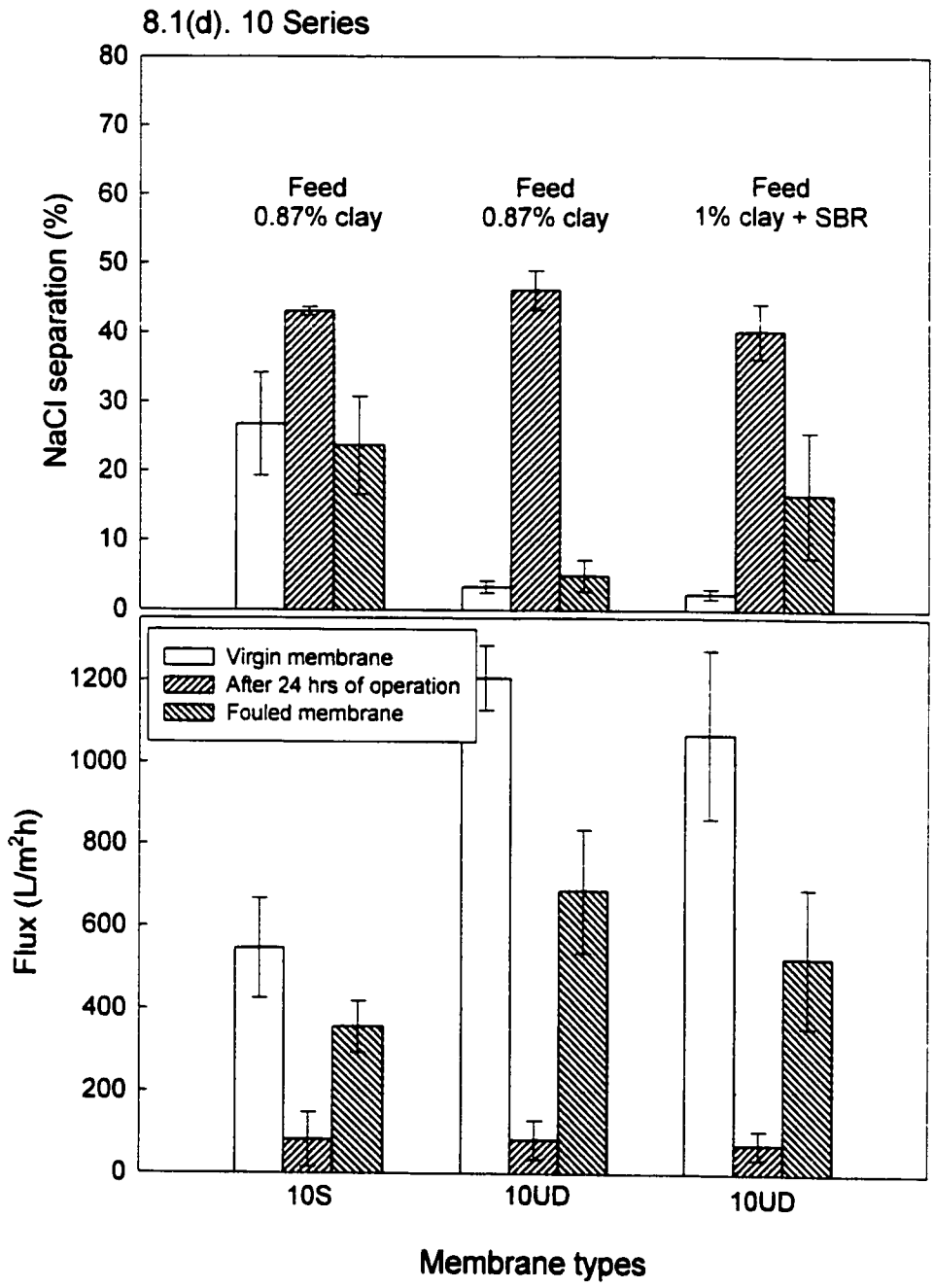

Figure 8.1. Pure water permeation (PWP) of virgin and fouled membranes, final permeate flux (PF) after 24 hours of operation and NaCl separation of various membranes (a) 20 Series, (b) 15 Series, (c) 12 Series and (d) 10 Series

NaCl concentration in the feed – 200 ppm, (Error bars indicate 95% confidence interval)

8.2(a). 20 Series

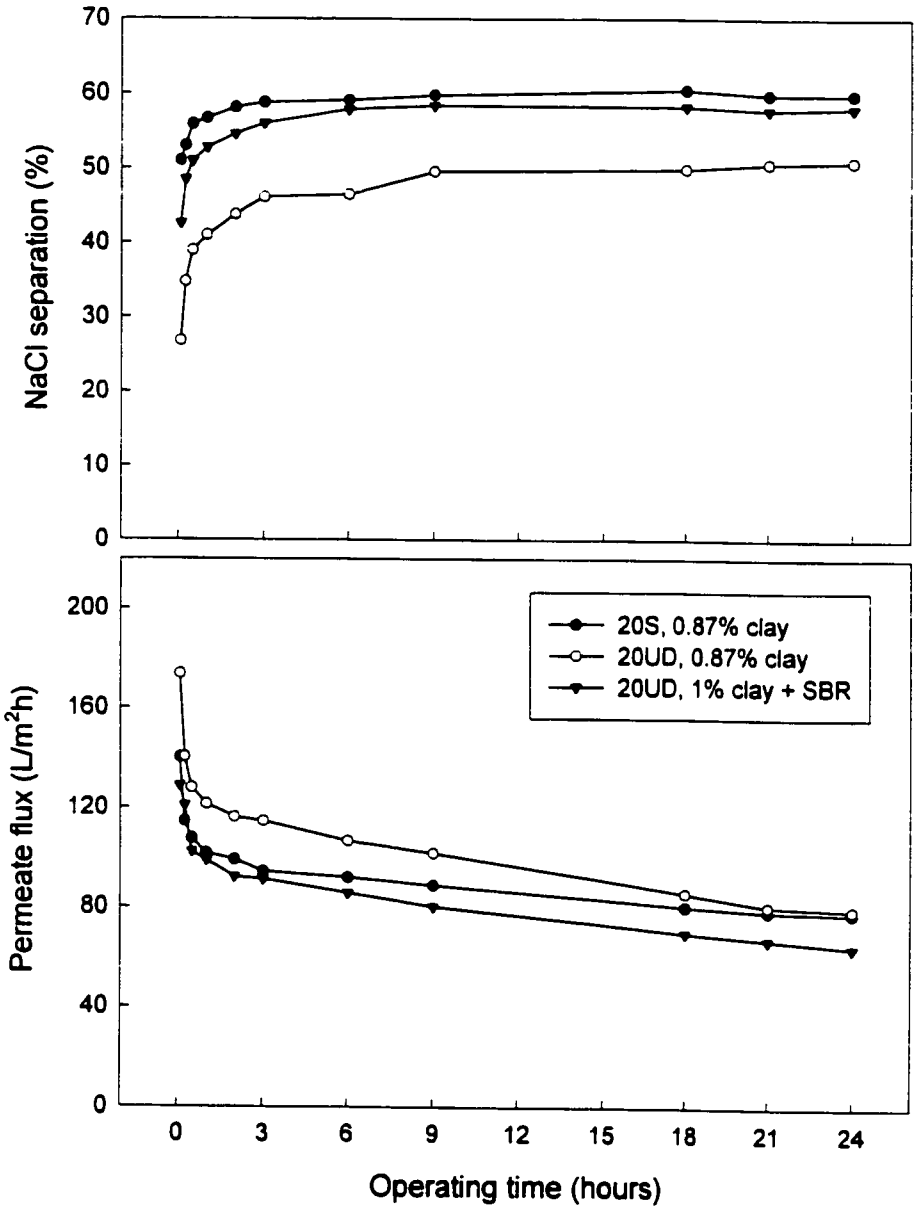

8.2(b). 15 Series

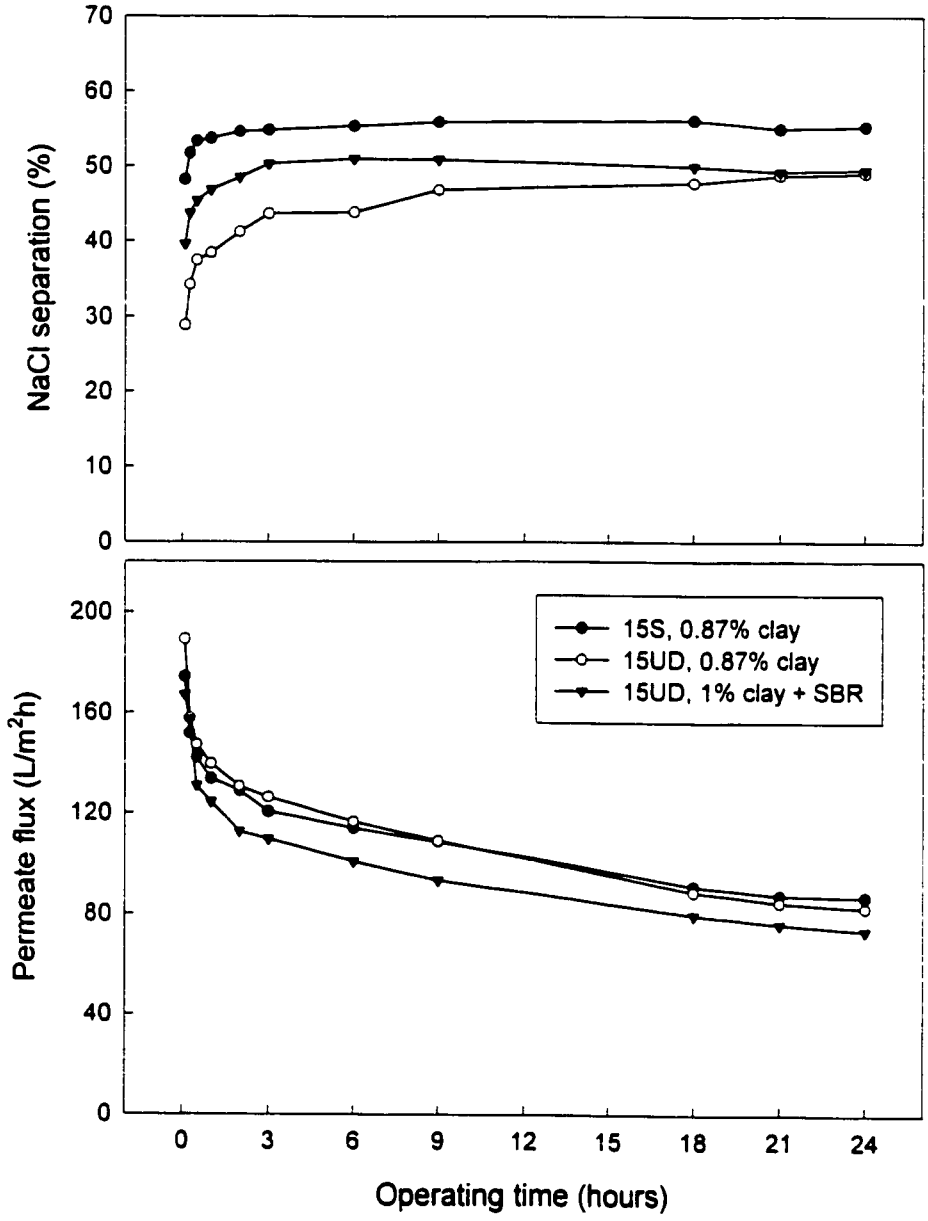

8.2(c). 12 Series

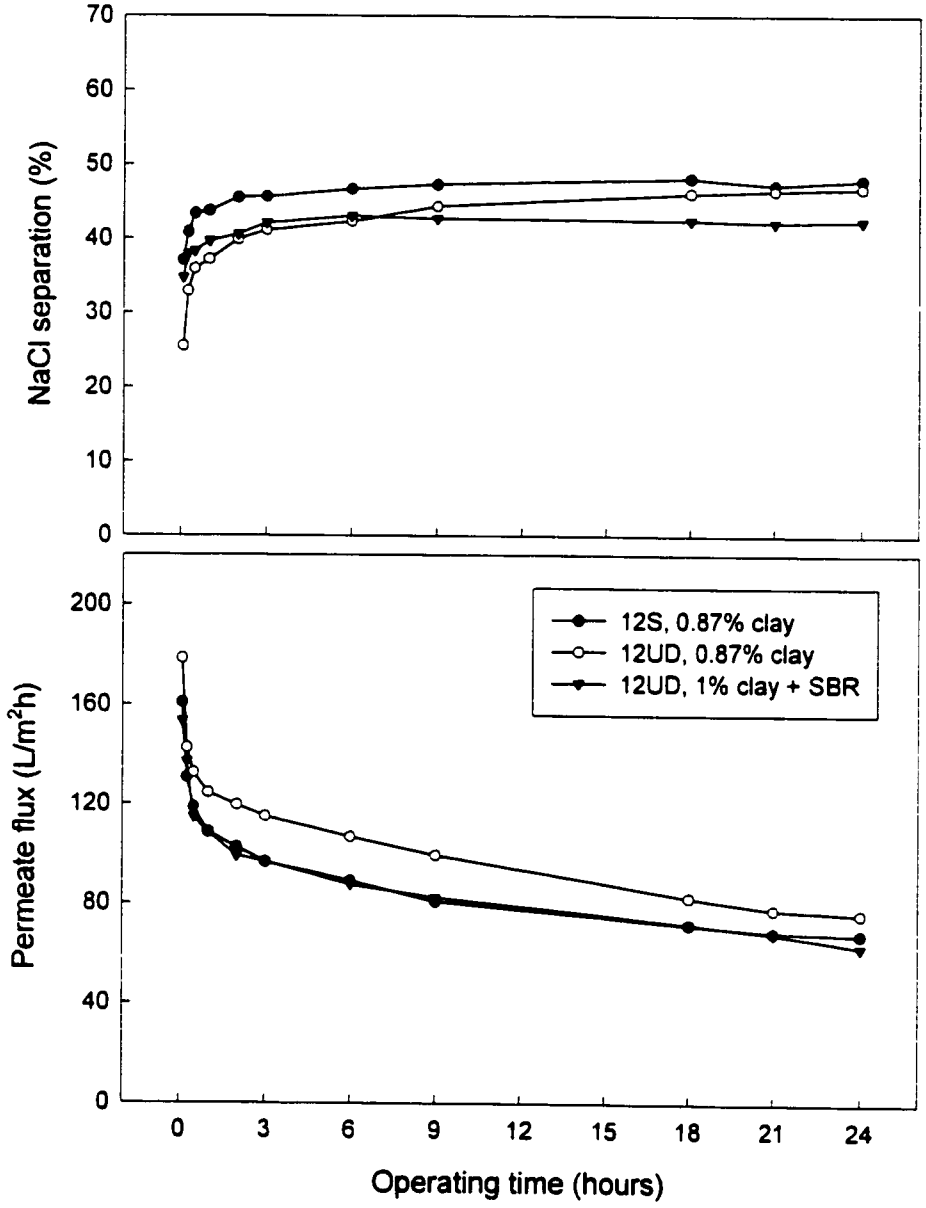

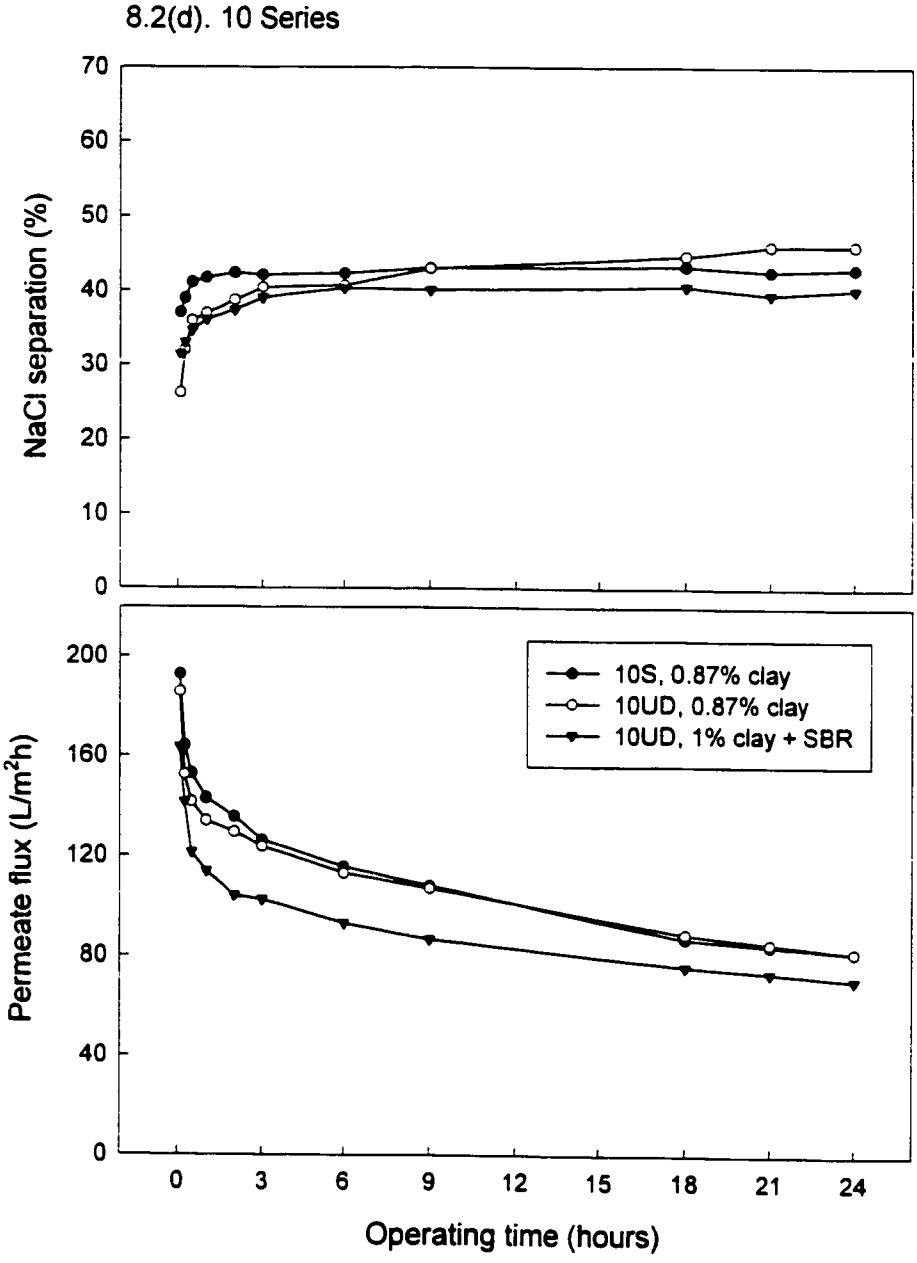

Figure 8.2. NaCl separation and permeate flux versus operating time for different feed solutions and membranes (a) 20 Series, (b) 15 Series, (c) 12 Series and (d) 10 Series. (First data point corresponds to 5 min of operation for each membrane)
NaCl concentration in the feed – 200 ppm

after 5 min of operation (Figure 8.2). Higher NaCl separations were mainly due to the partial pore plugging and the extra resistance exerted by the cake layer built on the membrane surface. SBR, when present in the feed solution, not only enhanced the deposition of clay particles on the membrane surface but also made the cake layer more compact. Moreover, in the presence of SBR, the clay particles were coated with a layer of SBR on their surface and tended to agglomerate as shown in the AFM micrograph (Figure 8.3a) of the membrane used for treating clay and SBR solution. The size of each agglomerate is about 2.5 μm containing 20 to 30 individual clay particles. No such agglomeration was observed when the feed solution contained clay only (Figure 8.3b).

The final NaCl separations were in the range of 46.1 to 50.9% when clay was present in the feed solution and were in the range of 40.2 to 58.1 % when both clay and SBR were present in the feed solution (Figure 8.1). It can also be noticed that the range of the final permeate fluxes (63 to 83 L/m^2h) is much smaller than that of the pure water permeation (476 to 1205 L/m^2h) of 'UD' membranes (Figure 8.1). This is understandable as it was the fouling resistance R_c and R'_p that controlled the permeate flux. It is to be noted that the fouling resistance after 24 hours of operation was substantially higher than the resistance of the membrane itself.

Figure 8.1, shows that the PWPs of the fouled 'UD' membranes are lower than those of their respective virgin membranes. This indicates that some irreversible fouling took place. Probably foulants in the pore that were not removed during the membrane washing process caused the irreversible fouling. NaCl separation of the fouled 20UD membrane which was

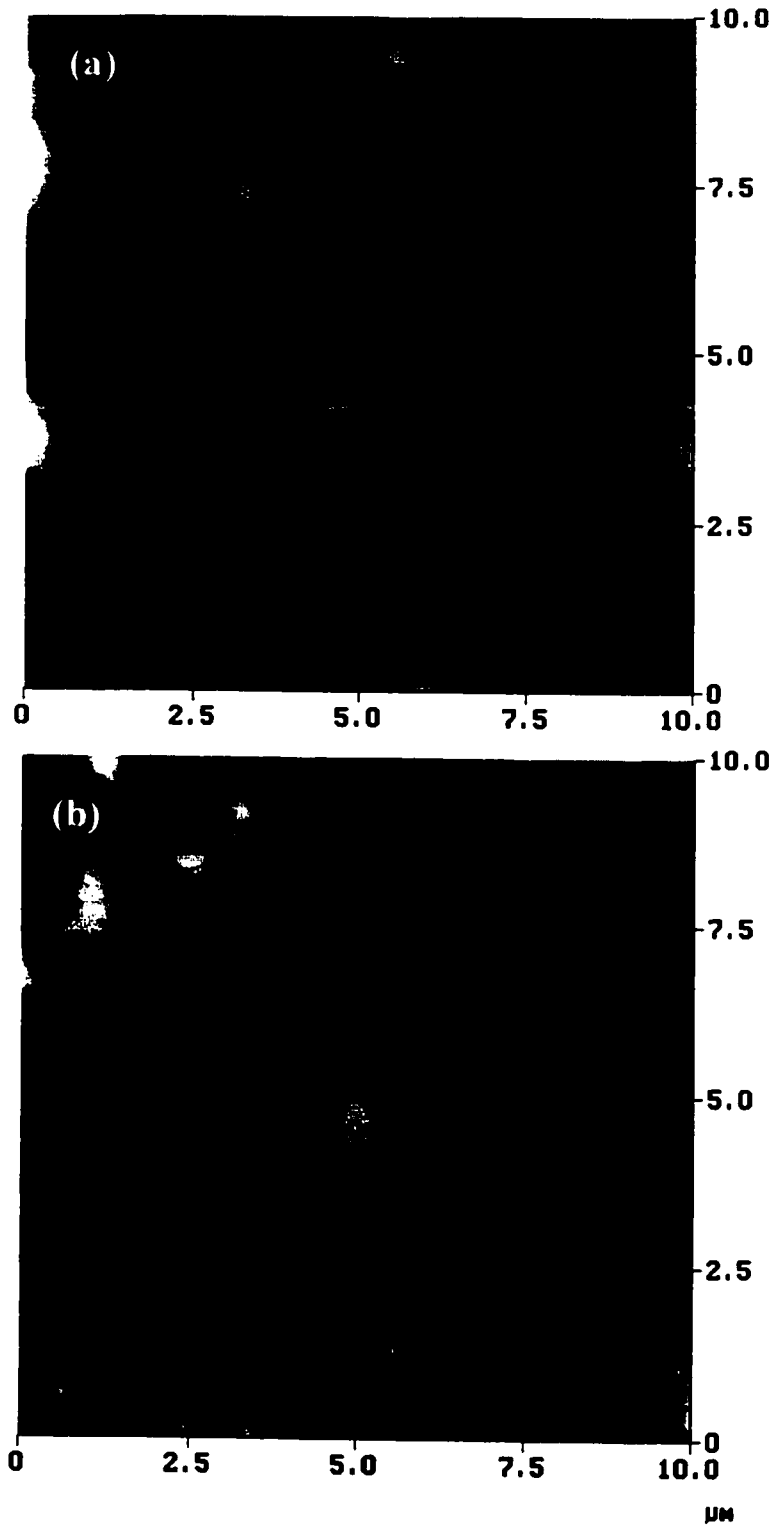

Figure 8.3. AFM micrographs of the surface of 20UD membrane used for 24 hours for treating (a) feed solution containing 1% of clay and SBR and (b) feed solution containing 0.87% of clay

used to treat the feed solution with 0.87% of clay was 27.5% while that of the virgin 20UD membrane was 5.5%. For other fouled membranes (15UD, 12UD and 10UD), the increase in the NaCl separation was not significant. Some of the large pores in 20UD membrane may have been blocked during ultrafiltration of the clay solution, thus reducing the effective pore sizes of the membrane. As for other fouled membranes, large pores seemed to remain unplugged.

Sodium chloride separations of all the fouled membranes which were used to treat a feed solution with 1% of clay and SBR were appreciably higher than those of their respective virgin membranes. For example, NaCl separation was increased from 2.7 to 43.6% for 20UD, 2.6 to 29.6% for 15UD, 2.6 to 19.6% for 12UD and 2.3 to 16.7% for 10UD membranes (Figure 8.1). PWPs of the fouled membranes which were used to treat the feed solution containing clay and SBR were lower than those of the fouled membranes which were used to treat the feed solution containing clay only, except for the 20UD membrane. On the other hand, NaCl separations of the former fouled membranes were higher than the latter fouled membranes. Apparently, the irreversible fouling was enhanced by the presence of SBR. It should be noted that the surface of the membranes was flushed with warm tap water and with distilled water to wash the membranes. Figure 8.1 shows that PWP could be partially recovered by flushing the membrane surface with water.

Sodium chloride separation and permeate flux as a function of operating time are shown in Figure 8.2. It can be seen that the curves representing permeate flux and NaCl separation are mirror images to each other. Permeate flux decreased and NaCl separation increased in the beginning of the experiment and then leveled off.

8.1.2.2. 'S' membranes

Sodium chloride separations were higher for virgin 'S' membranes (26.8 to 50.1%) compared to virgin 'UD' membranes (2.3 to 5.5%). High NaCl separation for 'S' membranes was partially due to the repulsive force between chloride ions and negatively charged sulfonate substituents on the membrane surface. High NaCl rejection was also observed by Chowdhury et al. (1994) when a polysulfone ultrafiltration membrane was coated with a thin layer of SPPO polymer with an IEC value of 2.0 meq/g of dry powder. The average pore sizes were also smaller (0.7 nm for 20S to 7.10 nm for 10S) in 'S' membranes than in 'UD' membranes (3.36 nm for 20UD to 10.38 nm for 10UD) (Table 5.1).

There was no significant increase in the NaCl separation in the first 5 min for 20S and 15S membranes while treating a feed solution containing 0.87% of clay and 200 ppm of NaCl. For instance, for 20S and 15S membranes, NaCl separations were 51.0 and 48.2% after 5 min of operation while they were 50.1 and 45.8% for their virgin membranes, respectively. The increase in NaCl separation was modest for 12S (from 32.1 to 37.1%) and 10S (from 26.8 to 37.0%) membranes. It should be recalled that there was a steep increase in NaCl separation for 'UD' membranes when they were used to treat the same feed solution. The following could be possible reasons for the different behavior of 'S' membranes.

Due to the repulsive force between clay particles and the negatively charged 'S' membrane, there was less cake layer build-up on the membrane surface. It was confirmed by the cake layer resistance (R_c) of 'S' membranes, which were lower than those of 'UD' membranes (Table 8.1). Although the formation of the cake layer increased the NaCl separation as observed for 'UD' membranes, the effective repulsive force between the membrane surface

and chloride ions, on the other hand, was reduced, resulting in a decrease in the NaCl separation.

The final NaCl separations were 59.9% for 20S, 55.3% for 15S, 48.0% for 12S and 43.0% for 10S (Figure 8.1). The final permeate fluxes (in terms of the percent of PWP of the virgin membrane) were 47% for 20S, 30% for 15S, 15% for both 12S and 10S membranes. NaCl separations for the fouled 'S' membranes were similar to those of their respective virgin membranes. PWPs of the fouled membranes were also not very different from their virgin membranes except for 10S membrane. For example, recovery of PWPs (PWP of the fouled membrane divided by PWP of the virgin membrane) was 112% for 20S, 89% for 15S, 84% for 12S and 65% for 10S. These results indicate that there was not much irreversible fouling in these membranes. No significant differences were found between the pore sizes of fouled and virgin 'S' membranes (Table 10.1, Chapter 10). Based on the recovery of PWPs, it can be stated that membranes were susceptible to pore plugging in the following increasing order: 20S, 15S, 12S, 10S. It should be recalled that the surface roughness was very similar for all 'S' membranes (Table 5.3). Their mean pore sizes (μ_p), on the other hand, were very different (Table 5.1). For example, mean pore size of 10S membrane (7.10 nm) was one order of magnitude higher than that of 20S membrane (0.70 nm). Therefore, it seems that membranes having larger pores are likely to be more susceptible to pore plugging.

8.1.2.3. Empirical equation for sodium chloride separation

Based on NaCl separation curve, it was attempted to fit the NaCl separation versus operating time to the following exponential equation for all the membranes and feed solutions used.

$$f_t = f_s - \beta_0 e^{-\beta_1 t} \qquad (8.1)$$

where

f_t = NaCl separation at time t (%)

f_s = Steady-state NaCl separation (%)

t = operating time (hour)

β_0, β_1 = constants

As shown in Figure 8.4 for 20 series membranes, the above mentioned equation fits the experimental data very well. Figures for 15 series, 12 series and 10 series membranes are given in Appendix E. Regression coefficients (r^2) between the calculated and experimental data ranged from 0.89 to 0.98, depending on the membrane type and the feed solution. The steady-state value for NaCl separation was obtained for each membrane from the above curve fitting and tabulated in Table 8.2. Steady-state NaCl separation was higher for 'S' membranes (42.3 to 59.6%) compared to 'UD' membranes (41.4 to 47.0%) for the feed solution containing 0.87% of clay and 200 ppm of NaCl.

8.2. Gel layer concentration and mass transfer coefficient

The correlation between permeate flux J_s (in m^3/m^2s) and feed concentration c_f (in %) is shown on a log scale in Figure 8.5 for the 20U, 15U, 12U and 10U membranes. Feed concentrations ranged from 0.1 to 30% of clay and SBR (clay/SBR = 100/15). As expected from Eq. (3.44), a linear correlation between permeate flux and feed concentration was obtained for all the membranes. According to Eq. (3.44), the gel layer concentration (c_g) corresponds to c_f at $J_s = 0$ and the mass transfer coefficient (k) corresponds to the slope of the line. From Figure 8.5, c_g and k are found to be 50% and 7.5×10^{-6} m/s respectively. The values of both mass transfer coefficient and gel layer concentration were in good agreement with the results found by other researchers (Woerner and Short, 1991).

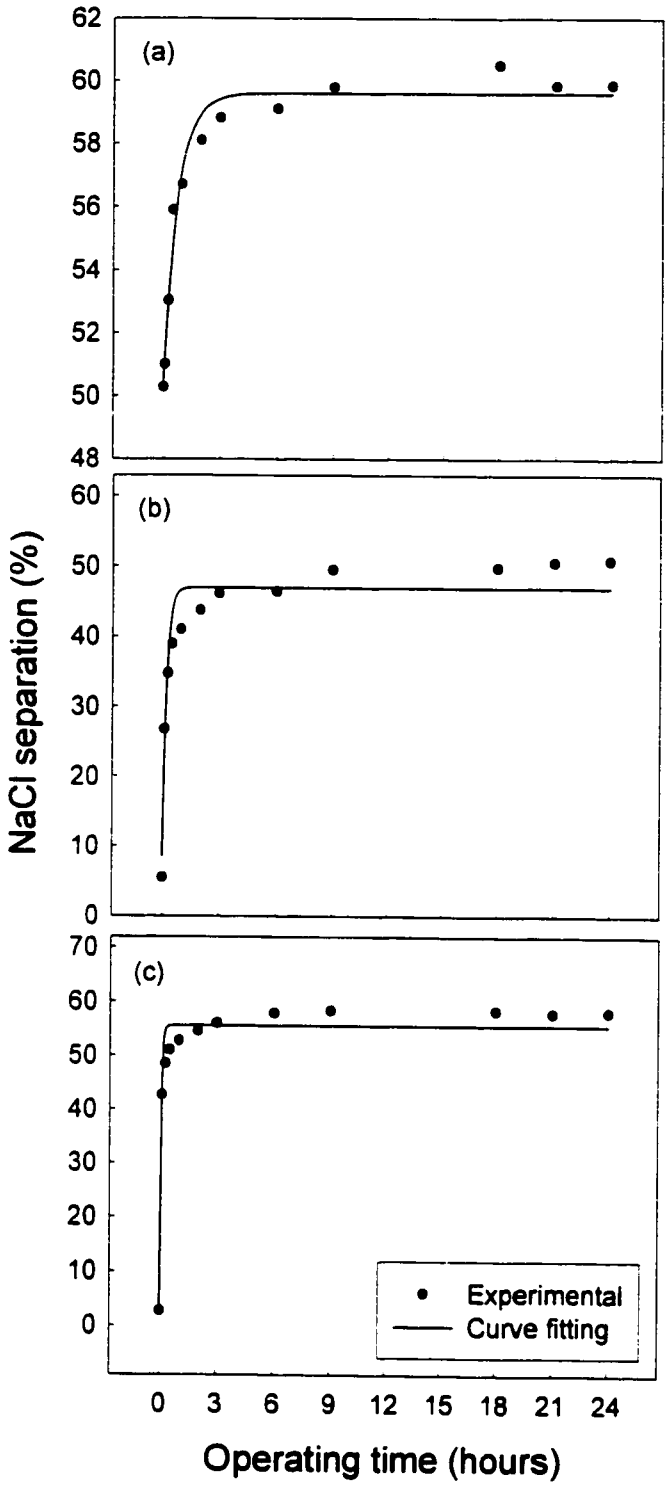

Figure 8.4. NaCl separation versus time for various membranes and feed solutions (a) 20S, feed: 0.87% of clay + 200 ppm of NaCl, (b) 20UD, feed: 0.87% of clay + 200 ppm of NaCl and (c) 20UD, feed: 1% of clay and SBR + 200 ppm of NaCl

Table 8.2 Steady-state NaCl separations and regression coefficients for different membranes obtained from the curve fitting based on Eq. (8.1)

Membrane	Feed solution	Steady-state NaCl Sep. f (%)	Regression coefficient, r^2
20UD	1*	55.6	0.96
15UD	1	48.6	0.97
12UD	1	41.2	0.98
10UD	1	38.2	0.95
20UD	2**	47.0	0.92
15UD	2	44.1	0.89
12UD	2	42.4	0.91
10UD	2	41.4	0.91
20S	2	59.6	0.97
15S	2	55.2	0.97
12S	2	46.7	0.94
10S	2	42.3	0.96

1* 1% of clay and SBR (clay/SBR = 100/15) + 200 ppm of NaCl
2** 0.87% of clay + 200 ppm of NaCl

8.3. Membrane performance stability

20S, 20UD, 12S and 12UD membranes were used to test their performance over an extended period with intermittent cleaning. In this experiment, the compaction of the membranes was carried out at a higher pressure (690 kPa or 100 psi) and for a period of 20 hours to eliminate the change in membrane performance due to additional compaction during the ultrafiltration experiment. The ultrafiltration experiment was carried out at 345 kPa (50 psi). The membrane performance was evaluated in terms of permeate flux and sodium chloride separation over time.

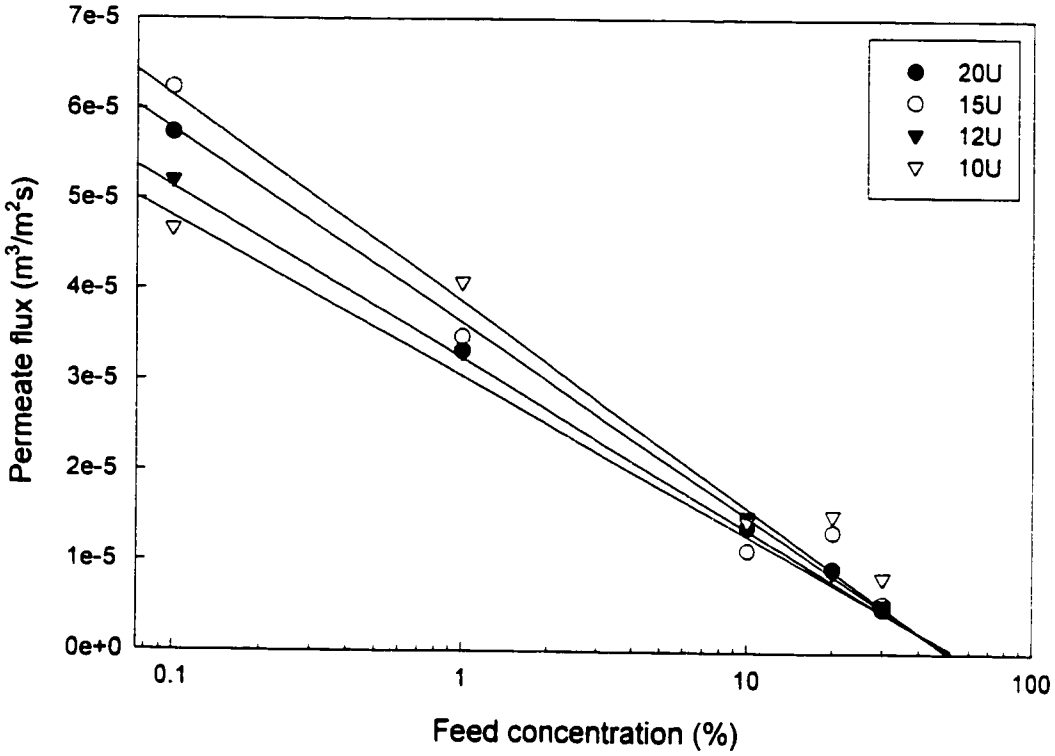

Figure 8.5. Permeate flux versus feed concentration (clay + SBR) for different 'U' membranes

First, the pure water permeation of each virgin membrane was measured at 50 psig. The sodium chloride separation experiment was also performed with a feed NaCl concentration of 200 ppm. Then the membranes were used to treat a feed solution containing 0.87% of clay and 200 ppm of NaCl. Permeate fluxes and NaCl separations were measured at various operating times. After 24 hours of operation, membranes were flushed with warm tap water and also with distilled water and the PWP and NaCl separation were measured. This operation was repeated for 4 days. After 4 days, the feed was changed to a solution containing 1% of clay and SBR and 200 ppm of NaCl. The ultrafiltration experiment was continued for 4 days with cleaning after each 24 hours of experiment. The sodium chloride separation and permeate flux were measured from time to time during the 8 days of experiment.

Sodium chloride separation and permeate flux data for 20S and 20UD membranes are presented in Figure 8.6 as a function of time. Data for 12UD and 12S are plotted in Figure F.1 in Appendix F.

It is clear from Figure 8.6 that the performance of the 20S membrane was very consistent over the period of 8 days. For the 20S membrane, for example, the NaCl separation after each cleaning operation was between 55 and 60% and the pure water permeation was between 62 to 72 L/m^2h. For the 20UD membrane, the NaCl separation slightly increased and the permeate flux slightly decreased when SBR was present in the feed solution. However, the performance of the 20UD membrane was consistent over time for a given feed solution. No significant changes were observed in the performance of 12UD and 12S

8.6(a). 20S membrane

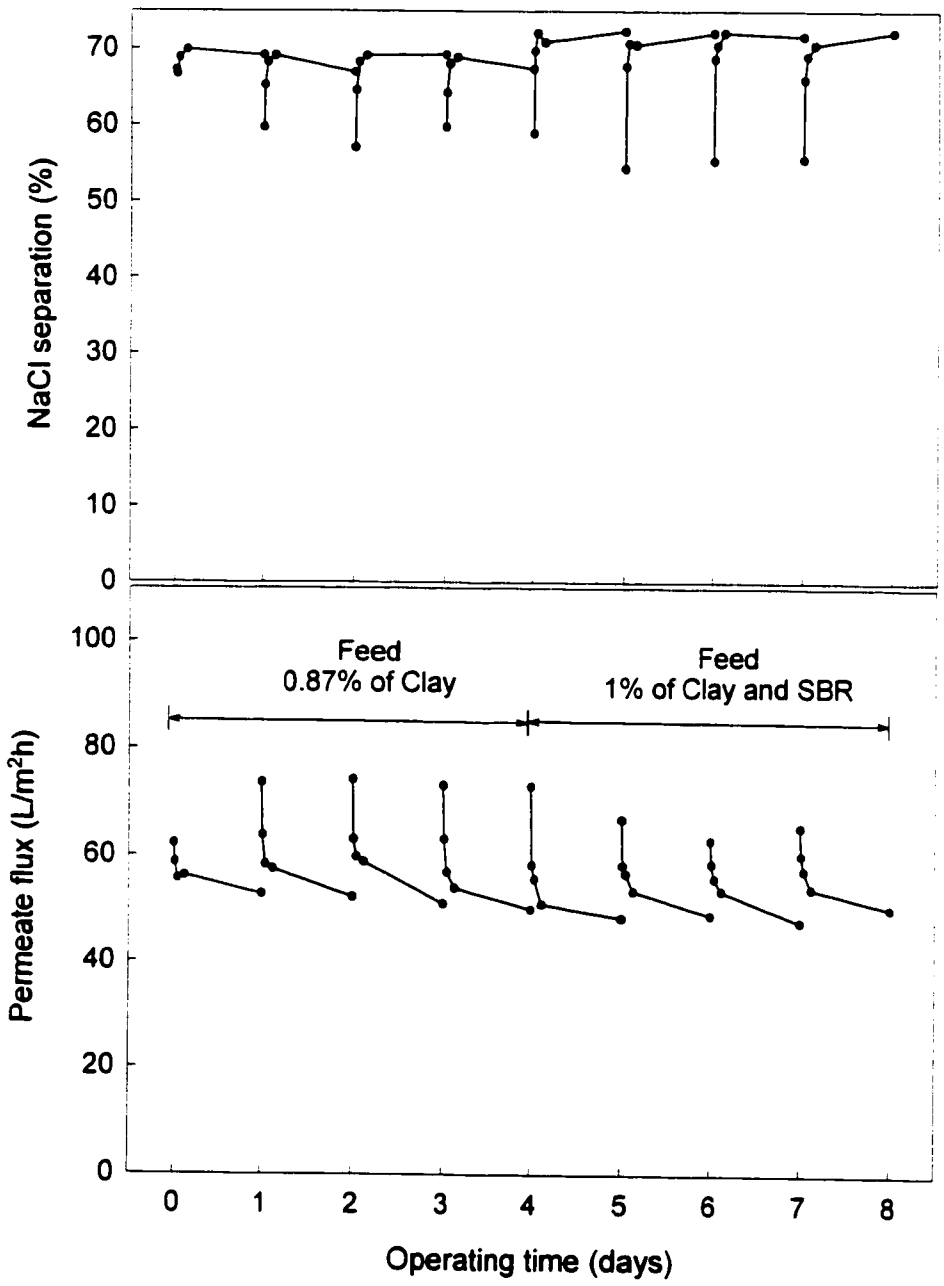

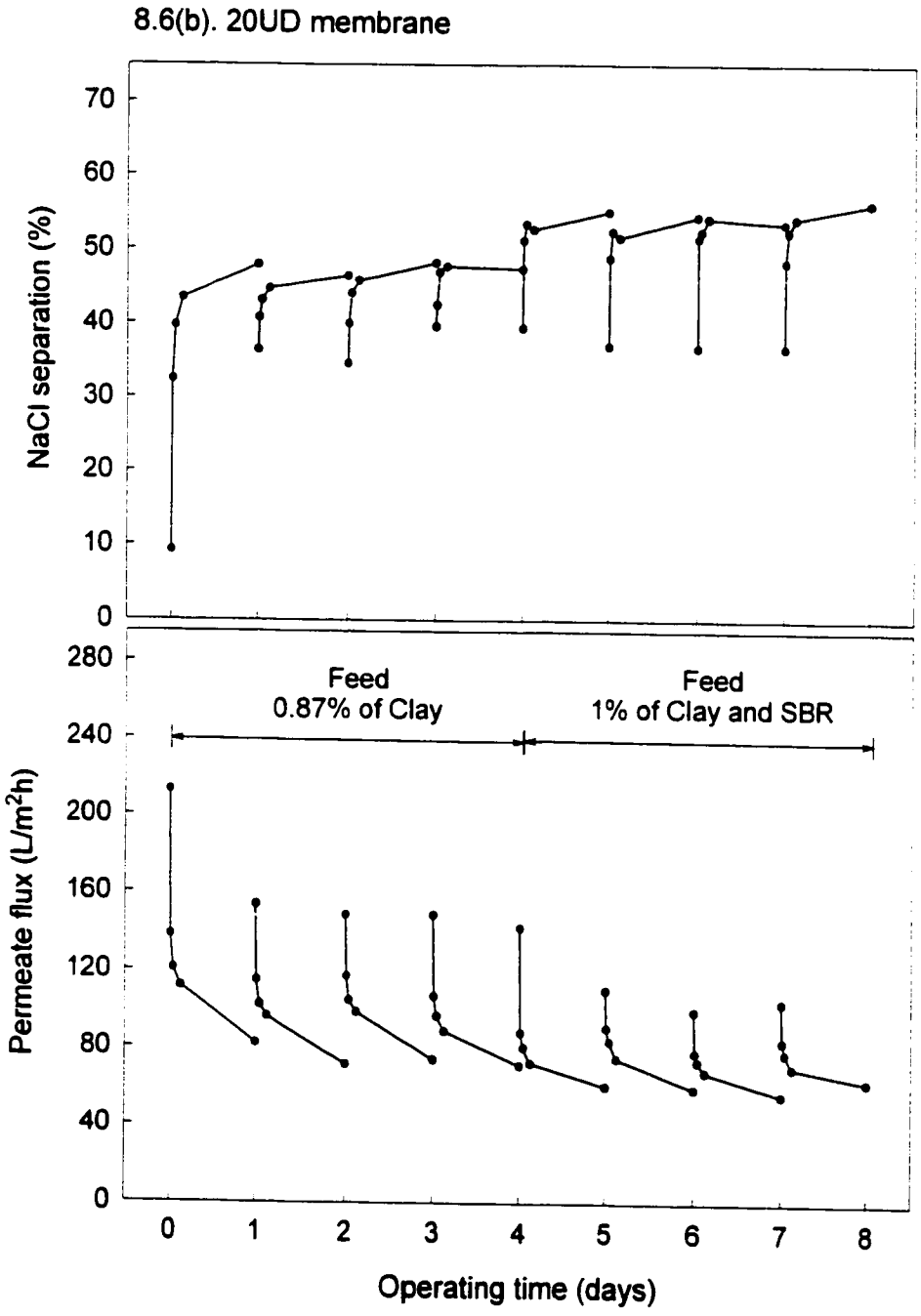

Figure 8.6. Performance of (a) 20S and (b) 20UD membranes in terms of permeate flux and NaCl separation over a period of 8 days. (Membranes were washed after every 24 hours of operation)

membranes over time (Appendix F). The consistent performance of the membranes over a long period of operation with intermittent cleaning demonstrated the reliability of these membranes.

8.4. Conclusions

Membrane fouling, which was most likely caused by the cake layer formation and pore plugging, was monitored with the change in the NaCl separation. There was a steep increase in the NaCl separation at the beginning of the ultrafiltration experiment with a feed solution containing clay and NaCl. The sodium chloride separation was higher when SBR was present in the feed solution. The sodium chloride separation could be well described by an empirical exponential function. The pure water permeation rate of the fouled membranes could not be fully recovered by cleaning the membranes after the experiment. This indicates that irreversible fouling took place. The cake layer resistance was higher when the feed solution contained clay and SBR compared to when only clay was present in the feed solution. In the presence of SBR, clay particles were agglomerated to form particles of larger sizes, each particle containing several individual clay particles. Less cake layer formation was observed when the membrane was coated with SPPO. More pore plugging was observed with the membranes having larger pores. The pore resistance was higher for the membranes having smaller pores.

The gel layer concentration and mass transfer coefficient for the feed solution containing clay and SBR were found to be 50% and 7.5×10^{-6} m/s, respectively. Membrane performance was very consistent over an extended period with intermittent cleaning.

CHAPTER 9

Fouling Study: II. Cake Layer Morphology

In the study of the morphology of the clay layer deposited on the membrane surface, the 20UD membrane was used and ultrafiltration experiments were conducted with the feed solution containing 0.87% of clay. SBR was not added in the feed as it would have enhanced agglomeration of the clay particles both in the feed and in the clay deposited on the membrane surface. Agglomeration of clay particles would lead to false results in the particle size analysis (PSA) by the Sedigraph 5100. Clay deposited on the membrane surface will be called the 'cake layer' hereafter. The 20UD membrane was used for different operational times and then taken out (without cleaning) for freeze/air drying to study the cake layer formed on the membrane surface in detail.

9.1. Surface observation of freeze/air dried membrane

Figure 9.1 shows the pictures of the membranes used for different operational times in an ultrafiltration experiment and then freeze-dried. The freeze drying process is described in Chapter 4. Scanning of the membrane surface was performed by ScanJet 4c (Hewlett Packard). As seen from the figure, all the membranes cracked during freeze drying process. And also most of the cake layer, which was deposited on the membrane during the ultrafiltration, fell off the membrane surface. The cake layer, when separated from the membrane surface, was too fragile to be used for its characterization by AFM/SEM.

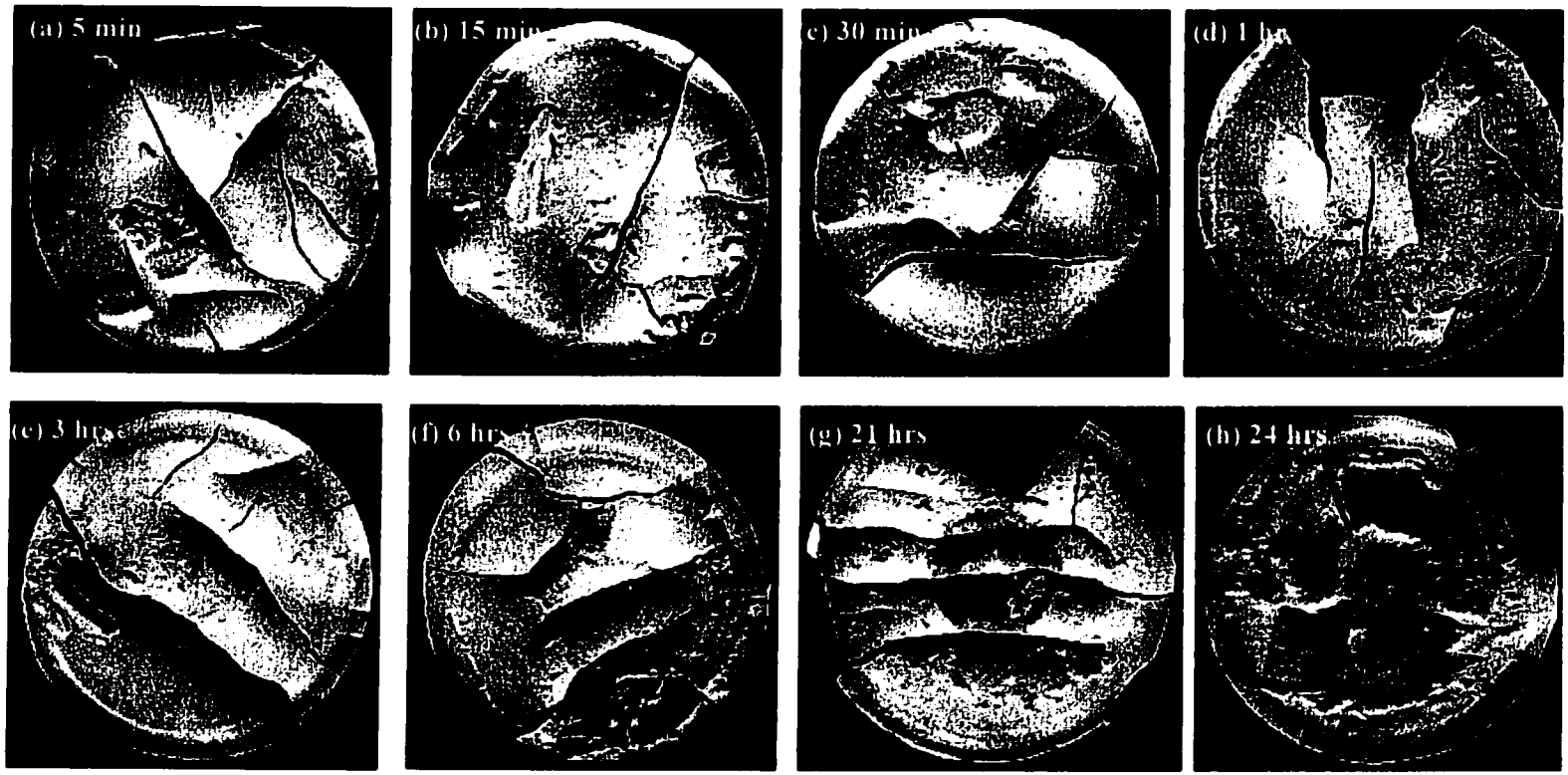

Figure 9.1. Scanned pictures of the freeze-dried 20UD membranes after treating a solution containing 0.87% of clay for different operational times (Cake layer fell off the membrane surface during freeze-drying)

Figure 9.2 shows the scanned pictures of the membranes used for different operational times in ultrafiltration experiments and then air-dried. Membranes were air-dried at room temperature for several days after being taken out from the cells. Clay deposition was seen on the membrane surface even after 5 min of operational time. However, the cake layer was thin and was not continuous. By visual observation, a clear pattern of clay deposition is seen on the surface of membranes which were used for three or more hours of operation. This pattern can also be seen in the scanned picture (Figure 9.2). As the feed solution hits the membrane at the centre (because of the cell configuration, Figure 4.2, Chapter 4), there was less deposition of clay near the center compared to the area near the periphery of the membrane.

9.2. Cross-sectional image of the air-dried membranes

It was attempted to measure the thickness of the cake layer at different operational times. SEM was used for imaging the cross-section of the membranes. However, in the sample preparation for SEM, the cake layer often separated from the membrane surface and fell off when a small piece of a membrane was dipped in liquid nitrogen. The same problem was faced when samples were prepared by cutting a small piece of membrane with a sharp blade. Figure 9.3 shows the cross-sectional images of the membranes used for different operational times. It can be seen that the cake layer was separated from the membrane surface in most cases. In some of the micrographs (b, g and h in Figure 9.3), only the cake layer is shown as the distance between the cake layer and the membrane was too large to include both in one picture at the given magnification level (×1500). The cake layer thickness was measured from the micrographs and results are given in Table 9.1. It shows that the cake layer thicknesses increased rapidly during the first hour of operation and then remained almost unchanged.

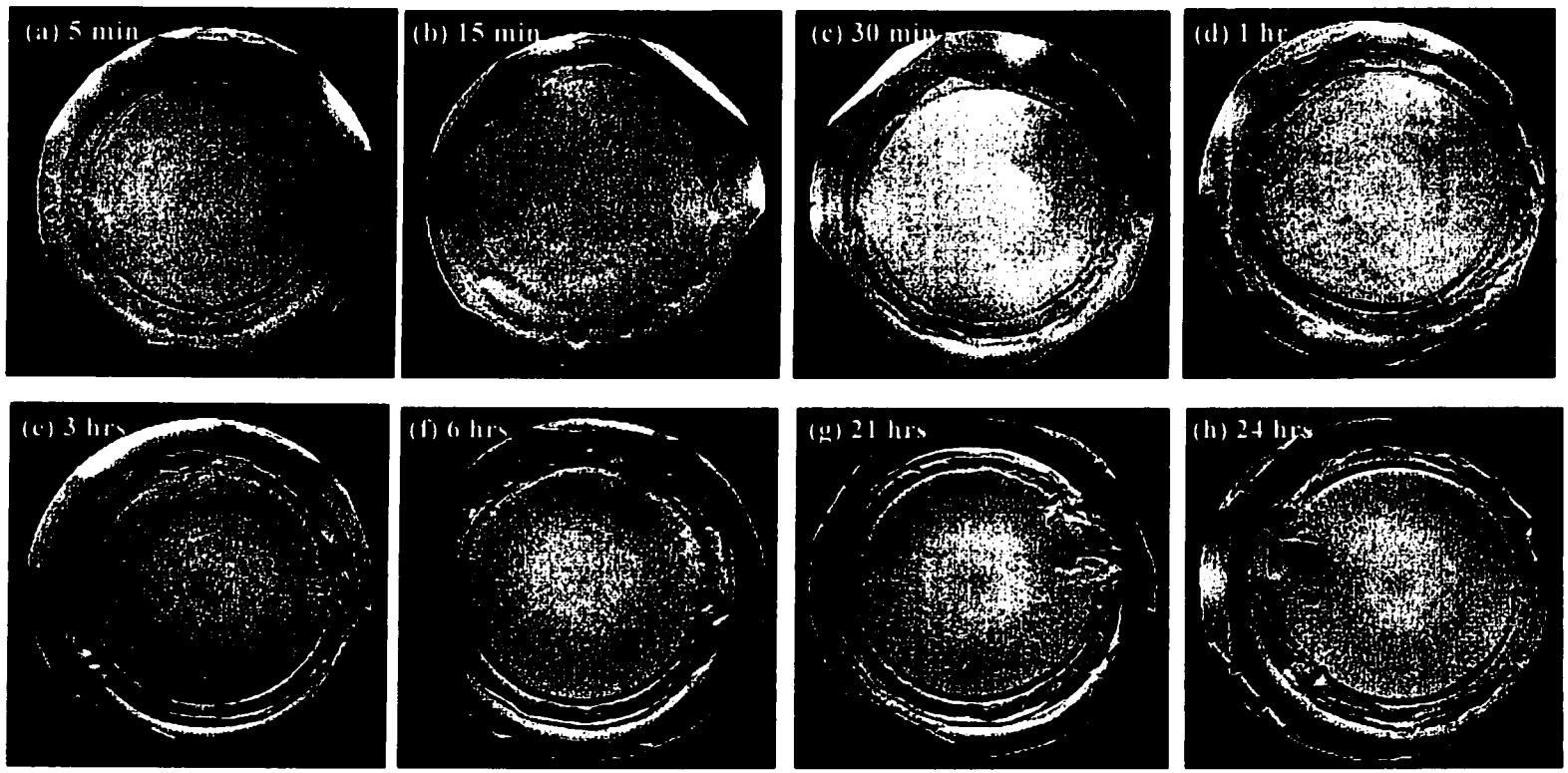

Figure 9.2. Scanned pictures of the air-dried 20UD membranes after treating a solution containing 0.87% of clay for different operational times

9.3. Particle size distribution of the clay in the cake layer and in the feed solution

The Sedigraph 5100 as described in Chapter 4 was used to perform particle size analysis of the clay present in the feed solution as well as in the cake layer. The results of the particle size analysis are shown in Figure 9.4a. It should be noted that clay (kaolin) particles have a plate type shape. However, the particle size obtained from Sedigraph is in term of 'Equivalent Spherical Diameter (ESD)'. ESD is defined as the diameter of a sphere which could be composed of the same material and that would have the same mass as the particle in question.

It can be seen from Figure 9.4a that 90% of clay in the cake layer is less than 0.6 μm in diameter while in the feed solution only 55% of clay is less than 0.6 μm. Therefore, it is clear that smaller particles were preferentially deposited on the membrane surface. Particle size distributions of the clay present in the cake layer and in the feed solution were also plotted on a log-normal probability paper (Figure 9.4b). Straight line regression with a high correlation coefficient ($r^2 \geq 0.96$) confirmed that the particle size distribution could be adequately expressed in terms of a log-normal distribution. The mean particle size and the standard deviation were calculated from Figure 9.4b and found to be 0.18 μm and 2.81 respectively in the cake layer and 0.56 μm and 3.52 in the feed solution. The mean particle size of the clay in the cake layer (0.18 μm) was one third of the mean particle size in the feed (0.56 μm). Lahoussine-Turcaud et al. (1990) also reported that maximum fouling was observed for the particle size of 0.2 μm, while particles greater than 3 μm in size had little effect on the fouling. The particle size distribution obtained in this work for the cake layer confirmed their results since more than 99% of clay in the cake layer had particle sizes less than 3 μm (Figure 9.4a). According to Lahoussine-Turcaud et al. (1990), particles with diameters of about 0.2

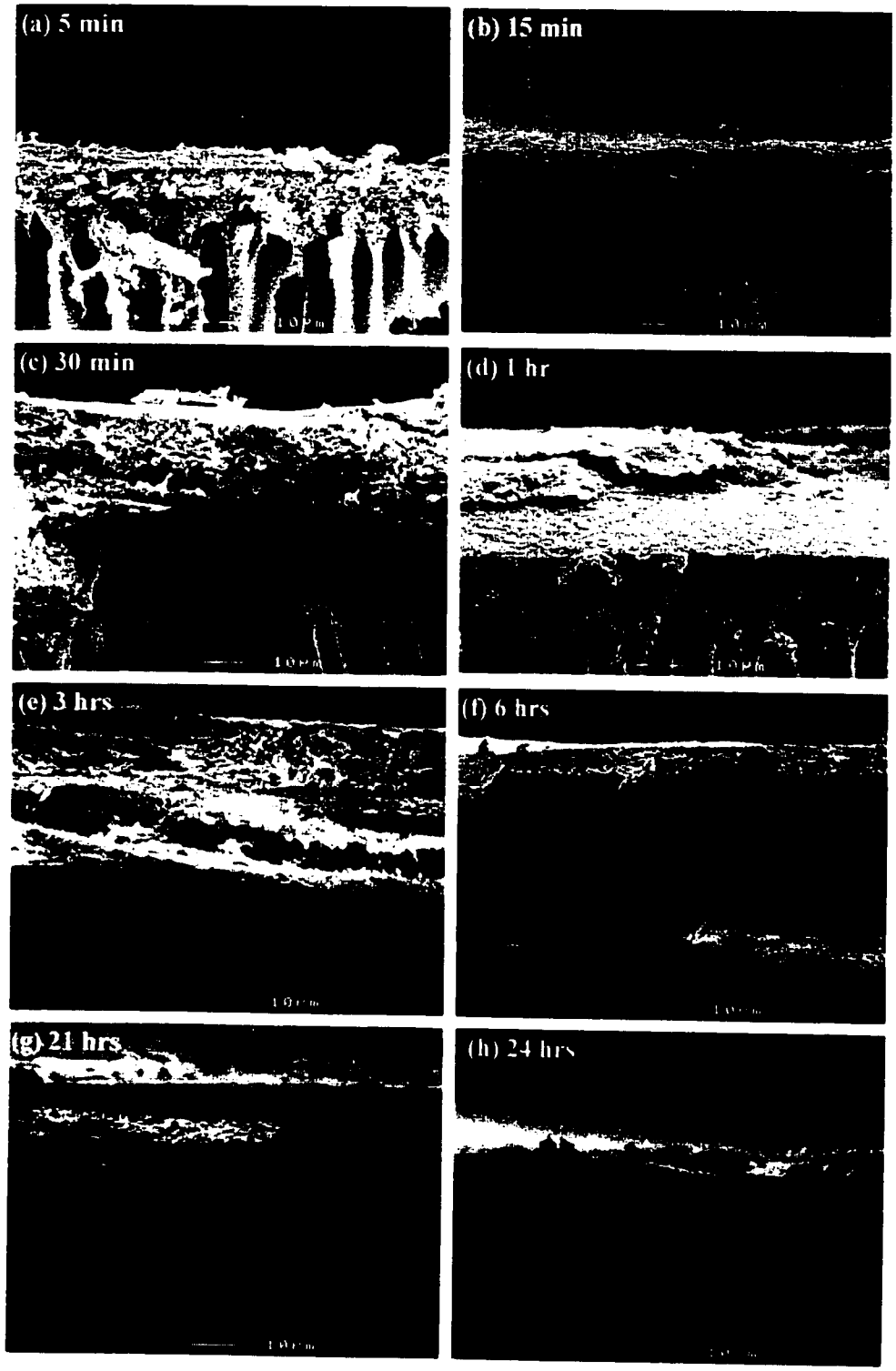

Figure 9.3. Cross-sectional images of the cake layer formed on the 20UD membranes after treating a solution containing 0.87% of clay for different operational times

μm are too large to be transported back by Brownian diffusion and are too small to be pulled from the surface by shear forces. The particles are also too large to penetrate into the pores of an ultrafiltration membrane.

Probability density functions in Figure 9.4c clearly demonstrate that the clay in the cake layer had a narrower particle size distribution than the clay in the feed solution and the distribution was shifted towards smaller particle sizes. Therefore, there was a selective deposition of the smaller clay particles on the membrane surface.

9.4. Mass of the cake layer

The amount of clay deposited on the membrane surface was measured (as per the procedure outlined in Chapter 4) and the mean value is reported in Table 9.1. There was a large variability among the clay mass obtained for a given operating time from different permeation cells as shown in Figure 9.5. However, there was a clear trend as the mass of the cake layer increased very quickly in the first hour of operation and then leveled off.

9.5. Specific resistance and void space of the cake layer

The specific resistance and the void space of the cake layer were calculated as described below. The specific resistance (α) of the cake layer can be determined from the cake resistance (R_c) (Fane , 1984; Baker et al., 1985) as

$$R_c = \frac{m}{A}\alpha \qquad (9.1)$$

where m is the mass of the cake layer and A is the surface area of the membrane. The value of the cake layer resistance (R_c) was calculated from Eq. (3.40). While calculating R_c at different operational times, it was assumed that R_2 did not depend on the operational time.

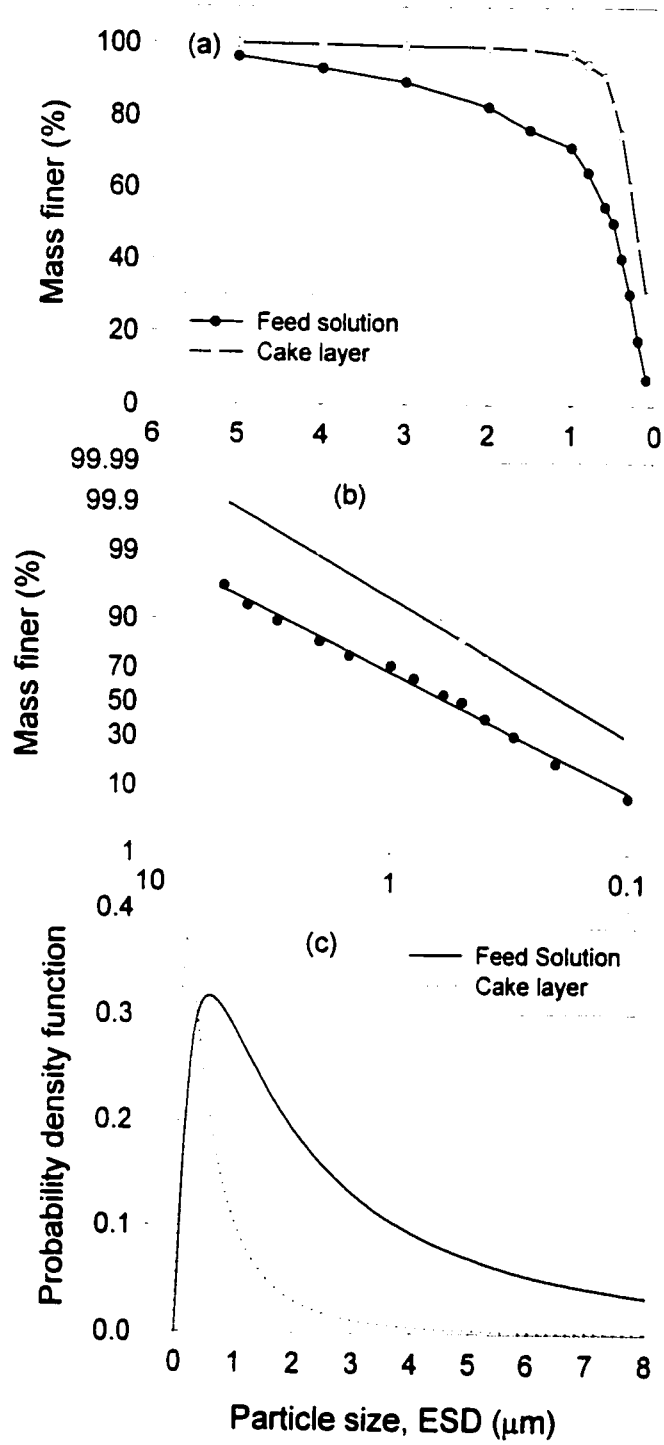

Figure 9.4. Particle size distribution of the clay in the cake layer and in the feed solution measured by Sedigraph 5100 (a) plotted on a normal paper, (b) plotted on a log-normal probability paper and (c) probability density function curves.
Feed solution – 0.87% of clay, Membrane – 20UD

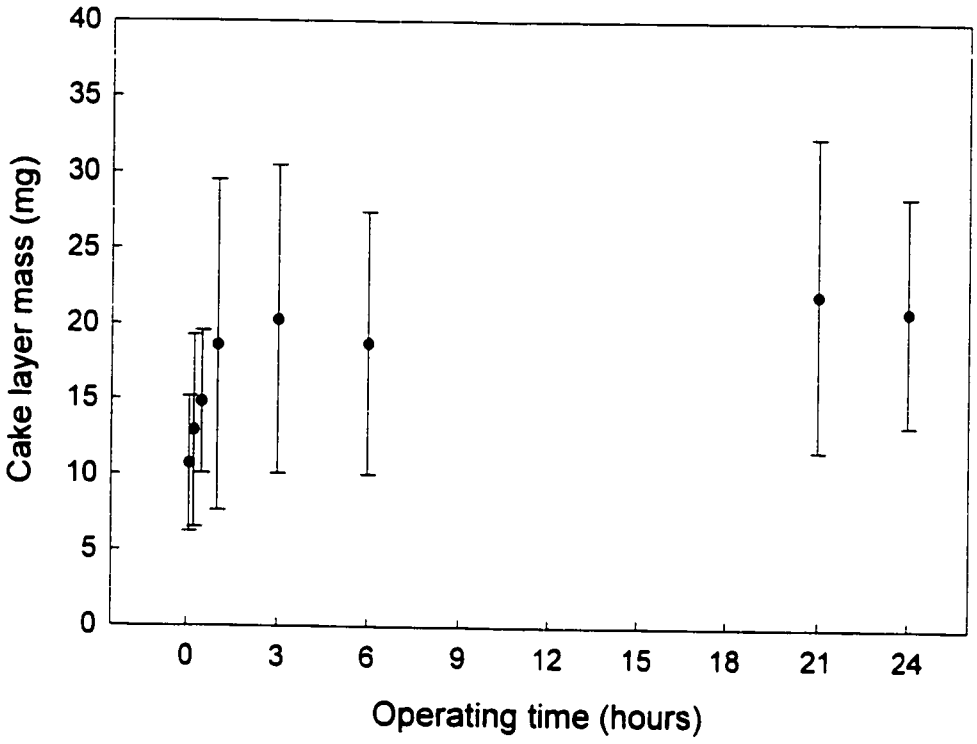

Figure 9.5. Mass of the clay deposited on the membrane surface versus operating time (Error bars indicate 95% confidence interval)

This is based on the assumption that pore blocking mainly occurred in the early stage of the ultrafiltration experiment and remained unchanged thereafter, and it is the cake layer resistance only which changed with time. Hence, the resistance due to the pores in the fouled membrane (R'_p in Figure 3.1b) and the resistance of the membrane matrix (R_m in Figure 3.1b) remained unchanged, and therefore, according to Eq. (3.21) R_2 is independent of the operational time.

Using the Carman-Kozeny equation (Baker et al., 1985), the void space (ε) of the cake layer can be calculated from the value of the specific resistance as

$$\alpha = \frac{180(1-\varepsilon)}{\rho D_p^2 \varepsilon^3} \tag{9.2}$$

where ρ is the density of clay particles (2.66 g/cm^3), D_p is the mean 'Effective Particle Diameter (EPD)' of clay particles in the cake layer. D_p is defined as

$$D_p = \frac{6}{a_v} \tag{9.3}$$

where a_v is the specific surface area and is defined as

$$a_v = \frac{S}{V} \tag{9.4}$$

S and V are the surface area and the volume of the particle, respectively.

The values of R_c, α and ε were calculated based on Eqs. (3.40), (9.1) and (9.2) and are given in Table 9.1. It is evident from the table that the specific resistance (α) increased progressively with operational time with exceptions occurring at 1 and 3 hours. For instance, the value of α increased from 5.20×10^{14} m/kg to 8.71×10^{14} m/kg when the operational time

Table 9.1. Specific resistance, void space and thickness of the cake layer deposited on 20UD membrane surface during an ultrafiltration experiment with a feed solution of 0.87% of clay.

Operating time (hr)	Cake resistance $R_c \times 10^{-12}$ (m^{-1})	Cake layer mass m (mg)	Specific resistance $\alpha \times 10^{-14}$ (m/kg)	Void space ε	Cake thickness from SEM δ^1 (μm)	Cake thickness calculated δ^2 (μm)
0.083	4.21	10.7	5.20	0.273	-	4.2
0.25	6.11	12.9	6.25	0.259	10	5.0
0.50	7.07	14.8	6.30	0.258	20	5.7
1	7.66	18.6	5.44	0.270	23	7.3
3	8.33	20.3	5.41	0.270	27	7.9
6	9.24	18.7	6.52	0.256	19	7.2
21	13.46	22.0	8.08	0.240	20	8.2
24	13.78	20.9	8.71	0.234	16	7.8

[1] measured from SEM micrographs (Figure 9.3)
[2] calculated from Eq. (9.5)

was increased from 5 min to 24 hours. The decrease in void space with the operational time indicates that the cake layer was becoming denser with time. For example, void space was 0.273 and 0.234 after the operational time of 5 min and 24 hours, respectively. From these observations it can be stated that the increase in the specific resistance of cake layer with time was mainly due to the decrease in the void space. Smaller values of void space also indicate that the clay particles which are plate type in structure are densely packed in the cake layer.

Both mass (Figure 9.5) and thickness (Figure 9.3) of the cake layer remained almost constant after 1 hour of operation. The reason may be that once a maximum of mass/thickness is attained for a given hydrodynamic condition, further deposition of clay is counter-balanced by the back diffusion and/or by the scouring effect.

Cake layer thickness (δ) was also calculated from its mass and void space by the following equation

$$\delta = \frac{m}{A(1-\varepsilon)\rho} \tag{9.5}$$

and the values of δ are given in Table 9.1. The cake thicknesses calculated (from the above equation) were smaller than those measured from the SEM micrograph.

9.6. Surface imaging of the cake layer by AFM/SEM

The surface of the membrane was covered completely by clay particles as evident from AFM (Figures 9.6) and SEM (Figure 9.7a) pictures. Figures 9.6 and 9.7a show the cake layer over the membrane that was used to treat a feed solution containing 0.87% of clay. Individual clay particles can be seen clearly in both the figures. Clay (kaolin) has a plate type structure. These plate-shaped particles are deposited horizontally one over the other. The SEM picture of the cross-section of the cake layer (Figure 9.7b) also confirms the horizontal pattern of clay particle deposition.

9.7. Particle size analysis of the cake layer by AFM

The size of the individual clay particles deposited on the membrane surface, which was used to treat a solution of 0.87% clay, was measured by the image analysis software in AFM. Sizes of 150 particles were measured. The clay particles were considered as square plates of length L and thickness t. When there was a significant difference between length and width of the particle, their average was taken. Particle sizes measured by AFM were converted to 'Equivalent Spherical Diameter (ESD)'. The following equations were used.

$$L^2 t = \frac{\pi D^3}{6} \tag{9.6}$$

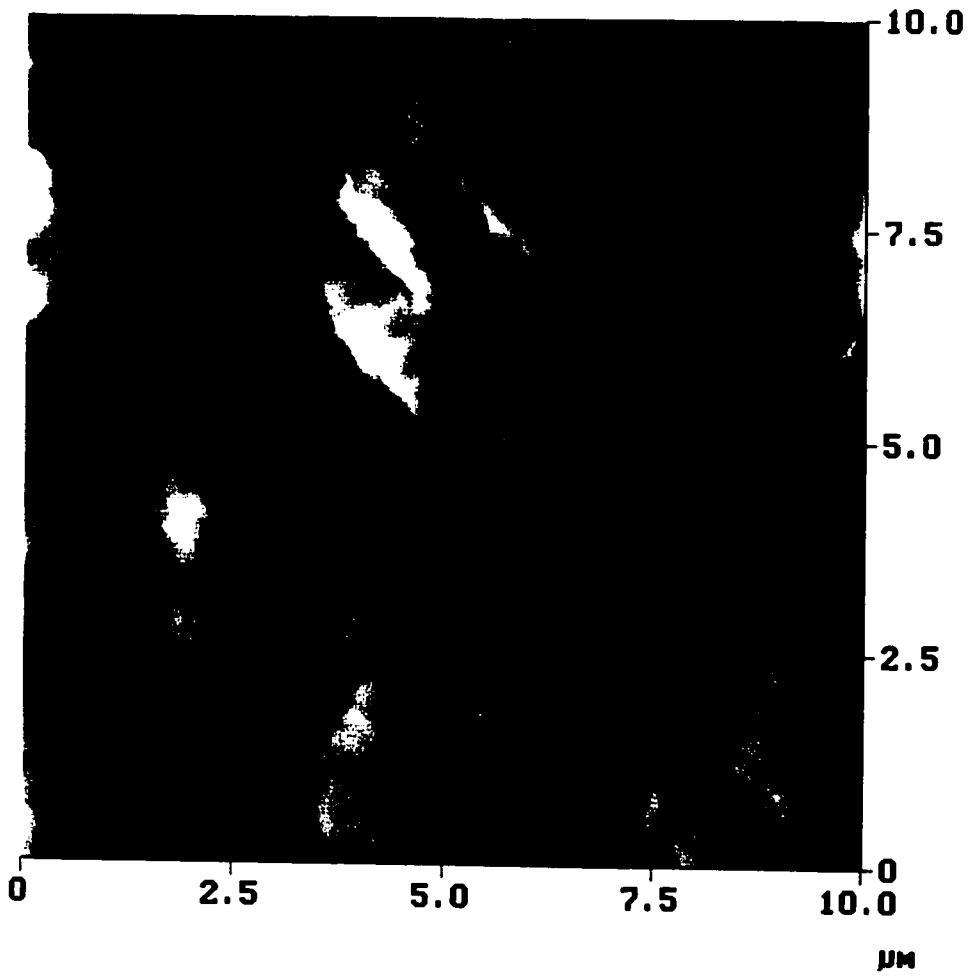

Figure 9.6. AFM micrograph of the surface of the cake layer deposited on 20UD membrane after treating a solution containing 0.87% of clay for 24 hours

(a)

(b)

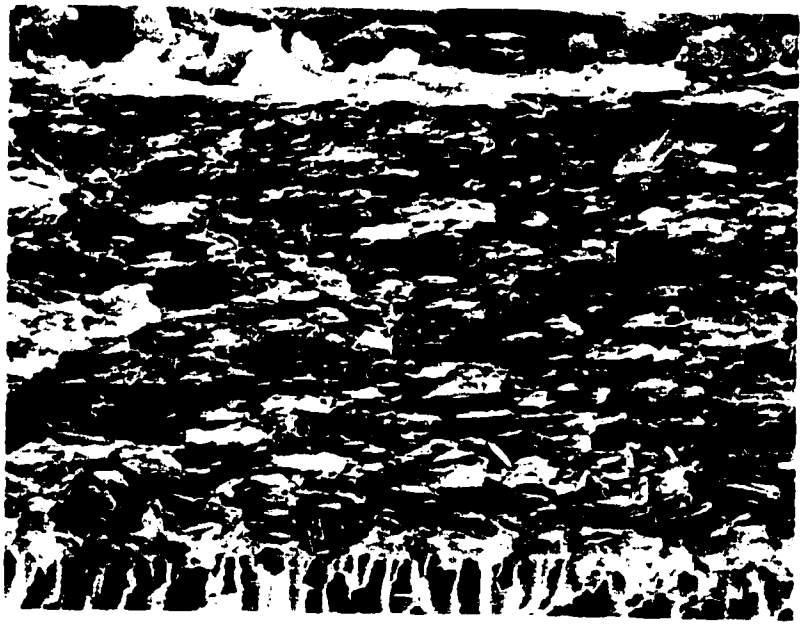

Figure 9.7. SEM micrographs of the cake layer deposited on 20UD membrane after treating a solution containing 0.87% of clay for 24 hours (a) surface of the cake layer and (b) cross-section of the cake layer

$$A_r = \frac{L}{t}$$

or
$$t = \frac{L}{A_r} \tag{9.7}$$

Substituting the value of t from Eq. (9.7) to Eq. (9.6) and rearranging yields

$$D = \left(\frac{6L^3}{\pi A_r} \right)^{\frac{1}{3}} \tag{9.8}$$

where,

D = ESD of clay particle

L = Length of clay particle

t = thickness of clay particle

A_r = aspect ratio of clay particle (13 as given by clay supplier)

All the sizes measured by AFM were converted to ESD by using Eq. (9.8) and plotted against median rank in Figure 9.8. It was also observed that these data could be adequately represented by a log-normal distribution. The mean particle size and the standard deviation were calculated to be 0.19 μm and 2.08, respectively. The values of the mean particle size measured by the AFM (0.19 μm) and by the Sedigraph (0.18 μm) are in excellent agreement. However, it should be noted that the particle size analysis by AFM is based on the number averaged while by Sedigraph it is based on the mass averaged. It is also confirmed by AFM that the cake layer was composed of mainly smaller particles, as 90% of the particles were smaller than 0.55 μm while more than 99% were smaller than 1.5 μm.

It is clearly demonstrated that the AFM can be used to study fouling. The AFM was used not only for imaging the surface of the foulants but also for the particle size analysis of the foulants.

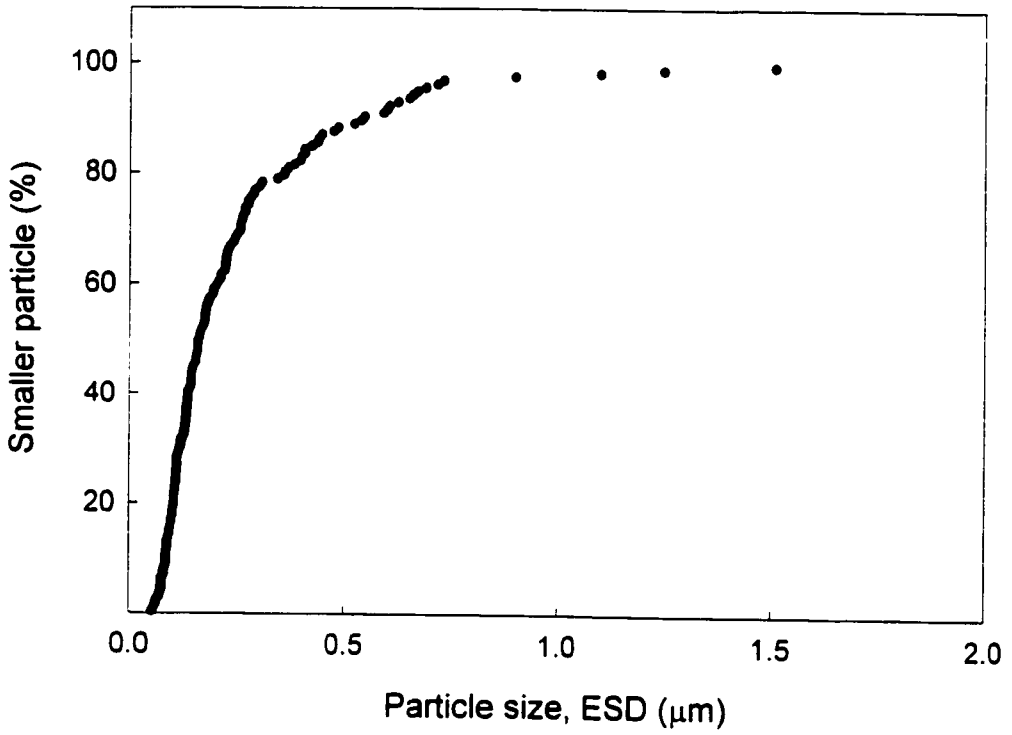

Figure 9.8. Particle size analysis of the clay in the cake layer performed by image analysis software build in AFM. Membrane was used for 24 hours of ultrafiltration experiment with a feed solution of 0.87% of clay.

9.8. Conclusions

A quick build-up of a cake layer was observed on the membrane surface while treating a clay solution by an ultrafiltration membrane. Both mass and thickness of the cake layer reached their maximum in the first hour of operation and remained unchanged thereafter as the deposition of clay to the membrane surface was counter-balanced by the back diffusion and/or scouring effect. Clay particles in the cake layer were substantially smaller than those in the feed solution, as 90% of the clay particles in the cake layer were smaller than 0.6 μm while only 55% of the clay particles were smaller than 0.6 μm in the feed solution. The mean particle size in the cake layer was 0.18 μm and in the feed solution was 0.56 μm. This confirms that particles with a diameter of about 0.18 μm were mainly responsible for the fouling, as these particles are too large to be transported back by Brownian diffusion and are too small to be pulled from the cake layer by shear force. The specific resistance of the cake layer increased with the operational time while its void space decreased. There was excellent agreement in the particle size analysis of the cake layer performed by AFM and Sedigraph. The usefulness of AFM and SEM was demonstrated in characterizing the cake layer morphology.

CHAPTER 10

Fouled Membrane Characterization

After a 24 hours of ultrafiltration experiment with the feed solution of either clay or clay and SBR, membranes were flushed with tap water of 45^{0}C for half an hour and then with distilled water for another half an hour at 70 kPa and at a feed flow rate of 4000 mL/min. These membranes are referred to as 'fouled membranes' hereafter. Fouled membranes were obtained after each set of the following ultrafiltration experiments and flushing the system thereafter.

1. **Fouled 'S' membranes:** 'S' membranes after ultrafiltration experiment with a feed solution of 0.87% clay
2. **Fouled 'UD' membranes:** 'UD' membranes after ultrafiltration experiment with a feed solution of 0.87% clay
3. **Fouled 'UD' membranes:** 'UD' membranes after ultrafiltration experiment with a feed solution of 1% clay and SBR (clay/SBR = 100/15)

In each experiment, fresh membranes were used. The membranes, which are freshly mounted on the permeation cell, are referred to as 'virgin membranes'. Fouled membranes were further subjected to ultrafiltration with aqueous solutions of PEG/PEO of different

molecular weights in order to determine the pore size distribution and other characteristic parameters of the membranes. This procedure has been explained in detail in Chapters 3 and 4. Various characteristic parameters such as geometric mean pore size, geometric standard deviation, pore density and surface porosity of the fouled membranes were determined from solute (PEG/PEO) separation data and were compared with those of virgin membranes. It should be noted that the membrane coupons used for the characterization of virgin and fouled membranes were not the same. However, they came either from the same lot or were prepared in exactly the same way.

10.1. Fouled sulfonated 'S' membrane after an ultrafiltration with 0.87% of clay solution

Figure 10.1a shows the results of ultrafiltration experiments with aqueous solutions of PEG/PEO for various fouled 'S' membranes. Before membranes were flushed and used for the ultrafiltration with PEG/PEO solutes, the membranes were challenged with the feed solution of 0.87% clay for 24 hours. The solute separations versus solute diameters are plotted on log-normal probability paper for different PEG/PEO solutes in Figure 10.1. A straight line relationship between solute separation and solute diameter, as in the case of virgin membranes, was obtained for each fouled membrane with reasonably high correlation coefficients ($r^2 \geq 0.94$). The correlation coefficient for each individual membrane is given in the Figure 10.1. The values of geometric mean pore size (μ_p) and geometric standard deviation (σ_p) were calculated using Figure 10.1 and are presented in Table 10.1. As can be seen from Table 10.1, the differences between virgin and fouled membranes (except 10S) in term of their μ_p and σ_p are small. More specifically, the mean

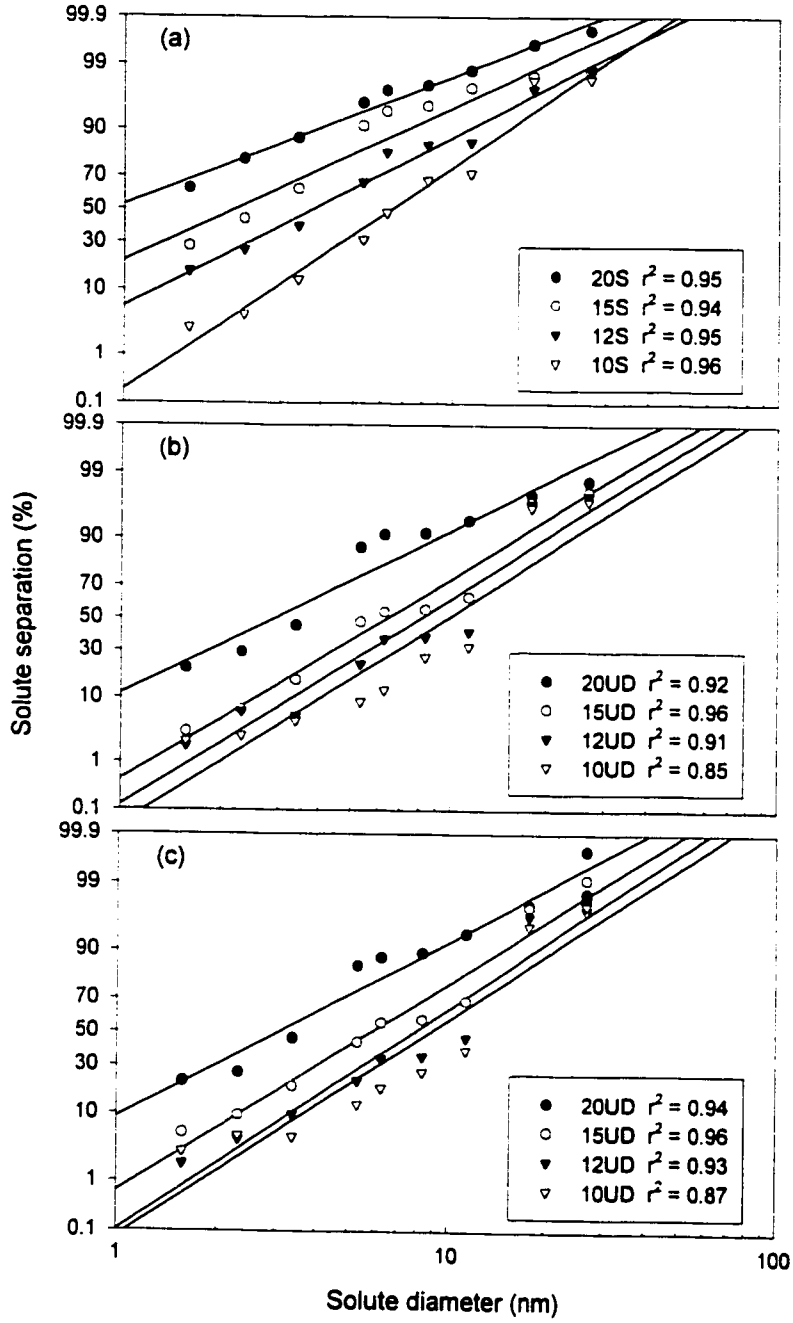

Figure 10.1 Solute separation curves (solute separation versus solute diameter) plotted on a log-normal probability paper for (a) Fouled 'S' membrane, 0.87% clay, (b) Fouled 'UD' membrane, 0.87% clay and (c) Fouled 'UD' membrane, 1% clay and SBR

Table 10.1. Geometric mean pore size (μ_p), and geometric standard deviation (σ_p) values of various fouled and virgin membranes.

Code for virgin membrane	Virgin membrane		Fouled membrane (0.87% Clay)		Fouled membrane (1% Clay + SBR)	
	μ_p (nm)	σ_p	μ_p (nm)	σ_p	μ_p (nm)	σ_p
20UD	3.36	2.29	2.91	2.41	3.04	2.40
15UD	7.18	1.84	6.36	2.04	5.93	2.09
12UD	9.14	1.74	8.04	2.00	8.03	1.99
10UD	10.38	1.78	9.71	1.98	9.15	2.05
20S	0.70	3.31	0.92	3.06		
15S	2.19	2.43	2.15	2.56		
12S	3.44	2.32	3.72	2.34		
10S	7.10	2.02	6.43	1.91		

All the parameters were calculated from the solutes (PEG/PEO) transport data. Data for virgin membranes are taken from Table 5.1 and are shown here to compare with the fouled membranes.

pore size (μ_p) was reduced from 7.10 nm for virgin 10S membrane to 6.43 nm for fouled 10S membrane. For the 15S membrane, μ_p was almost unchanged (2.15 nm for fouled membrane versus 2.19 nm for virgin membrane). μ_p was even slightly higher for fouled 20S (0.92 nm) and 12S (3.72 nm) membranes versus their virgin membranes (0.70 nm for 20S and 3.44 nm for 12S) (Table 10.1). However, differences between fouled and virgin membranes in terms of their μ_ps were very small and could be attributed to the experimental errors and/or to the variability among various membrane coupons of the same type. It should be noted that differences in the separation of sodium chloride were also small for fouled and virgin sulfonated membranes (Figure 8.1, Chapter 8).

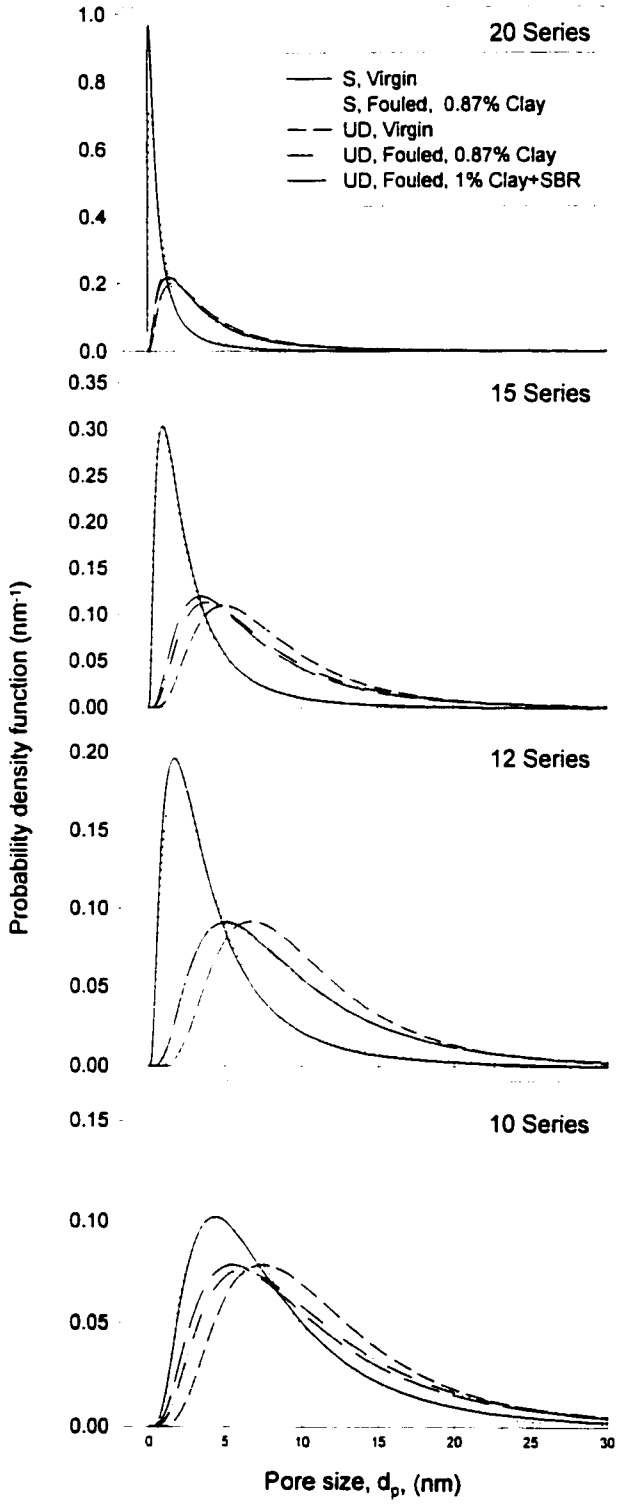

Figure 10.2. Probability density function curve for virgin and fouled membranes (a) 20 Series, (b) 15 Series, (c) 12 Series and (d) 10 Series

Table 10.2. Pore density and surface porosity of various fouled and virgin membranes.

Code for virgin membrane	Virgin membrane		Fouled membrane (0.87% Clay)		Fouled membrane (1% Clay + SBR)	
	Pore density (pores/μm^2)	Surface porosity (%)	Pore density (pores/μm^2)	Surface porosity (%)	Pore density (pores/μm^2)	Surface porosity (%)
20UD	231	0.76	170	0.50	145	0.46
15UD	122	1.02	55	0.47	45	0.36
12UD	84	1.01	25	0.33	21	0.27
10UD	51	0.80	15	0.28	11	0.20
20S	1291	0.60	778	0.53		
15S	447	0.73	221	0.44		
12S	170	0.61	91	0.39		
10S	49	0.50	52	0.39		

All the parameters were calculated from the solutes (PEG/PEO) transport data. Data for virgin membranes are taken from Table 5.2 and are shown here to compare with the fouled membranes.

From the probability density function curves generated from Eq. (3.5) and shown in Figure 10.2, it is evident that there was not much difference in the pore size distribution of fouled and virgin 'S' membranes.

The pore densities (calculated from Eq. (3.8)) of the fouled membranes are given in Table 10.2 along with those of virgin membranes. The table shows that the pore densities of the fouled membranes are smaller than the virgin membranes except for 10S membrane. For example, the number of pores per square μm for fouled 20S, 15S, 12S and 10S membranes are 778, 221, 91 and 52, respectively, while for the virgin membranes they are 1291, 447, 170 and 49, respectively. Despite having a higher pure water permeation (PWP) (Figure 8.1),

a lower pore density was found for fouled 20S membrane than for virgin 20S membrane. This was due to the slightly bigger pore sizes for fouled 20S membrane (μ_p: 0.92 nm) compared to that of virgin 20S membrane ((μ_p: 0.70 nm). For fouled 12S membrane, the lower PWP and the larger pore sizes contributed to lower pore density. There was practically no change in the pore density of the 10 series membrane. Smaller pore densities of the fouled membranes indicate that some of the pores were blocked either completely or partially Surface porosities of fouled membranes were slightly reduced (0.39 to 0.53%) from that of virgin membranes (0.50 to 0.73%).

10.2. Fouled 'UD' membranes after an ultrafiltration with 0.87% of clay solution

Solute separations versus solute Stokes diameters curves are presented in Figure 10.1b for PEG/PEO solutes for the fouled 'UD' membranes, which were used to treat a feed solution of 0.87% of clay for 24 hours. The values of μ_p and σ_p for all the fouled 'UD' membranes are given in Table 10.1. The μ_ps of all the fouled membranes were smaller than those of their respective virgin membranes. For instance, the μ_ps for the fouled 20UD, 15UD, 12UD and 10UD membranes were 2.91, 6.36, 8.04 and 9.71 nm, respectively, while for their respective virgin membranes, the μ_ps were 3.36, 7.18, 9.14 and 10.38 nm, respectively. Probability density function curves shown in Figure 10.2 indicate a shift to the left.

Both pore densities and surface porosities for all the fouled membranes were lower than virgin membranes. Pore densities ranged from 15 to 170 for fouled membranes and from 51 to 231 for virgin membranes (Table 10.2). The lower pore density and surface porosity confirmed that some of the pores were blocked either completely or partially.

The separation of sodium chloride for fouled 20UD membrane was much higher (27.5%) compared to that for the virgin 20UD membrane (5.5%) (Figure 8.1). However, for the other fouled membranes, the increase in the separation of sodium chloride (Figure 8.1) was only marginal, as their pore sizes were still too large to cause any significant salt separation.

10.3. Fouled 'UD' membranes after an ultrafiltration with 1% of clay and SBR solution

Solute separations versus solute Stokes diameter curves are presented in Figure 10.1c for PEG/PEO solutes for the fouled 'UD' membranes. Before these membranes were flushed and used for the ultrafiltration experiment with aqueous solution of PEG/PEO, the membranes were used to treat a feed solution of 1% clay and SBR for 24 hours. The values of μ_p were lower for the membranes fouled with 1% of clay and SBR solution compared to their respective virgin membranes. Pore densities and surface porosities were also lower for the fouled membranes. For example, pore densities were decreased from 51 to 11 per μm^2 for 10UD, from 84 to 21 per μm^2 for 12UD, from 122 to 45 per μm^2 for 15UD and from 231 to 145 per μm^2 for 20UD membranes. Surface porosities were between 0.20 to 0.46% for the fouled membranes and between 0.76 to 1.02% for virgin membranes.

10.4. Comparison of the membranes fouled during ultrafiltration experiment with 0.87% clay solution and with 1% clay and SBR solution

Mean pore sizes of the fouled 'UD' membranes, which were used for the feed solution of 1% of clay and SBR, were 3.04 nm, 5.93 nm, 8.03 nm and 9.15 nm, while the mean pore sizes of the fouled 'UD' membranes, which were used for the feed solution of 0.87% of clay, were 2.91 nm, 6.36 nm, 8.04 nm and 9.71 nm for 20UD, 15UD, 12UD and 10UD membranes, respectively. Therefore, there was no significant difference in the mean pore sizes of the membranes which were fouled either by clay solution or by clay and SBR solution.

However, both pore densities and surface porosities of the membranes fouled with 1% of clay and SBR solution were lower than those of the membranes fouled with 0.87% of clay solution (Table 10.2).

10.5. Conclusions

No significant differences were found in the mean pore sizes of fouled and virgin 'S' membranes. However, the former had comparatively smaller pore densities. The mean pore sizes of fouled 'UD' membranes were smaller than those of virgin 'UD' membranes. Reduction in the pore densities of the fouled membranes indicated that some of the pores were plugged during the ultrafiltration experiment. There was no significant difference in the mean pore sizes of the membranes (UD) which were fouled either by clay solution or by clay and SBR solution. However, both pore densities and surface porosities of the membranes fouled with 1% of clay and SBR solution were lower than those of the membranes fouled with 0.87% of clay solution.

CHAPTER 11

Low Pressure Reverse Osmosis

During ultrafiltration experiments, it was observed that some of the membranes had good separation for electrolytes. Therefore, membranes (15S and 20S) were tested along with some other membranes for their potential for low-pressure reverse osmosis (RO) application. A total of six membranes, characteristic details of which are given in Table 11.1, were tested for low-pressure reverse osmosis performance.

Membranes made from the casting solution having 25 wt.% polyethersulfone, 20 wt.% polyvinylpyrrolidone and 55 wt.% N-methylpyrrolidone were labeled as 25-20UD. The 25-20UD membrane was further coated with a thin layer of SPPO polymer and the membrane after coating was named 25-20S. 20S3 and 15S3 membranes were made by coating 20UD and 15UD membranes, respectively, with 3 layers of the SPPO polymer. After each coating, membranes were dried for 24 hours at room temperature. Preparation techniques of 20S and 15S membranes are outlined in Chapter 4. The procedure of casting a substrate membrane (UD) and its subsequent coating is also explained in Chapter 4.

Table 11.1. Characteristics of the membranes tested for the low-pressure reverse osmosis experiment. Operating pressure – 1034 kPa (150 psi)

Membrane	Layer of SPPO coatings	MWCO (kDa)	μ_p (nm)	σ_p
25-20UD	Nil			
25-20S	1	2.75	0.84	2.90
20S*	1	3.5	0.70	3.31
20S3	3			
15S*	1	11	2.19	2.43
15S3	3			

* Operating pressure – 345 kPa (50 psi)

All the membranes were compacted at 2758 kPa (400 psi) for 20 hours prior to the RO experiment which was conducted at 1034 kPa (150 psi) and at a feed flow rate of 800 mL/min. The concentration in the feed solution was kept at 500 ppm for NaCl and 1500 ppm for both $MgSO_4$ and Na_2SO_4.

Separation versus molecular weight is shown in Figure 11.1 for polyethylene glycol of different molecular weights for the 25-20S membrane. From this figure, the MWCO of the 25-20S membrane was obtained to be 2750 Daltons. The geometric mean pore size (μ_p) and geometric standard deviation (σ_p) were also calculated according to the procedure explained in Chapter 3. Values of μ_p and σ_p were found to be 0.84 nm and 2.90, respectively (Table 11.1).

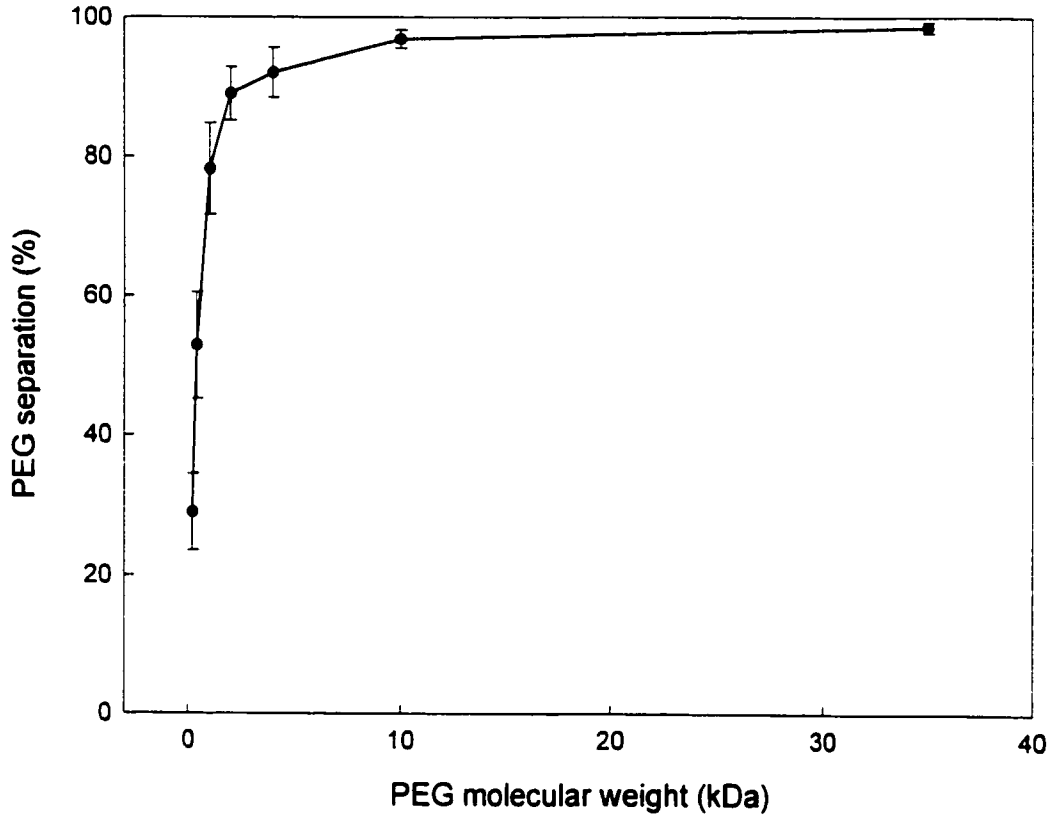

Figure 11.1. Separation of polyethylene glycol (PEG) versus its molecular weight for 25-20S membrane (Error bars indicate 95% confidence interval)

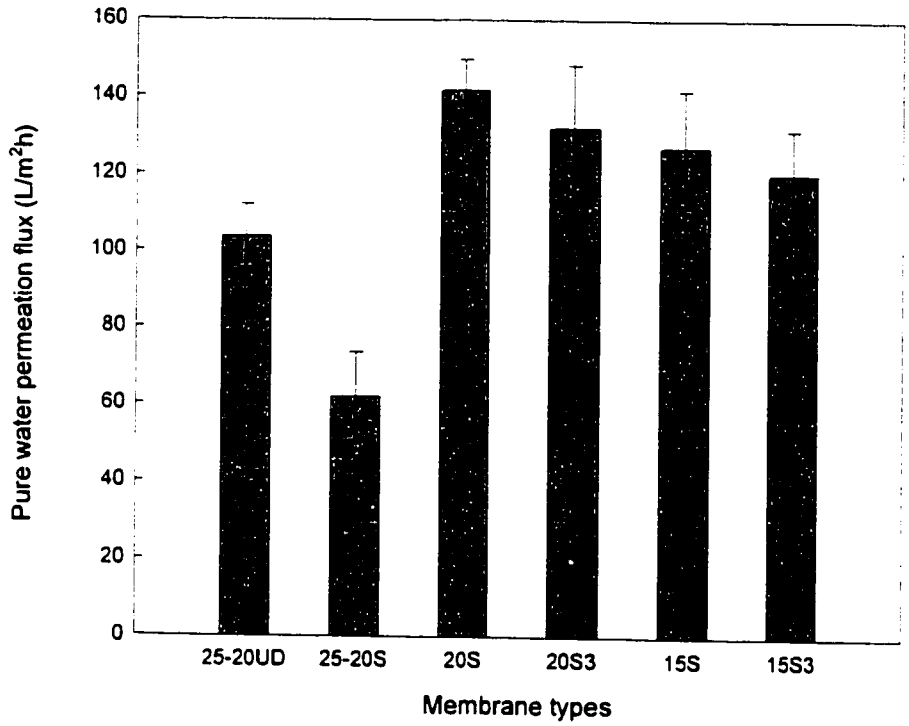

Figure 11.2. Pure water permeation flux of various membranes tested for RO experiment (Error bars indicate 95% confidence interval)
Operating pressure – 1034 kPa (150 psi)

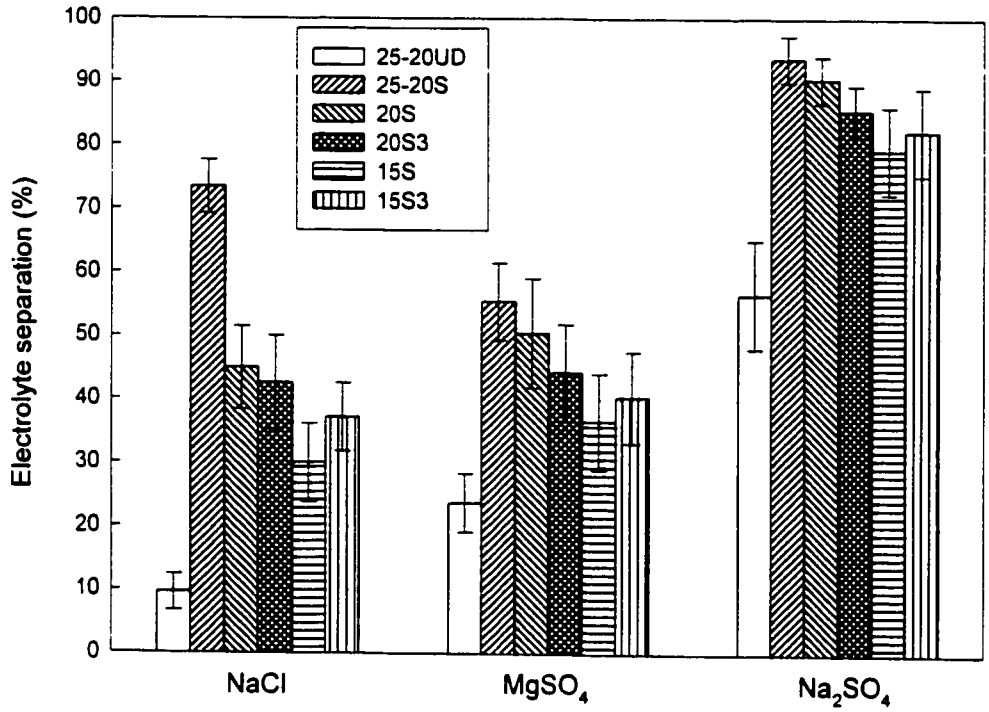

Figure 11.3. Electrolyte separation for various membranes tested for RO experiment.
(Error bars indicate 95% confidence interval)
Operating pressure – 1034 kPa (150 psi)

25-20S membrane had the lowest pure water permeation flux of 62 L/m^{2}h (Figure 11.2) among all the six membranes tested, while having the highest separations for electrolyte solutes (73.4% for NaCl, 55.5% for $MgSO_4$ and 93.6% for Na_2SO_4) as depicted in Figure 11.3. The performance of this membrane in terms of the permeate flux and the salt separation is one of the best among available commercial membranes. The separation of electrolyte solutes was the lowest (9.6% for NaCl, 23.7% for $MgSO_4$ and 56.6% for Na_2SO_4) for the 25-20UD membrane. 20S, 20S3, 15S and 15S3 membranes had both a higher PWP and higher separations for the electrolytes compared to the 25-20UD membrane. The higher salt separation of 20S, 20S3, 15S and 15S3 membranes was due to the negatively charged surface of these membranes. Salt separation of the 25-20UD membrane was significantly improved by coating a layer of SPPO. In general, for the feed electrolyte concentrations used in this study, the $MgSO_4$ separation was slightly higher than the NaCl separation for all the membranes except for 25-20S membrane. For the 25-20S membrane the NaCl separation (73.4%) was much higher than the $MgSO_4$ separation (55.5%). On the other hand, the Na_2SO_4 separation (56.6 to 93.6%) was higher than both the $MgSO_4$ (23.7 to 55.5%) and the NaCl (9.6 to 73.7%) separation without exception.

It was expected that an increase in the number of coating layers of SPPO on an ultrafiltration 'UD' membrane would result in an increase in electrolyte separation. However, electrolyte separation was lower for the 20S3 membrane compared to the 20S membrane. In the case of the 15S3 membrane, the electrolyte separation was slightly higher than that of the 15S membrane. There was not much difference in the pure water permeation fluxes of the membranes having one or three coating layer(s) of SPPO. For example the PWP of the 20S and 20S3 were 142 L/m^{2}h and 132 L/m^{2}h while for the 15S and 15S3, the PWP were 126 L/m^{2}h and 120 L/m^{2}h, respectively.

PART III

Conclusions and Recommendations

CHAPTER 12

Conclusions and Recommendations

12.1. Conclusions

Based on the results presented in Chapter 5 to Chapter 11, the following conclusions can be drawn.

- All the membranes were thoroughly characterized in terms of the mean pore size, pore size distribution, surface porosity, surface roughness and pore density.
- Using techniques such as solute transport, the atomic force microscope (AFM) and the scanning electron microscope (SEM), it was found that the pore size distribution of various membranes was well represented by a log-normal distribution.
- There was no significant difference between the 'U' (wet) membranes and 'UD' (glycerol-treated and air-dried) membranes in terms of their mean pore size, pore size distribution, pore density and surface porosity. It was confirmed that the treatment of the membranes by glycerol solution did not let the pores collapse on drying.
- The mean pore sizes ranged from 0.70 to 11.12 μm, pore densities ranged from 38 to 1291 per μm^2 and surface porosities ranged from 0.50 to 1.02%, as calculated from solute transport data for various membranes. Pore density was the highest for the 20 series membranes and was the lowest for the 10 series membranes.

- The mean pore sizes measured by the AFM were substantially larger than those calculated from the solute transport data.
- When a thin layer of SPPO polymer was coated on the surface of the 'UD' membranes, the mean pore sizes and surface roughness were reduced, while pore densities were increased. It was concluded that there were several pores in the coated layer of SPPO over a single pore in the skin layer of the uncoated membrane.
- No significant differences were found in the mean pore sizes of the fouled and virgin 'S' membranes. However, the fouled membranes had comparatively smaller pore densities. The mean pore sizes of fouled 'UD' membranes were smaller than those of virgin 'UD' membranes indicating that some of the pores were plugged during the ultrafiltration experiments.
- Separations of both clay and SBR were very high for all the membranes studied.
- A sharp flux decline was observed immediately after the start of the experiment. Flux reduction was higher for the membranes having bigger pore sizes. Flux reduction was lower when membranes were coated with SPPO layer.
- A method to calculate individual resistances contributed by the membrane matrix, membrane's pores and cake layer was developed in analogy to an electric circuit model. Fouling resistance to the permeate flow was substantially higher than the resistance of the membrane and hence was the controlling factor.
- Clay particles in the cake layer were substantially smaller in size compared to those in feed solution. This indicated that smaller particles were mainly responsible for the fouling.
- The specific resistance of the cake layer increased with operating time while its void space decreased with operating time.

- AFM micrograph revealed that in the presence of SBR, the clay particles were agglomerated to form large particles containing several individual clay particles.
- The usefulness of microscopic tools such as AFM and SEM was demonstrated in characterizing membrane and cake layer morphology.

12.2. Recommendations

In any continuation of this research work, following recommendations are made.

- The particle size analysis of the cake layer should be determined for different operating times to find if there is any change in the particle size of the cake layer. This could help to explain the change in the specific resistance of the cake layer with time.
- The study of the cake layer was performed with 'UD' membranes. It could be worthwhile to repeat the same study with 'S' membranes and compare the results with those of 'UD' membranes.
- Measurement of cake layer thickness experiment could be repeated with the feed solution containing both clay and SBR. The presence of SBR will probably prevent the cake layer falling off in freeze-drying and during the sample preparation for SEM, thus enabling more precise measurement of cake thickness. Freeze-drying will also help to keep the structure of the cake layer from being altered during drying.
- Most of the experiments described here were conducted at a feed flow rate of 2600 mL/min. Experiments may also be conducted at various feed flow rates to determine the flow rate for a minimum fouling.
- The experiments with the actual waste–water from a pulp and paper mill should be conducted to evaluate the performance of the membranes.

References

Aimar, P., M. Meireles and V. Sanchez, "A Contribution to the Translation of Retention Curves into Pore Size Distribution for Sieving Membranes", J. Membrane Sci. **54**, 21-338 (1990).

Anon., "How to Filter Out a Better Lye", Pulp Paper Int. **24**(3), 40 (1982).

Baker, R. J., A. G. Fane, C. J. D. Fell and B. H. Yod, "Factors Affecting Flux in Crossflow Filtration", Desalination **53**, 81-93 (1985).

Bansal, I. K., "Progress in Developing Membrane Systems for Treatment of Forest Products and Food Processing Effluents", AICHE Sym. Series **73**(166), 144-151 (1977).

Belfort, G. and N. Nagata, "Fluid Mechanics and Crossflow Filtration: Some Thoughts", Desalination **53**, 57-59 (1985).

Bessières, A., M. Meireles, R. Coratger, J. Beauvillain and V. Sanchez, "Investigations of Surface Properties of Polymeric Membranes by Near Field Microscopy", J. Membrane Sci. **109**, 271-284 (1996).

Blatt, W. F., A. Dravid, A. S. Michaels and L. Nelsen, "Solute Polarization and Cake Formation in Membrane Ultrafiltration: Causes, Consequences, and Control Techniques", In: Membrane Science and Technology, Industrial, Biological and Waste Treatment Processes, Edited by James E. Flinn. Plenum Press, New York, 1970, 47-97 (1970).

Bottino, A., G. Capanneli, A. Grosso, O. Monticelli, O. Cavalleri, R. Rolandi and R. Soria, "Surface Characterization of Ceramic Membranes by Atomic Force Microscopy", J. Membrane Sci. **95**, 89-296 (1994).

Bowen, W. R., A. W. Mohammad and N. Hilal, "Characterization of Nanofiltration Membrane for Predictive Purpose - Use of Salts, Uncharged Solutes and Atomic Force Microscopy", J. Membrane Sci. **126**, 91-105 (1997).

Bowen, W. R., N. Hilal, R. W. Lovitt and P. M. Williams, "Atomic Force Microscope Studies of Membranes: Surface Pore Structures of Cyclopore and Anopore Membranes", J. Membrane Sci. **110**, 233-238 (1996a).

Bowen, W. R., N. Hilal, R. W. Lovitt and P. M. Williams, "Visualisation of an Ultrafiltration Membrane by Non-Contact Atomic Force Microscopy at Single Pore Resolution", J. Membrane Sci. **110**, 229-232 (1996b).

Brain, P. L. T., "Concentration Polarization in RO Desalination with Variable Flux and Incomplete Rejection", Ind. Eng. Chem. Fundam. **4**, 439-445 (1965).

Brunner, G. and E. Okoro, "Reduction of Membrane Fouling by Means of an Electric Field During Ultrafiltration of Protein Solutions", Ber. Bunsenges. Phys. Chem. **93**, 1026-1032 (1989).

Chahboun, A., R. Coratger, F. Ajustron, J. Beauvillain, A. Aimar and V. Sanchez, "Comparative Study of Micro- and Ultrafiltration Membranes Using STM, AFM, and SEM Techniques", Ultramicroscopy **41**, 235-244 (1992).

Chowdhury, G., T. Matsuura and S. Sourirajan, "A study of Reverse Osmosis Separation and Permeation Rate for Sulfonated Poly (2,6-dimethyl-1,4-phenyleneoxide) Membranes in Different Cationic Forms", J. App. Polym. Sci., **51**, 1071-1075 (1994).

Chudacek, M. W. and A. G. Fane, "The Dynamics of Polarisation in Unstirred and Stirred Ultrafiltration", J. Membrane Sci. **21**, 145-160 (1984).

Cloutier, J. N., M. K. Azarniouch and D. Callender, "Electrolysis of Weak Black Liquor. Part I. Laboratory Study", J. Pulp Paper Sci., **19**(6), J244-J248 (1993).

Cohen, R. D. and R. F. Probstein, "Colloidal Fouling of Reverse Osmosis Membranes", J. Colloid Interface Sci. **114**, 194-207 (1986).

Cooper, A. R. and D. S. Van Derveer, "Characterization of Ultrafiltration Membranes by Polymer Transport Measurement", Sep. Sci. Technol. **14**, 551-556 (1979).

CPPA (Canadian Pulp and Paper Association) Standard Testing Method, Technical Section, 1996.

Crozes, G. F., J. G. Jacangelo, C. Anselme and J. M. Laine, "Impact of Ultrafiltration Operating Conditions on Membrane Irreversible Fouling", J. Membrane Sci. **124**, 63-76 (1997).

Dal-Cin, M. M., F. McLellan, C. N. Striez, C. M. Tam, T. A. Tweddle and A. Kumar, "Membrane Performance with a Pulp and Paper Effluent: Relative Contribution of Fouling Mechanisms", J. Membrane Sci. **120**, 273-285 (1996).

Davis, R. H. and D. T. Leighton, "Shear Induced Transport of a Particle Layer along a Porous Wall", Chem. Eng. Sci. **42**, 275-281 (1987).

Dharmappa, H. B., J. Verink, R. Ben Aim, K. Yamamoto and S. Vigneswaran, "A Comprehensive Model for Cross-flow Filtration Incorporating Polydispersity of the Influent", J. Membrane Sci. **65**, 173-185 (1992).

Dietz, P., K.-H. Herrmann, O. Inacker, H. D. Lehmann and P. K. Hansma, "Scanning Force Microscope of Synthetic Membranes in Air and Under Water: Surfaces, Cross Sections and Fouling", Scanning Probe Microscopies **1639**, 186-197 (1992b).

Dietz, P., P. K. Hansma, K.-H. Herrmann, O. Inacker and H.-D Lehmann, "Atomic Force Microscopy of Synthetic Ultrafiltration Membranes in Air and Under Water", Ultramicroscopy **35**, 155-159 (1991).

Dietz, P., P. K. Hansma, O. Inacker, H.-D. Lehmann and K.-H. Herrmann, "Surface Pore Structure of Micro- and Ultrafiltration Membranes Imaged with the Atomic Force Microscope", J. Membrane Sci. **65**, 101-111 (1992a).

Digital Instruments Inc., "Nano Scope III Control System Manual", Santa Barbara, USA, 1993.

Elefsiniotis, P., E. R. Hall and R. M. Johnson, "Removal of Contaminants from Recirculated White Water by Ultrafiltration and/or Biological Treatment", Can. J. Chem. Eng. **75**, 88-94 (1997).

Fane, A. G. and C. J. D. Fell, "A Review of Fouling and Fouling Control in Ultrafiltration", Desalination **62**, 117-136 (1987).

Fane, A. G., "Ultrafiltration of Suspensions", J. Membrane Sci. **20**, 249-259 (1984).

Fane, A. G., C. J. D. Fell and A. G. Waters, "The Relationship Between Membrane Surface Pore Characteristics and Flux for Ultrafiltration Membranes", J. Membranes Sci. **9**, 245-262 (1981).

Fritzsche, A. K., A. R. Arerado, M. D. Moore and C. O'Hara, "The Surface Structure and Morphology of Polyacrylonitrile Membranes by Atomic Force Microscope", J. Membrane Sci. **81**, 109-120 (1993).

Fritzsche, A. K., A. R. Arevalo, A. F. Connolly, M. D. Moore, V. Elings and C. M. Wu, "The Structure and Morphology of Skin of Polyethersulfone Ultrafiltration Membranes: A Comparative Atomic Force Microscope and Scanning Electron Microscope Study, J. Appl. Polym. Sci. **45**, 1945-1956 (1992a).

Fritzsche, A. K., A. R. Arevalo, M. D. Moore, C. J. Weber, V. B. Elings, K. Kjoller and C. M. Wu, "Image Enhancement of Polyethersulfone Ultrafiltration Membrane Surface Structure for Atomic Force Microscopy", J. Appl. Polym. Sci. **46**, 167-178 (1992b).

Gatenholm, P., C. J. Fell and A. G. Fane, "Influence of the Membrane Structure on the Composition of the Deposit Layer during Processing of Microbial Suspensions", Desalination **70**, 363-378 (1988).

Geraldes, V. M. and M. N. de Pinho, "National Report: Portugal", Water Supply, **14**, 289-322 (1996).

Green, G. and G. Belfort, "Fouling of Ultrafiltration Membranes: Lateral Migration and the Particle Trajectory Model", Desalination **35**, 129-147 (1980).

Hamza, A., G. Chowdhury, T. Matsuura and S. Sourirajan, "Study of Reverse Osmosis Separation and Permeation Rate for Sulfonated Poly(2,6-dimethyl-1,4-phenylene oxide) Membranes of Different Ion Exchange Capacities", J. Appl. Poly. Sci. **58**, 613-620 (1995).

Henis, J. M. S. and M. K. Tripodi, "A Novel Approach to Gas Separations using Composite Hollow Fiber Membrnaes", Sep. Sci. Technol. **15**, 1059-1068 (1980).

Henis, J. M. S. and M. K. Tripodi, "Composite Hollow Fiber Membranes for Gas Separation: The Resistance Model Approach", J. Membrane Sci. **8**, 233-246 (1981).

Hermia, J., "Constant Pressure Blocking Filtration Law – Application to Power-Law Non-Newtonian Fluids", Trans. Inst. Chem. Eng. **62**, 183-187 (1982).

Hirose, M., H. Ito and Y. Kamiyama, "Effect of Skin Layer Surface Structure on the Flux Behaviour of RO Membranes", J. Membrane Sci. **121**, 209-215 (1996).

Hoogland, M. R., C. J. D. Fell, A. G. Fane and D. A. R. Jones, "The Optimum Design of Cross-flow Filtration Elements for Mineral Slurry Processing", Proceedings of 5th World Filtration Congress, 1990, 604-610 (1990).

Hsieh, F. -U., T. Matsuura and S. Sourirajan, "Analysis of Reverse Osmosis Data for the System: Polyethylene Glycol-Water-Cellulose Acetate Membrane at Low Operating Pressures", Ind. Eng. Chem. Process Des. Dev. **18**, 414-423 (1979b).

Hsieh, F. -U., T. Matsuura and S. Sourirajan, "Reverse Osmosis Separations of Polyethylene Glycols in Dilute Aqueous Solutions Using Porous Cellulose Acetate Membranes", J. Appl. Polym. Sci. **23**, 561-573 (1979a).

Huang, R. Y. M. and J. J. Kim, "Synthesis and Transport Properties of Thin Composite Membranes II. Preparation of Sulfonated Polyphenylene Oxide Thin Composite Membranes for the Purification of Alberta Tar Sand Waste Waters", J. Appl. Polym. Sci. **29**, 4029(1984).

Hunt, J. W., C. J. Brouckaert, J. D. Raal and C. A. Buckley, "The Unsteady-state Modelling of Cross-flow Microfiltration", Desalination **64**, 431-442 (1987).

Imasaka, T., N. Kanekuni, H. So and S. Yoshino, "Cross-flow Filtration of Methane Fermentation Broth by Ceramic Membranes", J. Fermen. Bioeng. **68**, 200-206 (1989).

Ishiguro, M., T. Matsuura and C. Detellier, "A Study on the Solute Separation and the Pore Size Distribution of a Montmorillointe Membrane", Sep. Sci. Technol. **31**, 545-556 (1996).

Jantunen, E., G. Lindholm, L. M. Lindroos, A. Paavola, U. Parkkonen, R Pusa and M. Soderstrom, "The Effluent Free Newsprint Mill", Pulp Paper Timber **74**, 41-44 (1992).

Jonsson, A. S. and E. Petersson, "Treatment of C-stage and E-stage Bleaching Plant Effluent by Ultrafiltration", Nordic Pulp Paper Res. J. **4**(3), 184-187 (1989).

Jonsson, A. S. and E. Petersson, "Treatment of C-stage and E-stage Effluents from a Bleach Plant Using a Ceramic Membrane", Nordic Pulp Paper Res. J. **3**(1), 4-7 (1988).

Jonsson, A. S. and R. Wimmerstedt, "The Application of Membrane Technology in the Pulp and Paper Industry", Desalination **53**, 181-196 (1985).

Jonsson, A. S., "Influence of Shear Rate on the Flux During Ultrafiltration of Colloidal Substances", J. Membrane Sci. **79**, 93-99 (1993).

Jonsson, A. S., "Treatment of Effluent from Alkali Extraction with Ultrafiltration and Reverse Osmosis", Nordic Pulp Paper Res. J. **4**(1), 33-37 (1989).

Jonsson, A. S., "Ultrafiltration of Bleach Plant Effluent", Nordic Pulp Paper Res. J. **2**(1), 23-29 (1987).

Jonsson, A. S., C. Jonsson, M. Teppler, P. Tomani and S. Wannstrom, "Recovery of Dilute Coating Colour Effluents by Ultrafiltration", Filtration & Separation **33**, 31-38 (1996a).

Jonsson, A. S., C. Jonsson, M. Teppler, P. Tomani and S. Wannstrom, "Treatment of Paper Coating Colour Effluents by Membrane Filtration", J. Membrane Sci. **105**, 263-276 (1996b).

Joshi, V. S. and S. Basu, "Application of Electrolysis in Recovery of Chemical from Black Liquor," Chemical Age of India **24**(10), 671-676 (1973).

Kakuta, A., M. Kuramoto, M. Ohno, H. Kushida, A. Tanioka and K. Ishikawa, "Freeze-Dried Cellulose Acetate Membrane Fine Structure Observation", J. Polym Sci., Polym Chem. Ed. **18**, 3229-3243 (1980).

Kassotis, J., J. Shmidt, L. T. Hodgins and H. P. Gregor, "Modeling of the Pore Size Distribution of Ultrafiltration Membranes", J. Membrane Sci. **22**, 61-76 (1985).

Khatib, K., J. Rose, O. Barres, W. Stone, J-Y. Bottero and C. Anselme, "Physico-Chemical Study of Fouling Mechanisms of Ultrafiltration Membrane on Biwa Lake (Japan)", J. Membrane Sci. **130**, 53-62 (1997).

Khulbe, K. C., B. Kruczek, G. Chowdhury, S. Gagné and T. Matsuura, "Surface Morphology of Homogeneous and Asymmetric Membranes Made from Poly(phenylene oxide) by Tapping Mode Atomic Force Microscope", J. Appl. Polym. Sci. **59**, 1151-1158 (1996a).

Khulbe, K. C., B. Kruczek, G. Chowdhury, S. Gagné, T. Matsuura and S. P. Verma, "Characterization of Membranes Prepared from PPO by Raman Scattering and Atomic Force Microscopy", J. Membrane Sci. **111**, 57-70 (1996b).

Kim, K. J., A. J. Fane and C. J. D. Fell, "Quantitative Microscopic Study of Surface Characteristics of Ultrafiltration Membranes", J. Membrane Sci. **54**, 89-102(1990).

Kozinski, A. A. and E. N. Lightfoot, "Protein Ultrafiltration; A General Example of Boundary Layer Filtration", AICHE J. **18**, 1030 (1972).

Lafrenière, L. Y., F. D. F. Talbot, T. Matsuura and S. Sourirajan, "Effect of Polyvinylpyrrolidone Additive on the Performance of Polyethersulfone Ultrafiltration Membranes", Ind. Eng. Chem. Res. **26**, 2385-2389 (1987).

Lahoussine-Turcaud, V., M. R. Wiesner and J-Y. Bottero, "Fouling in Tangential-Flow Ultrafiltration: The Effect of Colloid Size and Coagulation Pretreatment", J. Membrane Sci. **52**, 173-190 (1990).

Leonard, E. F. and C. S. Vassilief, "The Deposition of Rejected Matter in Membrane Separation Processes", Chem. Eng. Comm. **30**, 209-217 (1984).

Leypoldt, J., "Determining Pore Size Distributions of Ultrafiltration Membranes by Solute Sieving- Mathematical Limitations", J. Membrane Sci. **31**, 289-305 (1987).

Lindstrom, T., C. Soremark and L. Westman, "The Influence on Paper Strength of Dissolved and Colloidal Substances in the White Water", Sevensk Papperstidning **11**, 341-345 (1977).

Lipson, C. and N. J. Sheth, "Statistical Tools, in: Statistical Design and Analysis of Engineering Experiments", McGraw-Hill, New York, 18 (1973).

Lundahl, H. and L. Mansson, "Ultrafiltration for Removing Color Form Bleach Plant Effluent", Tappi J. **63**(4), 97-101 (1980).

Mackley, M. R. and N. E. Sherman, "Cross-Flow Cake Filtration Mechanisms and Kinetics", Chem. Eng. Sci. **47**, 3067-3084 (1992).

Manttari, M., J. Nuortila-Jokinen and M. Nystrom, "Evaluation of Nanofiltration Membrane for Filtration of Paper Mill Total Effluent", Filtration & Separation **34**, 275-280 (1997).

Matsumoto, Y., Y. Totsuka, T. Sakata, T. Higashi and W. Takahashi, "Characteristic of Filtration for Methane Fermentation Suspension by Ceramic Membranes- Study of Filtration Condition", Kagaku Kogaku Ronbunshu **14**, 462-469 (1988)

McLeod, M., "Mill Achieves Maximum Reuse of Water with Reverse Osmosis", Pulp & Paper **48**(11), 62-64 (1974).

Meireles, M., A. Bessieres, I. Rogissart, P. Aimar and V. Sanchez, "An appropriate Molecular Size Parameter for Porous Membranes Calibration", J. Membrane Sci. **103**, 105-115 (1995).

Michaels, A. S., "Analysis and Prediction of Sieving Curves for Ultrafiltration Membranes: A Universal Correlation?", Sep. Sci. Technol. **15**, 1305-1322 (1980).

Michaels, A. S., "New Separation Technique for the CPI", Chem. Eng. Progress **64**, 31-43 (1968a).

Michaels, A. S., "Ultrafiltration. In Progress in Separation and Purification edited E. S. Perry, Vol. 1. New York, Wiley Interscience, 1968b.

Michaels, A. S., L. Nelsen and M. C. Porter, "Ultrafiltration in; M. Bier (Ed), Membrane Process in Industry and Biomedicine", Plenum Press, New York, 197 (1971).

Miner, R., and J. Unwin, "Progress in Reducing Water Use and Waste Water Loads in U.S. Paper Industry", Tappi J. **74**(8), 127 (1991).

Muralidhara, H. S., "Membrane Fouling: Techno-Economic Implications", Key Engineering Materials **61&62**, 301-306 (1991).

Nabi, G., "Light-Scattering Studies of Aqueous Solutions of Poly(ethylene oxide)", Pakistan J. Sci. **20**, 136-140 (1968).

Nakao, S., "Determination of Pore Size and Pore Size Distribution. 3. Filtration Membranes", J. Membrane Sci. **96**, 131-165 (1994).

Nakao, S., S. Nomura and S. Kimura, "Transport Phenomena of the Cross-flow Microfiltration Process", Proceedings of 5th World Filtraiton Congress, 1990, 564-570 (1990).

Nelson, W. R., G. O. Walraven and D. C. Morris, "Process Water Reuse and Upset Control Modification at an Integrated NSSC mill", Tappi J. **56**(7), 54-57 (1973).

Nurotila-Jokinen, J. and M. Nystrom, "Comparison of Membrane Separation Processes in the Internal Purification of Paper Mill Water", J. Membrane Sci. **119**, 99-115 (1996).

Nurotila-Jokinen, J., P. Martin and M. Nystrom, "UF and NF as Internal Methods for the Make-up Waters of a Neutral MFC Machine", Proceedings of Euromembrane, 1995, I521-I529 (1995a).

Nurotila-Jokinen, J., P. Soderberg and M. Nystrom, "UF and NF Pilot Scale Studies on Internal Purification of Paper Mill Make-up Waters", Proceedings of TAPPI International Environmental Conference, 1995, 847-859 (1995b).

Paine, P. L. and P. Scherr, "Drag Coefficient for the Movement of Rigid Sphere Through Liquid Filled Pores", Biophysical J. **15**, 1087-1091 (1975).

Paleologou, M., J. N. Cloutier, P. Ramamurthy, R. M. Berry, M. K. Azarniouch and J. Dorica, "Membrane Technologies for Pulp and Paper Applications", Pulp Paper Can. **95**(10), T386-T390 (1994).

Paleologou, M., P-Y. Wong and R. M. Berry, "A Solution to Caustic/Chlorine Imbalance: Bipolar Membrane Electrolysis", J. Pulp Paper Sci. **18**(4), J138-J145 (1992).

Panchapakesan, B., "White Water Reuse and Saveall: In Paper Machine Operation", Vol. 7., Published by TAPPI press Atlanta, 173-1991 (1991).

Pepper, D. and J. Tingle, "Reverse Osmosis and Ultrafiltration for Energy Conservation and Pollution Control", Pulp Paper Can. **4**(10), T219-T221 (1983).

Perry's Chemical Engineering Handbook, Edited by R. H. Perry, D. W. Green and J. O. Maloney, McGraw-Hill Inc., New York, 1984.

Pichon, M., R. Camatta, G. Tardy and D. Woerner, "Ultrafiltration Applied to the Treatment of Effluents to the Paper and Paper Board Coating Plants", Proceeding of Tappi Environmental Conference, 1992, 731-736 (1992).

Pinho, M. N. D., V. M. Geraldes, M. J. Rosa, M. D. Afonso, H. Figueira, F. Taborada, G. Almeida, R. Ganho, R. Creusen, J. Hanemaaijer, S. Gaeta, P. Amblard, C. Gavach and C. Guizard, "Water Recovery from Bleached Pulp Effluents", Tappi J. **79**, 117-124 (1996).

Plummer, C. W., G. Kimura, and A. B. La Conte, "Development of Sulfonated Polyphenylene oxide Membranes for Reverse Osmosis", Research and Development Progress Report # 551, Office of Saline Water, United States Department of Interior, (1970).

Porter, M. C., "Concentration Polarization with Membrane Ultrafiltration", Ind. Eng. Chem. Prod. Res. Develop. **11**, 234-248 (1972b).

Porter, M. C., "Ultrafiltration of Colloidal Suspension", AICHE Symp. Ser. **68**, 21-30 (1972a).

Ramamurthy, P., R. Poole and J. G. Dorica, "Fouling of Ultrafiltration Membranes during Treatment of CTMP Screw Press Filtrates", J. Pulp Paper Sci. **21**, J50-J54 (1995)

Rautenbach, R. and G. Schock, "Ultrafiltration of Macromolecular Solutions and Cross-flow Mircofiltration of Colloidal Suspensions. A Contribution to Permeate Flux Calculations", J. Membrane Sci. **36**, 231-242 (1988).

Riesmeier, B., K. H. Kroner and M. R. Kula, "Studies of Secondary Layer Formation and its Characterization during Cross-flow Filtration of Microbial Cells", J. Membrane Sci. **34**, 245-266 (1987).

Riley, R., J. O. Gardner and U. Merten, "Cellulose Acetate Membranes: Electron Microscopy of Structure", Science **143**, 801-803 (1964).

Romero, C. A. and R. H. Davis, "Experimental Verification of the Shear-induced Hydrodanamic Diffusion Model of Crossflow Micorfiltration", J. Membrane Sci. **62**, 249-273 (1991).

Romero, C. A. and R. H. Davis, "Global Model of Crossflow Microfiltration based on Hydrodanamic Particle Diffusion", J. Membrane Sci. **39**, 157-185 (1988).

Shimizu, Y., K. Shimodera and A. Watanabe, "Cross-flow Microfiltration of Bacterial Cells", J. Fermen. Bioeng. **76**, 493-500 (1993).

Shimizu, Y., M. Rokudai, S. Tohya, E. Kayawake, T. Yazawa, H. Tanaka and K. Eguchi, "Effect of Membrane Resistance on Filtration Characteristics for Methanogenic Waste", Kagaku Kogaku Ronbunshu **16**, 145-151 (1990).

Shirato, M., T. Murase, E. Iritani and S. Nakatsuka, "Experimental Analysis of Flux Decline Mechanism of Batch Ultrafiltration (Filtration Characteristics of Gel Layer)", Filtration & Separation **28**, 104-109 (1991).

Sierka, R. A., H. G. Folster and J. J. Avenell, "The Treatment of Whitewaters by Adsorption and Membrane Techniques", Proceedings of Tappi International Environmental Conference, 1994, 249-257 (1994).

Silva, M., M. E. D. Zaniquelli and F. Galembeck, "Paralled Electric Field in Flux Restoration during Ultrafiltration", Sep. Sci. Technol. **26**, 831-840 (1991).

Skowronski, J. and P. Lepoutre, "Water Interactions during Paper Coating, Part II. Network and Intrafibre Stress Relaxation", Proceedings of CPPA 72nd Annual Meeting, 1986, A45-A51 (1986).

Sourirajan, S. and T. Matsuura, "Reverse Osmosis/Ultrafiltration Process Principles", National Research Council of Canada, 1985.

Strathmann, H., K. Kock, P. Amar and R. W. Baker, "The Formation Mechanism of Asymmetric Membranes", Desalination **16**, 179-203 (1975).

Stridsberg, S., T. Nyberg and L. Robinson, "Recovery of Waste Coating by Ultrafiltration", Proceeding of Tappi Environmental Conference, 1992, 737-745 (1992).

Suki, A., A. G. Fane and C. J. D. Fell, "Modeling Fouling Mechanisms in Protien Ultrafiltration", J. Membrane Sci. **27**, 181-193 (1986).

Tardif, O. and E. R. Hall, "Alternatives for Treating Recirculated Newsprint Whitewater at High Temperatures", Wat. Sci. Tech. **35**, 57-65 (1997).

Tardy, G., J. Kuhbok and D. Woener, "Pollution Control of Coating Effluents", Paper Age **28** (5), 30-31 (1992).

Tunney, J. J., "New Nanocomposite Materials from Kaolinite as a Mineral Precursor", A Ph. D. Thesis at Department of Chemisty, University of Ottawa, 212 (1995).

Vanden Berg, G. B. and C. A. Smolders, "The Boundary Layer Resistance Model for Unstirred Ultrafiltration: A New Approach", J. Membrane Sci. **40**, 149-172 (1989).

Wakeman, R. J. and E. S. Tarleton, "Membrane Fouling Prevention in Crossflow Microfiltraton by the Use of Electric Fields", Chem. Eng. Sci. **42**, 829-842 (1987).

Wijmans J. G., S. Nakao and C. A. Smolders, "Flux Limitation in Ultrafiltration: Osmotic Pressure Model and Gel Layer Model", J. Membrane Sci., **20**, 115-124 (1984).

Wijmans, J. G., S. Nakao and C. A. Smolders, "Hydrodynmic Resistance of Concentration Polarizaton Boundary Layer in Ultrafiltration", J. Membrane Sci. **22**, 117-135 (1985).

Woerner, D. L. and J. L. Short, "Recovery of Coating Losses", Proceedings of Tappi Coating Conference, 1991, 251-257 (1991).

Yao, W. X, K. J. Kennedy, C. M. Tam and J. D. Hazlett, "Pre-treatment of Kraft Pulp Bleach Plant Effluent by Selected Ultrafiltration Membranes", Can. J. Chem. Eng. **72**, 991-999 (1994).

Youm, K. H. and W. S. Kim, "Prediction of Intrinsic Pore Properties of Ultrafiltration Membrane by Solute Rejection Curves: Effect of Operating Conditions on Pore Properties", J. Chem. Eng. Japan **24**, 1-7 (1991).

Zeman, L. and M. Wales, "Steric Rejection of Polymeric Solutes by Membranes with Uniform Pore Size Distribution", Sep. Sci. Technol. **16**, 275-290 (1981).

Zydney, A. L. and C. K. Colton, "A Concentration Polarization Model for the Filtrate Flux in Cross-flow Microfiltration of Particulate Suspensions", Chem. Eng. Comm. **47**, 1-21 (1986).

PART IV

Appendices

Appendix A

A.1. Determination of the stoichiometric amount of chlorosulfonic acid for sulfonation of poly(2,6-dimethyl-1,4-phenylene oxide) (PPO)

The following equation was used to determine the stoichiometric amount of chlorosulfonic acid for sulfonation of PPO.

$$v_c = \frac{m_c \times w_p}{\rho_c}\left(\frac{I}{1000 - 80.I}\right) \qquad (A.1)$$

where

v_c = volume of chlorosulfonic acid required (mL),

m_c = molecular weight of chlorosulfonic acid (116.52 g/mol),

ρ_c = density of chlorosulfonic acid (1.753 g/cm^3),

w_p = weight of polymer (PPO) used for sulfonation (g), and

I = Target value of ion exchange capacity (meq/g of polymer powder)

As per Eq. (A.1), 1.58 mL of chlorosulfonic acid will be required to sulfonate 10 g of PPO polymer for achieving an IEC value of 2.0 meq/g of polymer.

A.2. Determination of IEC value of sulfonated PPO (SPPOH)

The IEC of SPPOH polymer was measured by using acid-base titration method. A known amount (about 0.5 g) of vacuum dried SPPOH was soaked in 25 mL of 0.1N NaOH for two days. The H^+ of sulfonate groups in SPPOH are replaced with Na^+ from the NaOH solution. The liberated H^+, consequently, consumes a stoichiometric quantity of OH^- ions. Treating the

excess NaOH with 0.1N HCl then gives the meq of OH^- consumed per unit weight of dry polymer. Phenolphthalein was used as an indicator in titration. The following equation was used to calculate the IEC value

$$I = \frac{(v_1 - v_2)}{w_s} \times 0.1 \qquad (A.2)$$

where

v_1 = volume of 0.1N NaOH used for soaking the polymer (mL),

v_2 = volume of 0.1N HCl consumed in titration (mL), and

w_s = weight of SPPOH polymer soaked in 0.1N NaOH (g)

Appendix B

B.1. Relationship between operating pressure and permeation rate

The Figure B.1 (a&b) confirms the linear relationship between operating pressure and permeation rate.

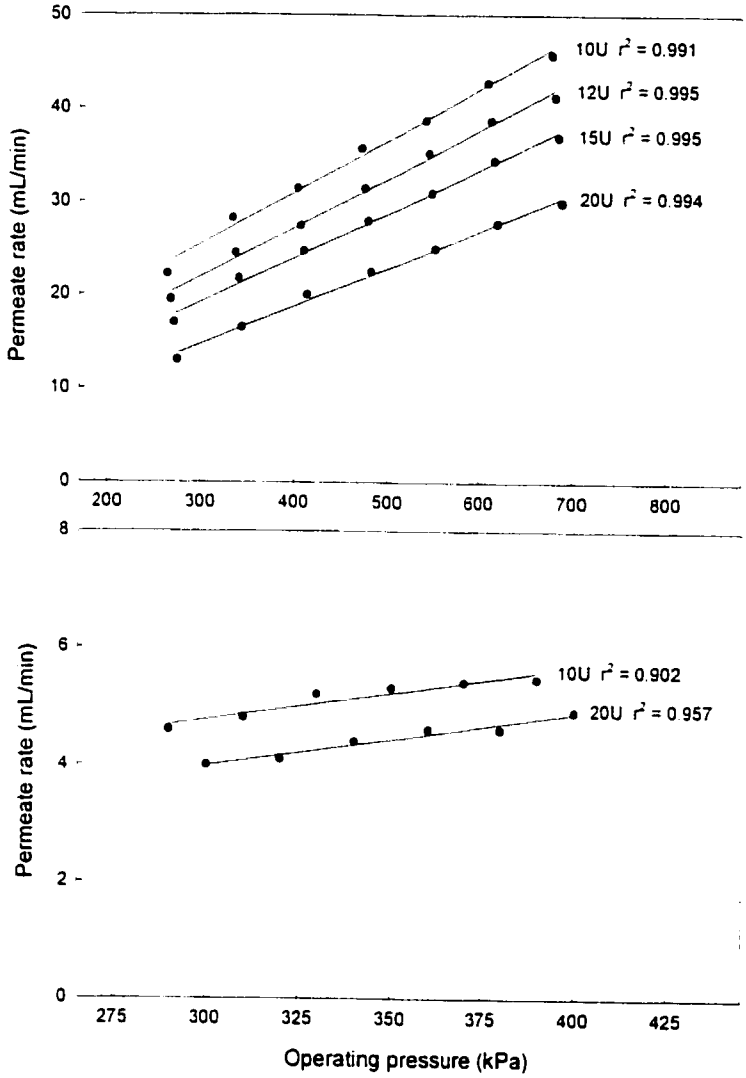

Figure B.1. Operating pressure versus permeate rate for the feed solution (a) deionised water and (b) 1% of clay and SBR (clay/SBR = 100/15)

Appendix C

C.1. Conversion of permeate flux data to the value at 25^{0}C

Permeate flux data were converted to the values at 25^{0}C by the following equation using density and viscosity data of water which were taken form Perry's Chemical Engineer's Handbook (1984)

$$J_{p(25)} = \alpha J_{p(T)} \tag{C.1}$$

where

$$\alpha = \frac{\rho_{25}\eta_T}{\rho_T\eta_{25}} \tag{C.2}$$

where α is a conversion factor and is defined in Eq. (C.2). $J_{fp(25)}$ and $J_{fp(T)}$ are the permeate flux at 25^{0}C and at operating temperature T^{0}C respectively. Similarly ρ_{25}, ρ_T and η_{25}, η_T are density and viscosity of water at 25^{0}C and at operating temperature T^{0}C. Typical temperature range for feed solution in the ultrafiltration experiment was 22 to 29^{0}C. Values of α for different temperatures are given in Table C.1.

Table C.1. Values of conversion factor α for various temperatures to convert permeate flux data to the value at 25^{0}C

Operating temperature (^{0}C)	Conversion factor α	Operating temperature (^{0}C)	Conversion factor α	Operating temperature (^{0}C)	Conversion factor α
15	1.273	22	1.071	29	0.916
16	1.241	23	1.047	30	0.897
17	1.210	24	1.023	31	0.879
18	1.180	25	1.000	32	0.861
19	1.151	26	0.978	33	0.844
20	1.123	27	0.957	34	0.827
21	1.097	28	0.936	35	0.811

Appendix D

D.1. Particle Size Analysis by Sedigraph 5100

For particle size analysis (PSA), Sedigraph 5100 uses the principle of sedimentation in order to determine the diameter of particles in a suspension. Sedimentation size analysis is based upon the fact that the measured equilibrium velocity of a particle through a viscous medium, resulting from the action of the gravitational force, can be related to the size of the particle by Stoke's law. For a spherical particle of diameter D with a falling velocity of v, Stoke's law can be written as

$$D = \left[\frac{18\eta v}{(\rho - \rho_0)g}\right]^{\frac{1}{2}} \qquad (D.1)$$

where ρ and ρ_0 are the densities of the particle and fluid respectively, η is the viscosity of fluid and g is the acceleration of gravity. In practice, however, particles are not usually spherical and adopt a large variety of irregular shapes: this is especially true of clay (kaolin), whose particles have a plate type shape. The diameter in the above Eq. (D.1), thus refers to the 'Stoke's Diameter' or 'Equivalent Spherical Diameter (ESD)' for such particles, representing the mean diameter of a sphere which would be composed of the same material and that would have the same mass as the particle in question. The falling velocity v can be further expressed as the distance h fallen by the particle during a period of time t, and the Stokes equation can be reformulated as:

$$D = \left[\frac{18\eta h}{(\rho - \rho_0)gt}\right]^{\frac{1}{2}} \qquad (D.2)$$

Therefore, after a given time t, all particles larger than the corresponding diameter D will have fallen below a given distance h from the surface of suspension. If the initial (uniform) concentration of material is C_0 g/cm^3 and the concentration after time t_i at distance h is C_i g/cm^3, then P_i the weight percent of particles finer than D_i can be expressed as:

$$P_i = 100\left(\frac{C_i}{C_0}\right) \tag{D.3}$$

In the PSA experiment, a suspension of a material is allowed to settle in a cell through which a collimate X-ray beam is passed at a fixed point. The intensity of X-ray is reduced as it passes through the suspension and the X-ray transmittance T_i can be related to the particle mass concentration C_i in the beam's path. Thus, the particle size distribution can be expressed as:

$$P_i = 100\left(\frac{\ln T_i}{\ln T_0}\right) \tag{D.4}$$

where T_0 is the initial X-ray transmittance (at t = 0) of the suspension.

The P_i values measured by X-ray transmittance can, therefore, be plotted as a function of the D_i values obtained from the sedimentation time to give the particle size distribution graph for the material studied. This is most often presented as cumulative mass plot, where the percentage of particles with larger mass is plotted as a function of particle size. The percent of particles found in different size intervals can likewise be determined.

Appendix E

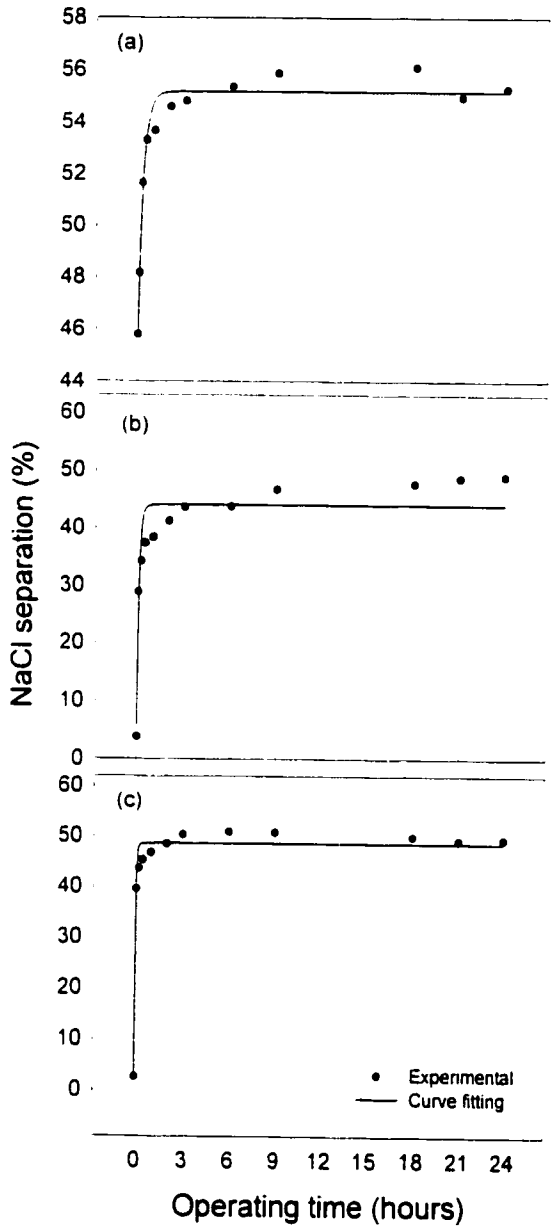

Figure E.1. NaCl separation versus time for various membranes and feed solutions (a) 15S, feed: 0.87% of clay + 200 ppm of NaCl, (b) 15UD, feed: 0.87% of clay + 200 ppm of NaCl and (c) 15UD, feed: 1% of clay and SBR + 200 ppm of NaCl

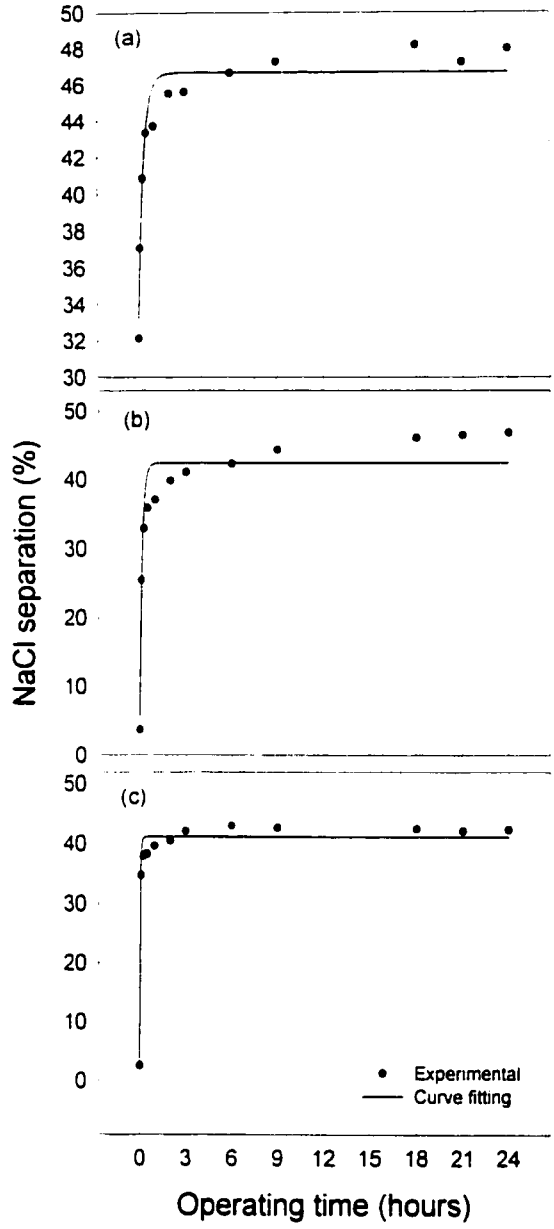

Figure E.2. NaCl separation versus time for various membranes and feed solutions (a) 12S, feed: 0.87% of clay + 200 ppm of NaCl, (b) 12UD, feed: 0.87% of clay + 200 ppm of NaCl and (c) 12UD, feed: 1% of clay and SBR + 200 ppm of NaCl

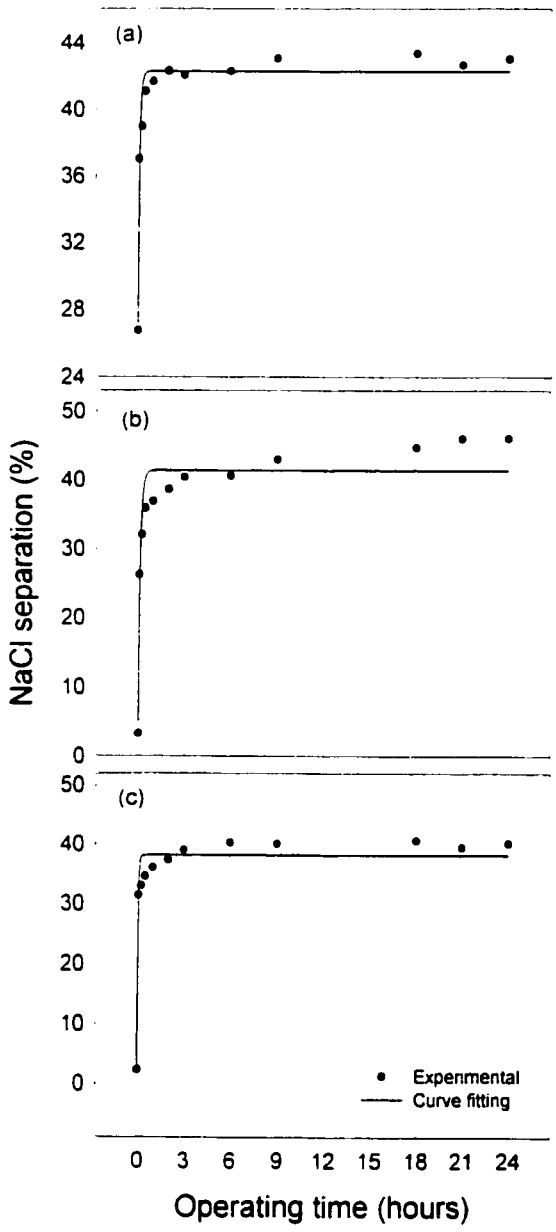

Figure E.3. NaCl separation versus time for various membranes and feed solutions (a) 10S, feed: 0.87% of clay + 200 ppm of NaCl, (b) 10UD, feed: 0.87% of clay + 200 ppm of NaCl and (c) 10UD, feed: 1% of clay and SBR + 200 ppm of NaCl

Appendix F

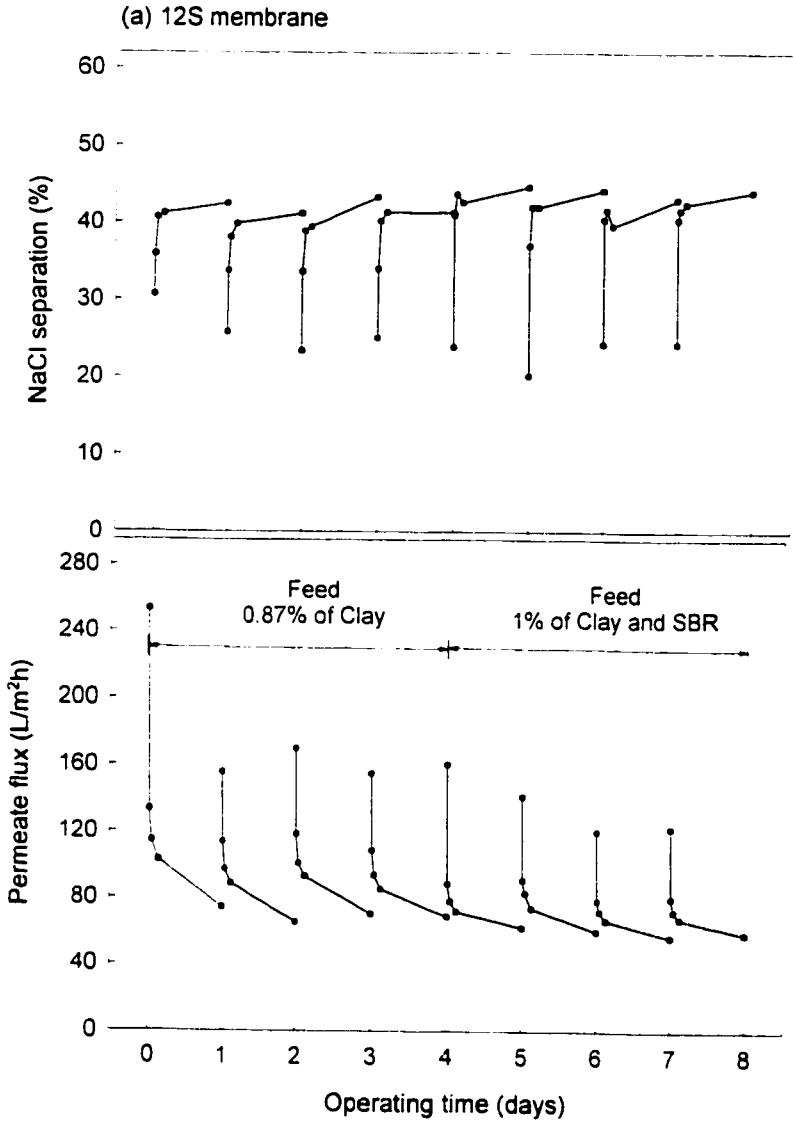
(a) 12S membrane
NaCl separation (%)
60
50
40
30
20
10
0
Permeate flux (L/m²h)
280
240
200
160
120
80
40
0
Feed
0.87% of Clay
Feed
1% of Clay and SBR
0
1
2
3
4
5
6
7
8
Operating time (days)

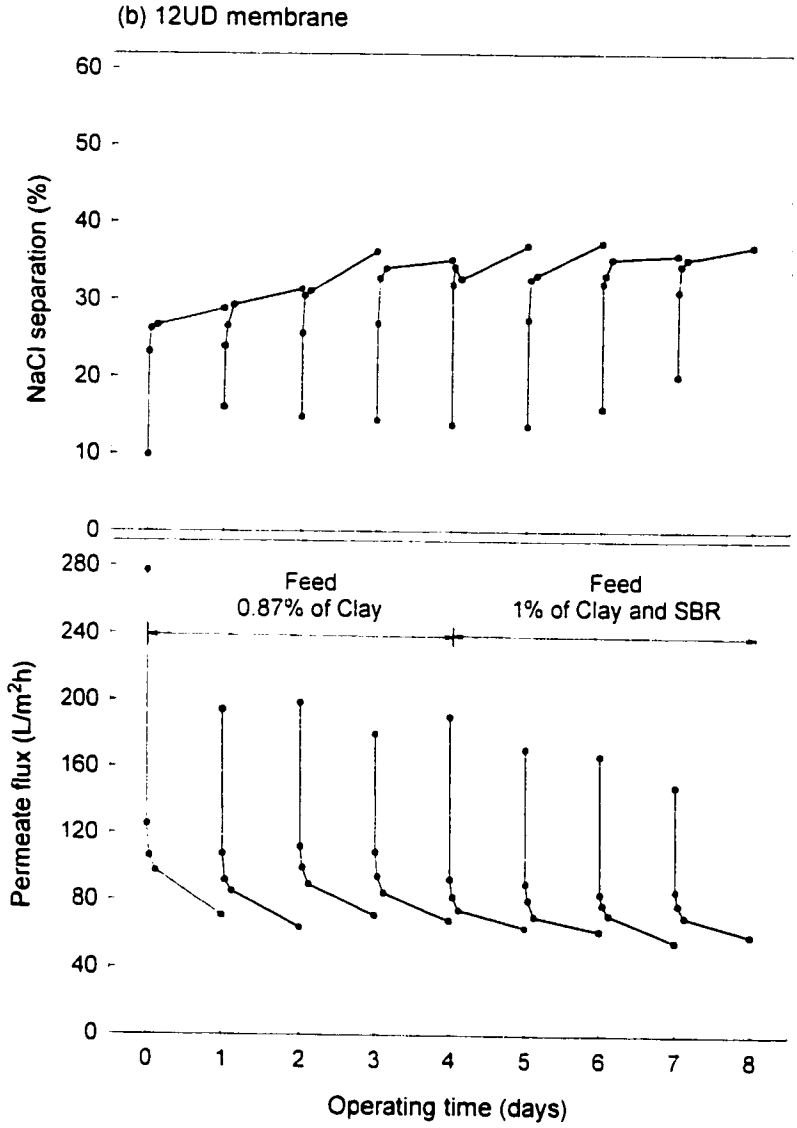

Figure F.1. Performance of (a) 12S and (b) 12UD membranes in terms of permeate flux and NaCl separation over a period of 8 days. (Membranes were washed after every 24 hours of operation)